Detailed Study of the 21 May 2016 Landslide on the Natural Hillside above Slope No. 8SE-A/F34 at Sai Kung Sai Wan Road, Sai Kung

GEO Report No. 336

AECOM Asia Company Limited

Geotechnical Engineering Office
Civil Engineering and Development Department
The Government of the Hong Kong
Special Administrative Region

Detailed Study of the 21 May 2016 Landslide on the Natural Hillside above Slope No. 8SE-A/F34 at Sai Kung Sai Wan Road, Sai Kung

GEO Report No. 336

AECOM Asia Company Limited

This report was originally produced in October 2017 as GEO Landslide Study Report No. LSR 3/2017

First published, March 2018

Prepared by:

Geotechnical Engineering Office,
Civil Engineering and Development Department,
Civil Engineering and Development Building,
101 Princess Margaret Road,
Homantin, Kowloon,
Hong Kong.

Preface

In keeping with our policy of releasing information which may be of general interest to the geotechnical profession and the public, we make available selected internal reports in a series of publications termed the GEO Report series. The GEO Reports can be downloaded from the website of the Civil Engineering and Development Department (http://www.cedd.gov.hk) on the Internet.

W.K. Pun
Head, Geotechnical Engineering Office
March 2018

Foreword

This report presents the findings of a detailed study of a landslide incident (Incident No. 2016/05/1823) that occurred on a natural hillside above Sai Kung Sai Wan Road, Sai Kung East Country Park following the intense rainstorm during the early morning of 21 May 2016. The landslide involved a total source volume of about 2,100 m^3 and comprised a translational rock slide. The detached material travelled a distance of about 500 m down the hillside eventually coming to rest in a natural drainage line above High Island Reservoir. Sai Kung Sai Wan Road was completely blocked with debris and the fill slope below (Slope No. 8SE-A/F34) was partly eroded, undermining the road and resulting in road closure for several months. Some outwash debris was transported into the reservoir. No casualties were reported as a result of the landslide.

The key objectives of the study were to document the facts about the landslide, present relevant background information and establish the probable causes of the failure. The discussion and views expressed in this report are not intended to establish the existence of any duty at law on the part of the Government of the Hong Kong Special Administrative Region (HKSARG), its employees or agents, contractors, their employees or agents, or subcontractors, or any other party. This report neither determines nor implies liability towards any particular organization or individual except so far as necessary to achieve the said objectives.

The report was prepared for the Geotechnical Engineering Office of the Civil Engineering and Development Department, under Agreement No. CE 46/2015 (GE). This is one of a series of reports produced during the consultancy by AECOM Asia Company Limited. Unless otherwise agreed in writing, AECOM Asia Company Limited accepts no responsibility for any use of, or reliance on any contents of this Report by any person other than HKSARG or its employees or agents, and shall not be liable to any person other than HKSARG or its employees or agents, on any ground, for any loss, damage or expense arising from such use or reliance.

Patrick A Chao
Project Director
AECOM Asia Company Limited

Agreement No. CE 46/2015 (GE)
Study of Landslides Occurring in Kowloon and the New Territories between 2016 and 2018 - Feasibility Study

Contents

List of Tables

List of Figures

1 Introduction

Following the intense rainstorm during the early morning of 21 May 2016, a total of 34 natural terrain landslides occurred in the vicinity of Sai Kung Sai Wan Road, Sai Kung East Country Park (Figure 1.1). This report presents the findings of the landslide investigation on one of these landslides, Incident No. 2016/05/1823 (thereafter referred to as 'the landslide'), which was the largest of the 34 landslides, with a source volume of about 2,100 m^3, occurring on a natural hillside above Sai Kung Sai Wan Road, about 600 m west of Sai Wan Pavilion (Figures 1.1 and 1.2). The debris resulted in complete blockage of Sai Kung Sai Wan Road (Figure 1.3) which is a country park road with restricted vehicular access. The fill slope (Slope No. 8SE-A/F34) supporting Sai Kung Sai Wan Road was severely eroded, undermining the road and resulting in road closure for several months (Figures 1.4 and 1.5). No casualties were reported as a result of the landslide.

Following the incident, AECOM Asia Company Limited (AECOM) carried out a detailed study for the Geotechnical Engineering Office (GEO) of the Civil Engineering and Development Department (CEDD), under Agreement No. CE 46/2015 (GE).

The key objectives of the study were to document the facts about the landslide, present relevant background information and establish the probable causes of the landslide. Recommendations for follow-up actions are reported separately.

This report presents the findings of the detailed landslide study, which comprised the following key tasks:

(a) review of all known relevant documents relating to the study area,

(b) aerial photograph interpretation (API),

(c) topographical surveys, detailed field observations and measurements,

(d) ground investigation,

(e) analysis of rainfall records,

(f) engineering analyses, and

(g) diagnosis of the probable causes of the landslide.

2 The Site

2.1 Site Description

The landslide is located on a southeast-facing natural hillside defined by an extensive broad catchment (thereafter referred to as the 'study area') approximately 450 m wide and 650 m long with a plan area of about 19.2 hectares (Figure 1.1). The top of the study area is at

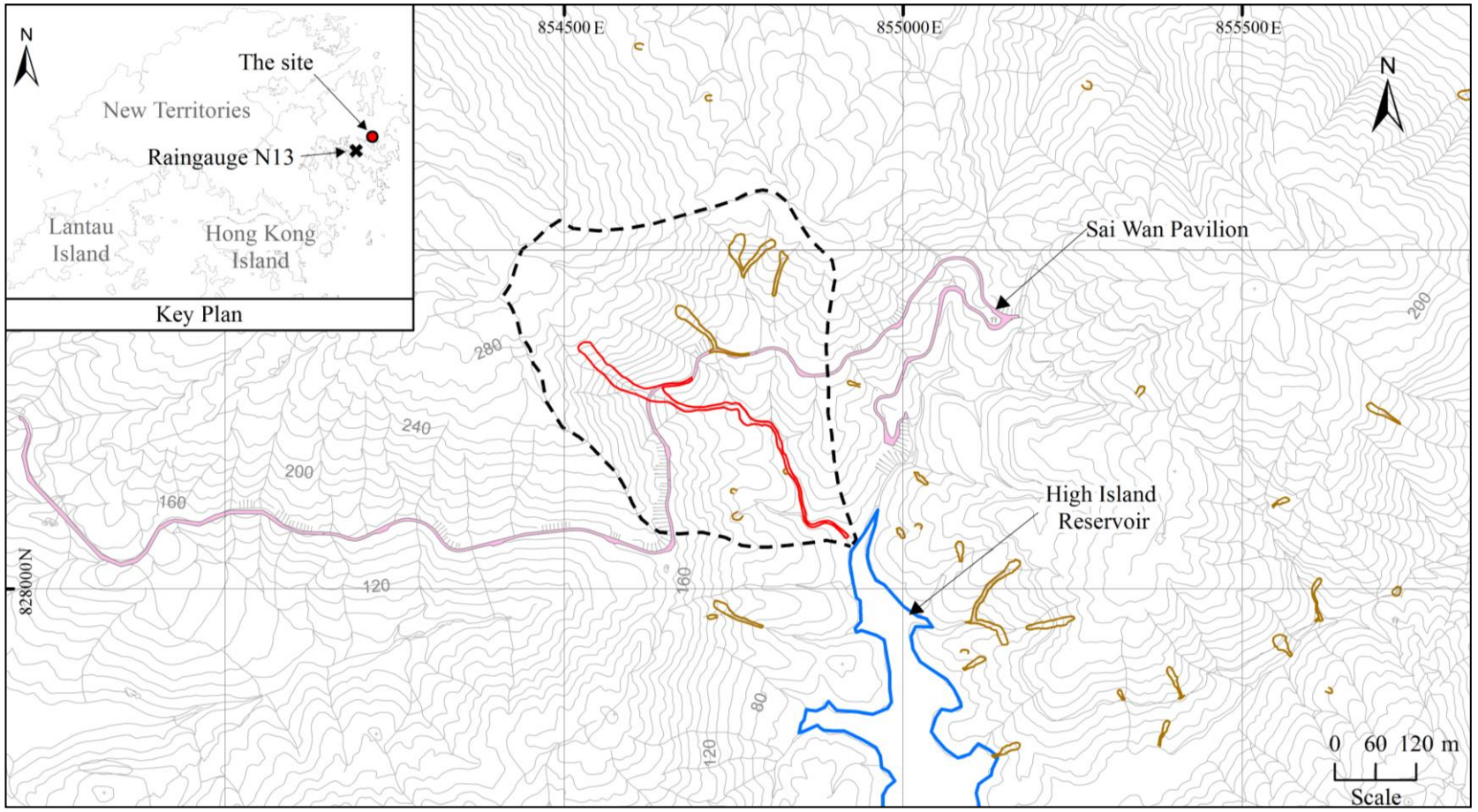

Legend:

The landslide — Study area — Other 21 May 2016 landslides — Sai Kung Sai Wan Road

Note: Based plan is extracted from 1:20000 survey sheet No. 8 dated March 2016.

Figure 1.1 Location Plan

Figure 1.2 General View of the Study Area Showing the Landslide (Photograph taken on 30 May 2016)

Figure 1.3 View of the Debris Deposited on Sai Kung Sai Wan Road Resulting in Complete Road Blockage (Photograph taken on 21 May 2016 by GEO Emergency Duty Officer)

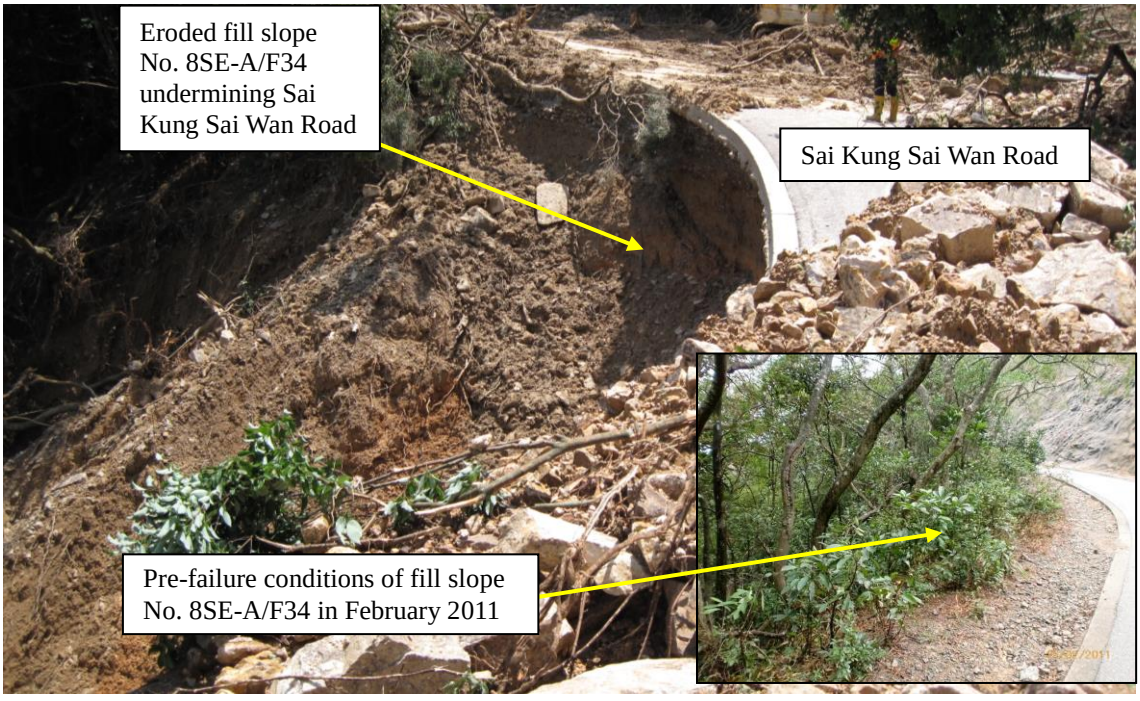

Figure 1.4 View of Slope No. 8SE-A/F34 (Photograph taken on 22 May 2016)

Figure 1.5 View of the Source Area and Upper Debris Trail of the Landslide (Photograph taken on 30 May 2016)

an elevation of about 300 mPD, and the toe of the study area, at High Island Reservoir, is at an elevation of about 60 mPD. Sai Kung Sai Wan Road traverses the middle of the study area and is at an elevation of about 150 mPD. The landslide crown is located about 100 m above Sai Kung Sai Wan Road at an elevation of about 250 mPD (Figures 2.1 and 2.2).

The hillside adjacent to the source area is generally densely vegetated with tall shrubs and mature trees and is inclined at an angle of about 35° to 45° (Figure 1.5). Locally, rock outcrops in linear bands cross the study area and this is typically characterised by an increase in local slope angle and decrease in vegetation.

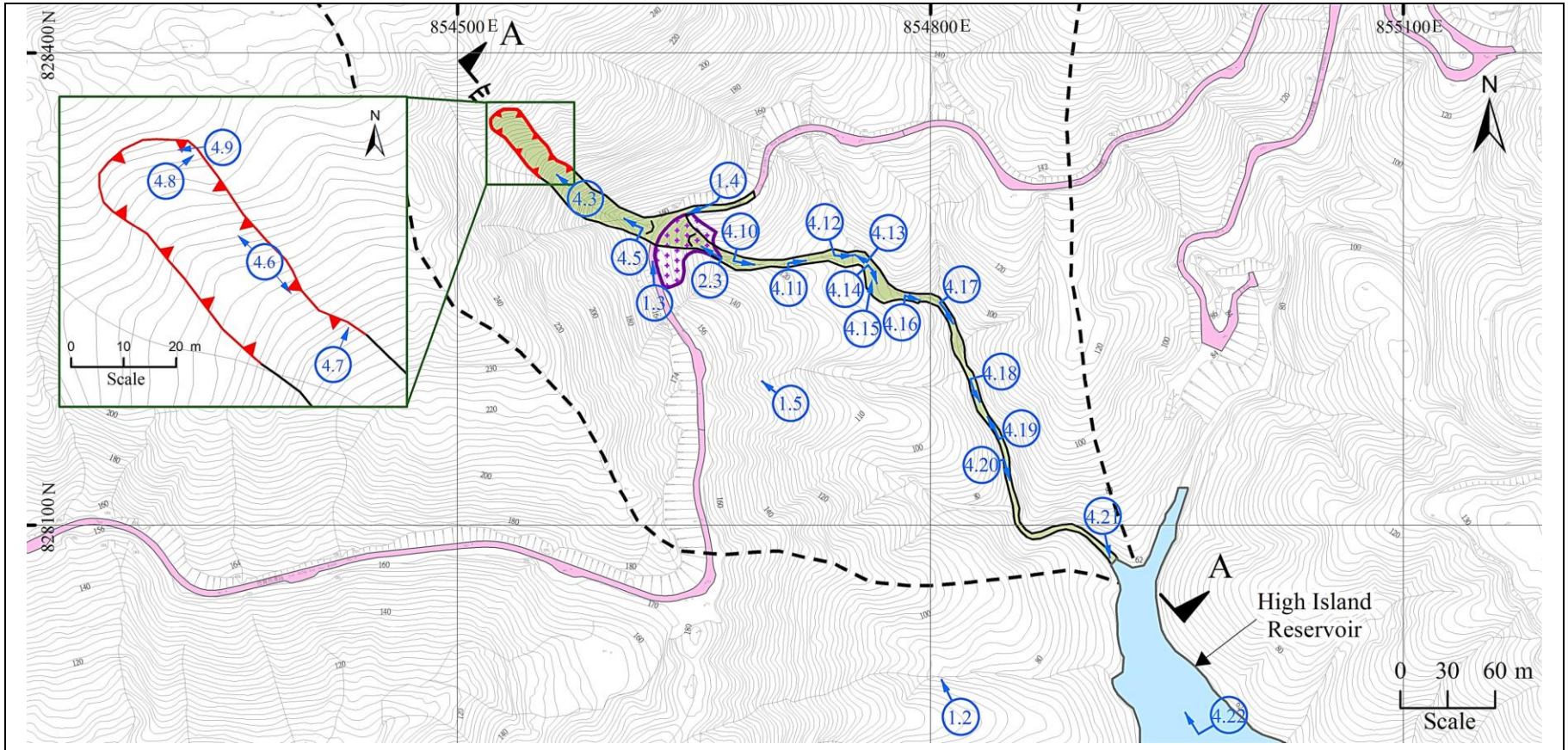

Legend:

The landslide main scarp — Study area — Vertical 'Step' — Sai Kung Sai Wan Road

The landslide — Culvert — Fill slope No. 8SE-A/F34 — (1.2) Location and direction of photograph as shown in Figure 1.2

Notes: (1) Base plan is extracted from 1:1000 survey sheet Nos. 8SE-7A, 8SE-7B, 8SE-7C and 8SE-7D dated March 2016.

(2) Refer to Figure 5.2 for location and direction of photograph as shown in Figure 5.4.

Figure 2.1 Site Layout Plan

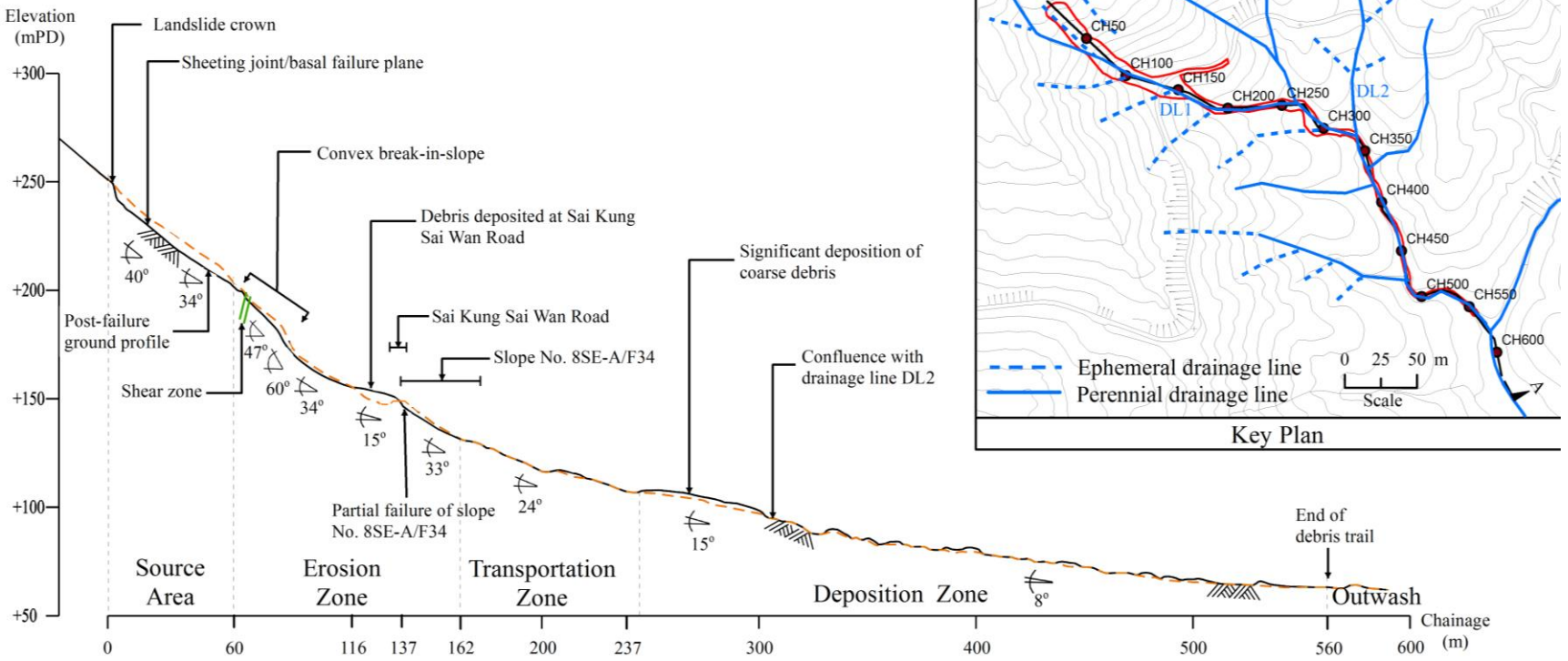

2100	210	20	250	40	30	17	Erosion (m^3)
10	80	460	200	90	510	875	Deposition (m^3)
2090	2220	1780	1830	1780	1300	442	Mass Balance (m^3)

Legend:

- - - - Pre-failure ground profile

Note: See Figures 4.1 and 4.2 for geological details.

Figure 2.2 Longitudinal Section A-A

The study area contains several perennial and ephemeral drainage lines which drain down to the northern part of High Island Reservoir (Figure 2.2). The landslide scar intersects one perennial drainage line (DL1) just below the source area and another minor ephemeral drainage line is located along the west flank of the source area. A culvert carries the drainage water below Sai Kung Sai Wan Road, through fill slope (Slope No. 8SE-A/F34), and discharges into the confined natural drainage line below (Figures 2.1 and 2.3).

2.2 Regional Geology

According to the Hong Kong Geological Survey (HKGS) 1:20 000 scale Solid and Superficial Geology Map Sheet No. 8 - Sai Kung (GCO, 1989), the study area is mostly underlain by volcanic rocks of the High Island Formation (Figure 2.4). These rocks, as described on the map sheet, comprise undivided fine ash tuff. The fine ash tuff is underlain by undivided trachydacite and rhyolite lava of the Clear Water Bay Formation which is indicated outcropping across the lower portion of the study area. The geological map also indicates the presence of extensive Pleistocene and Holocene debris flow deposits within the High Island Reservoir area. Flow fabric in the volcanic rocks is shown to dip east at about 20°. No faults are shown in close proximity to the source area, although a north trending cross-fault is shown about 250 m east of the source area, intersecting the debris trail at about Chainage 300. The HKGS 1:100 000 scale Pre-Quaternary Geology of Hong Kong

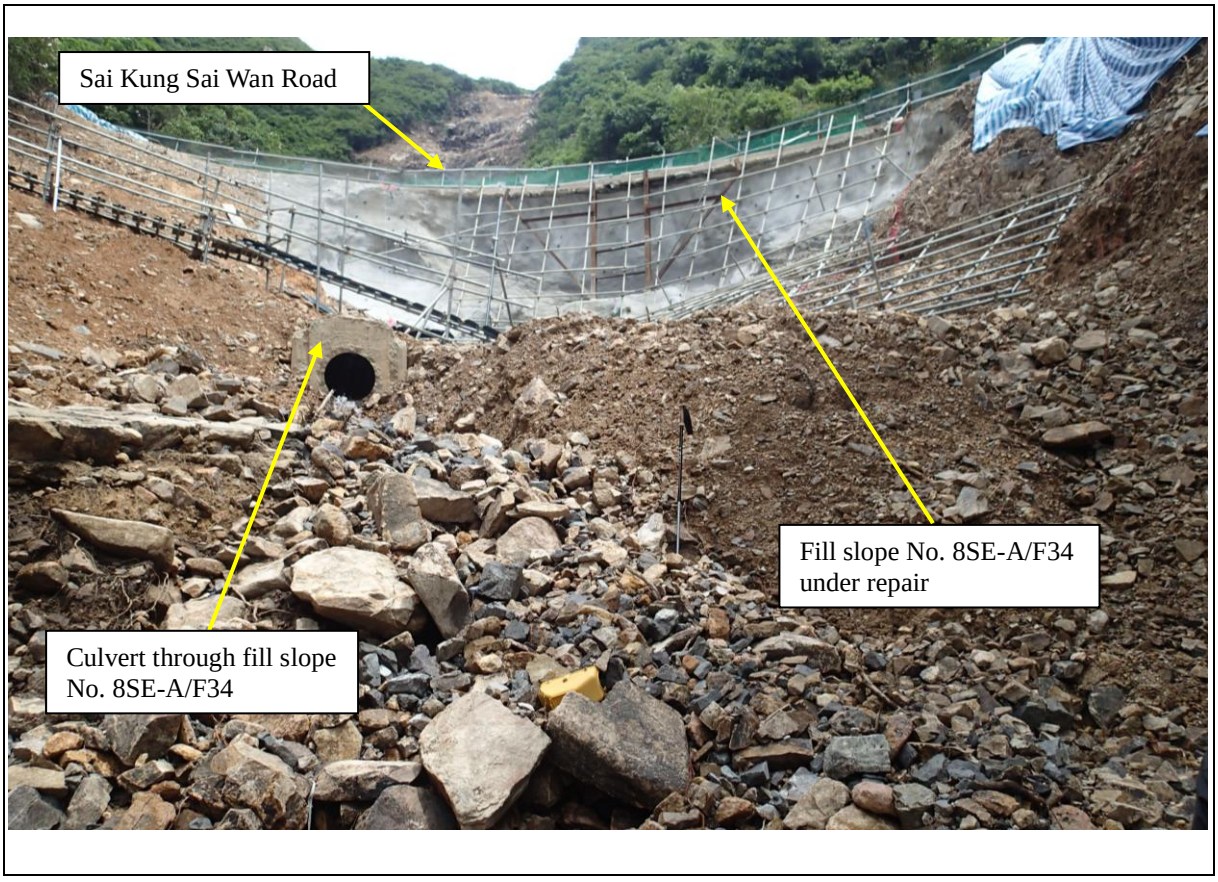

Figure 2.3 View Upslope from CH136 to CH165 (Photograph taken on 14 June 2016)

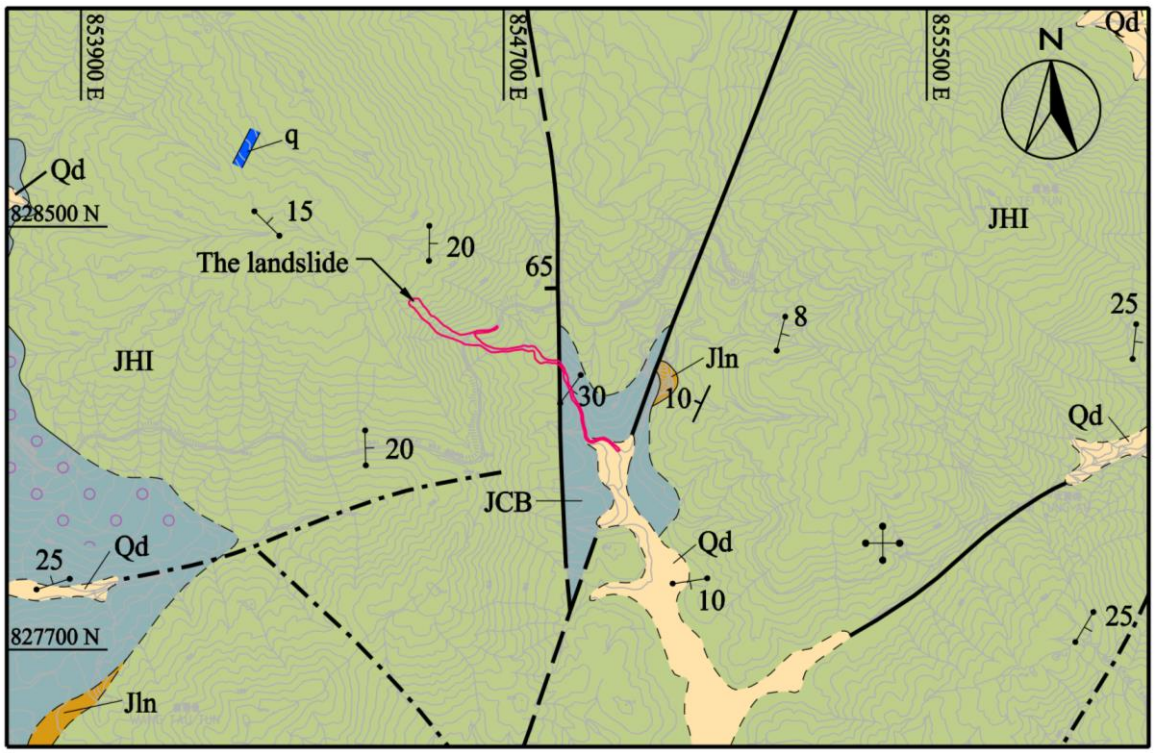

Legend:

0 100 200 m
Scale

Superfical deposits

Qd — Debris flow deposits — Unsorted sand, gravel, cobbles and boulders; clay/silt matrix

Soild geology

JHI — Undivided, mainly fine ash tuff

JCB — Undivided, mainly trachydacite and rhyolite lava

Jln — Tuffite and tuff

q — Quartz vein

Autobrecciated

Geological lines

Photogeological lineament

Fault

Geological boundary, superficial deposits

Structural symbols

20 — Bedding

20 — Inclined flow fabric

Horizontal flow fabric

Note: Extracted from Hong Kong Geolgical Survey, Map Series HGM 20, Sheet 8. 1:20000 scale (GCO, 1989).

Figure 2.4 Regional Geology

(Sewell et al, 2000) also indicates that volcanic rocks (Kkh) of High Island Formation underlie the study area. These are described on the map as welded fine ash vitric tuff with minor tuff breccia and tuffaceous sandstone.

3 Site History and Past Instabilities

3.1 General

The site history has been determined from an interpretation of the available aerial photographs, together with a review of relevant documentary information (Figure 3.1). Detailed observations from the aerial photograph interpretation (API) are summarised in Appendix A, with the salient observations given below.

3.2 Site History

The study area is located in a remote natural terrain catchment of Sai Kung East Country Park. Consequently, the main anthropogenic activity observed in the vicinity is the construction of Sai Kung Sai Wan Road and associated slope formation, traversing across the mid-slope of the study area, which was largely completed in 1974. This was probably related to the construction of High Island Reservoir downslope of the study area in the 1970s.

3.3 Past Instabilities

3.3.1 Enhanced Natural Terrain Landslide Inventory (ENTLI)

The ENTLI database records 31 relict and three recent landslides within the study area (Figure 3.1). One of the 31 relict landslides (Tag No. 8SEA0034E) has its crown located immediately above the source area of the landslide (Figure 3.1). This relict landslide was likely identified based on the geomorphological depression observed in API under this study. The relict landslide has been assigned 'Class C1' under the ENTLI classification system, which defines it as a poorly defined feature with broad rounded morphology and likely a relatively old feature. The remaining relict landslides are predominately located at the head of drainage lines and along the over-steepened flanks of incised drainage lines.

Three recent landslides (Tag Nos. 8SEA0589E, 8SEA0623E and 8SEA0626E) occurred at the lower portion of the study area (the nearest one is about 300 m from the source area) and have runout distances of approximately 10 m to 50 m.

3.3.2 Large Landslide Database

According to the GEO's Large Landslide Database (Scott Wilson, 1999), there are no observed or reported landslides within the study area.

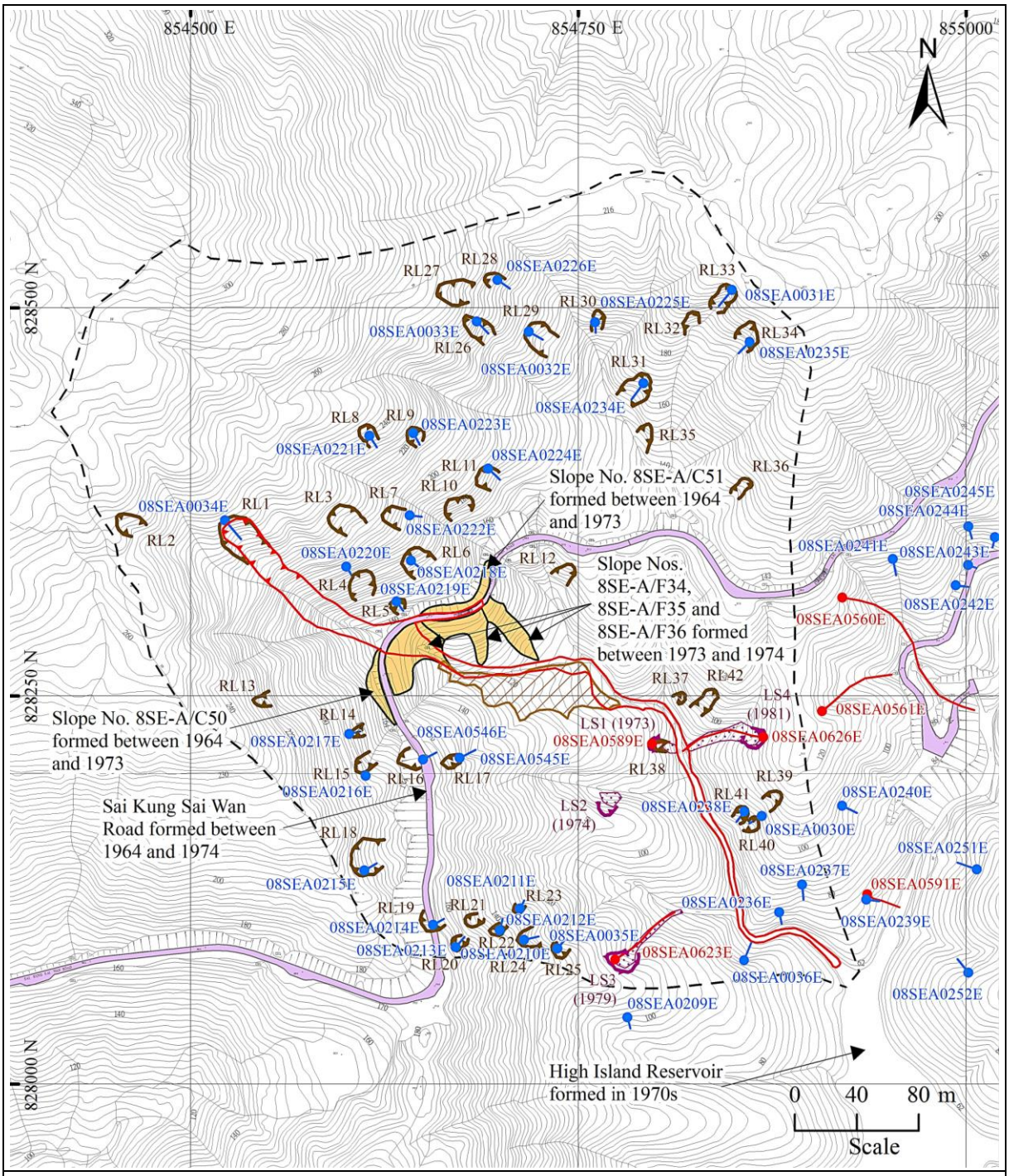

Figure 3.1 Site History and Past Instabilities

3.3.3 GEO's Database of Reported Landslides

According to the GEO's landslide database, there are no recorded landslides within the study area.

3.3.4 Historical Landslide Catchments

Although there are some historical landslides recorded within the study area, there are no existing Historical Landslide Catchments (HLCs) identified, as the only affected facility is Sai Kung Sai Wan Road which is not a high consequence facility. The nearest HLC are Nos. 8SE-A/DF1, 8SE-A/OH1 and 8SE-A/OH2, located about 1,500 m to the northeast of the study area.

3.3.5 Aerial Photograph Interpretation

The high-resolution 1963 photographs clearly show the geomorphology of the study area and following review of these photographs, some additional relict and recent landslides have been identified with reference to the ENTLI database. In total, the study area contains 42 relict landslides (RL1 to RL42), which are mainly concentrated on the mid-slope area (Figure 3.1). Relict landslide RL1, identified under the ENTLI as Tag No. 8SEA0034E, is located within a rounded, degraded depression, as evident in the Digital Terrain Model (Figure 3.2) composed from pre-failure LiDAR survey data, and which appears to be in the same location as the source area. The depression is approximately 23 m wide by 30 m long, and with a depth of about 2 m estimated from pre- and post-failure topographic contours, API and field observations. This gives a source volume of approximately 720 m^3, based on an ellipsoidal landslide shape (IAEG Commission on Landslides, 1990). A thin strip of rock outcrop (about 4 m wide) is observed adjacent to the west flank of landslide RL1 and an ephemeral drainage line is apparent at the same location, draining approximately southeast (Figure 3.3). Rock outcrop is also observed in perennial drainage line DL1, between the source area of the landslide and Sai Kung Sai Wan Road, and a narrow band of rock outcrop extends eastwards from the toe of the source area, traversing across the hillside at a similar elevation. To the west of the source area, intermittent rock outcrop is observed, some with apparent planar joint surfaces dipping downslope.

Below Sai Kung Sai Wan Road, hummocky hillside morphology indicates the presence of a distinct lobe of probable colluvial deposits (Figure 3.1) along the debris trail, about 170 m downslope of the landslide crown. The other relict landslides could be seen as shallow depressions covered with thin vegetation, typically on steep valley flanks, and with estimated source volumes ranging from 15 m^3 to 260 m^3. Four recent landslides, LS1 to LS4 occurring between 1973 and 1981, are visible within the lower portion of the study area with debris probably entering the main drainage line from LS1 and LS4.

No signs of distress were apparent in the hillside prior to the 21 May 2016 failure, and there were no significant observable past instabilities in the study area since 1981, since when there has been a general increase in vegetation density.

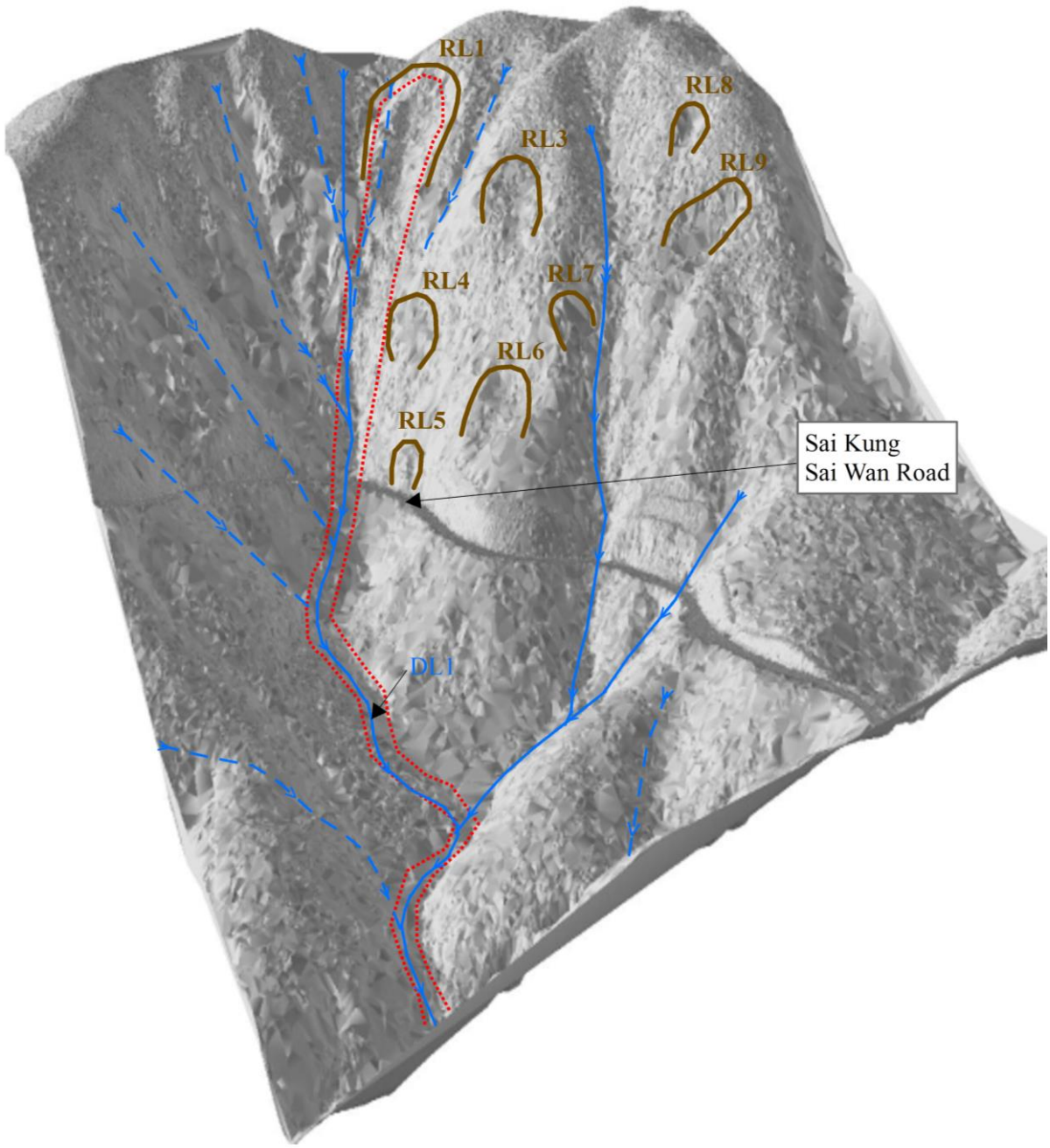

Legend:

	The landslide		Perennial drainage line
RL1	Relict landslide		Ephemeral drainage line

Note: 3D Digital Terrain Model composed with 2010 LiDAR survey data and overlayed with 1963 aerial photograph.

Figure 3.2 Digital Terrain Model

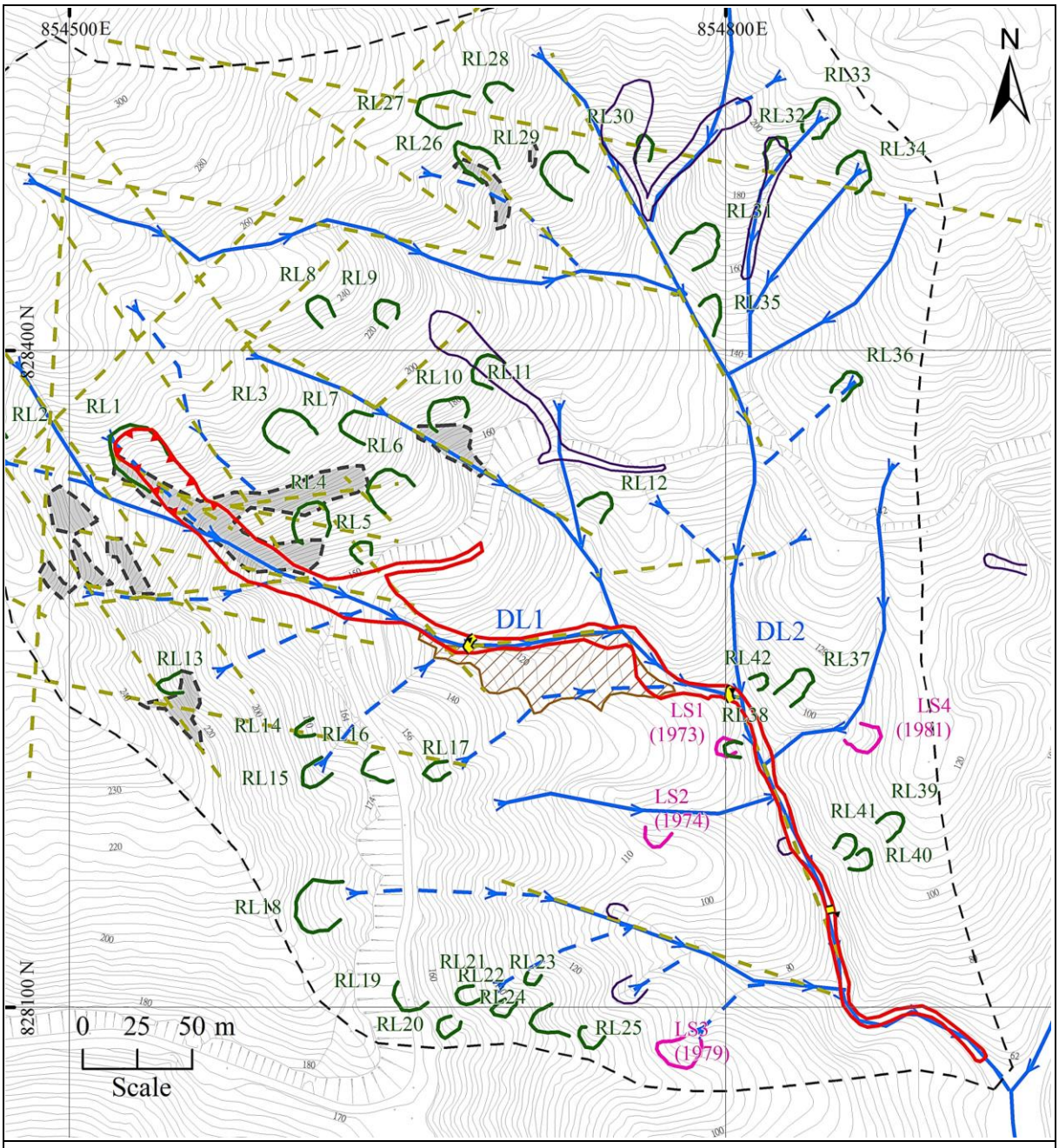

Legend:

- The landslide
- Other 21 May 2016 landslides
- Study area
- Perennial drainage line
- Ephemeral drainage line
- Photolineament
- LS1 (Year) — Recent landslide from API
- RL1 — Relict landslide from API
- Lobe of relict colluvial deposits
- Rock outcrop
- 'Step' in topography

Note: Base plan is extracted from 1:1000 survey sheet Nos. 8SE-7A, 8SE-7B, 8SE-7C and 8SE-7D dated March 2016.

Figure 3.3 Geomorphological Setting

4 Description of the Landslide and Post-failure Observations

4.1 General

The exact time of failure of the landslide is not known as there were no eyewitnesses to the event, which occurred in a remote country park area. However, it was first reported by the Fire Services Department (FSD) at about 8:30 a.m. on 21 May 2016.

The landslide was a structurally controlled, translational rock slide with a detached source volume of about 2,100 m^3 and subsequently entrained about 570 m^3 within the debris trail. The source area was located approximately 100 m above Sai Kung Sai Wan Road (Figures 1.5 and 2.1), below which the debris entered perennial drainage line DL1 where the debris became confined and channelized before coming to rest, giving a total travel distance of about 500 m.

The following sections present a description of the source area and the debris trail.

4.2 Site Observations

The landslide was initially inspected by AECOM on 21 May 2016, however, due to difficulties in accessing the upper part of the landslide, the source area was not inspected until 31 May 2016. Subsequently, several field inspections were carried out over the next few months. During this exercise, evidence of dominant landslide processes was looked for. The processes comprised erosion, where existing material within the debris trail has been incorporated into the landslide debris by entrainment; deposition, where landslide debris is deposited; and transportation, where the debris is transported over the substrate with little erosion or deposition. In many cases both erosion and deposition processes could be observed although only the dominant process was recorded on the debris mass balance summary (Table 4.1).

As the landslide is predominantly a rock slide in columnar jointed tuff, a large proportion of the observed debris was coarse clastic material comprising boulder-sized, joint-defined rock blocks, and fragmented rock blocks observed as gravel- and cobble-sized clasts. On the periphery of the debris trail, typically higher up on the flanks, remoulded debris could be observed comprising a mixture of clastic debris within a fine sandy silt matrix. This material was considered evidence of debris flow processes and the last observation of this material was considered as the end of the landslide deposition at about Chainage 560. Some intermittent debris lobes of mainly sand, gravel- and cobble-sized rock fragments could be seen along the remaining drainage line until the reservoir is reached. However, this material is considered outwash material as the drainage line catchment is large with many tributaries, and it is likely that significant post-failure washing and movement of debris has occurred.

A longitudinal section of the landslide is shown in Figure 2.2, associated 1:1 000 scale landslide mapping plans are shown in Appendix B, and a summary of the debris mass balance along the debris trail is shown in Table 4.1. A plan and sections through the source area are shown in Figures 4.1 and 4.2 respectively.

Table 4.1 Mass Balance of Debris during the Landslide

Chainage (m)	Average Slope Gradient (°)	Trail Width/ Depth (m)	Channel Width/ Depth (m)	Erosion (m^3) & MT (substrate)	Post-Landslide erosion by water (m^3) & MT	Deposition (m^3) & MT	Active Volume (m^3)	Max. Clast Diameter (m)	Fines (%)
Toe of Rupture at CH60						MT = Material Type			
0-60	37	Source Area		2100 MT1,2,3	0	10 MT5	2090	2	35
60-80	47	18/1.5	15-16/ 1.5	100 MT1,3	442 MT5,6 (CH0 to CH560)	15 MT5	2175	0.8	60
80-86	60	21/0.5	16-17/ 0.5	10 MT1,3		35 MT5	2150	0.5	60
86-116	34	15/1.5	9-12/1.5	100 MT1,3		30 MT5	2220	0.8	60
116-137	15	11.5-20/2-4.5	9-15/1.5	20 MT1,3		460 MT5,6	1780	1.5	25
137-162	33	10-26/ 2-4	7-15/1	250 MT9		200 MT5,6	1830	0.7	50
162-180	24	6.5/1.5	5-7/1.5	15 MT1		35 MT5,6	1810	0.7	50
180-237		5/1.5	3-7/1.5	25 MT1		55 MT5,6	1780	1	40
237-300	15	7-13/2	4-8/2	30 MT1		510 MT6	1300	1.5	20
300-335	21	5/1.5	3.5-4.5/ 1.5	5 MT1		95 MT5,6	1210	1	60
335-397	10	3-6/1	2-5/1	5 MT1		225 MT5,6	990	0.8	50
397-450		3.5-5/ 0.7	2-5/0.7	1 MT1		135 MT6	856	0.7	20
450-470	9	2.5-3.5/1.5	2-5/1.5	1 MT1		105 MT6	752	0.7	20
470-485	8	4.5/1	3-4.5/1	0		90 MT6	662	1	30
485-500		3/1	3/1	5 MT1		80 MT5,6	587	1	50
500-535	5	5/1	3-4/1	0		75 MT5,6	512	0.5	60
535-560		5/0.8	3-5/0.7	0		70 MT5,6	442	1	30

Notes:
(1) Mass Balance is negative 442 m^3. This was probably related to the debris derived by washing out of finer.
(2) For descriptions of substrate materials (MT1 to MT4), deposition materials (MT5 and MT6) and erosion material (MT9), please refer to Appendix B.
(3) From Chainage CH60 to CH86, the hillside is an open hillslope catchment and the channel width presented in the above table is the topography width.

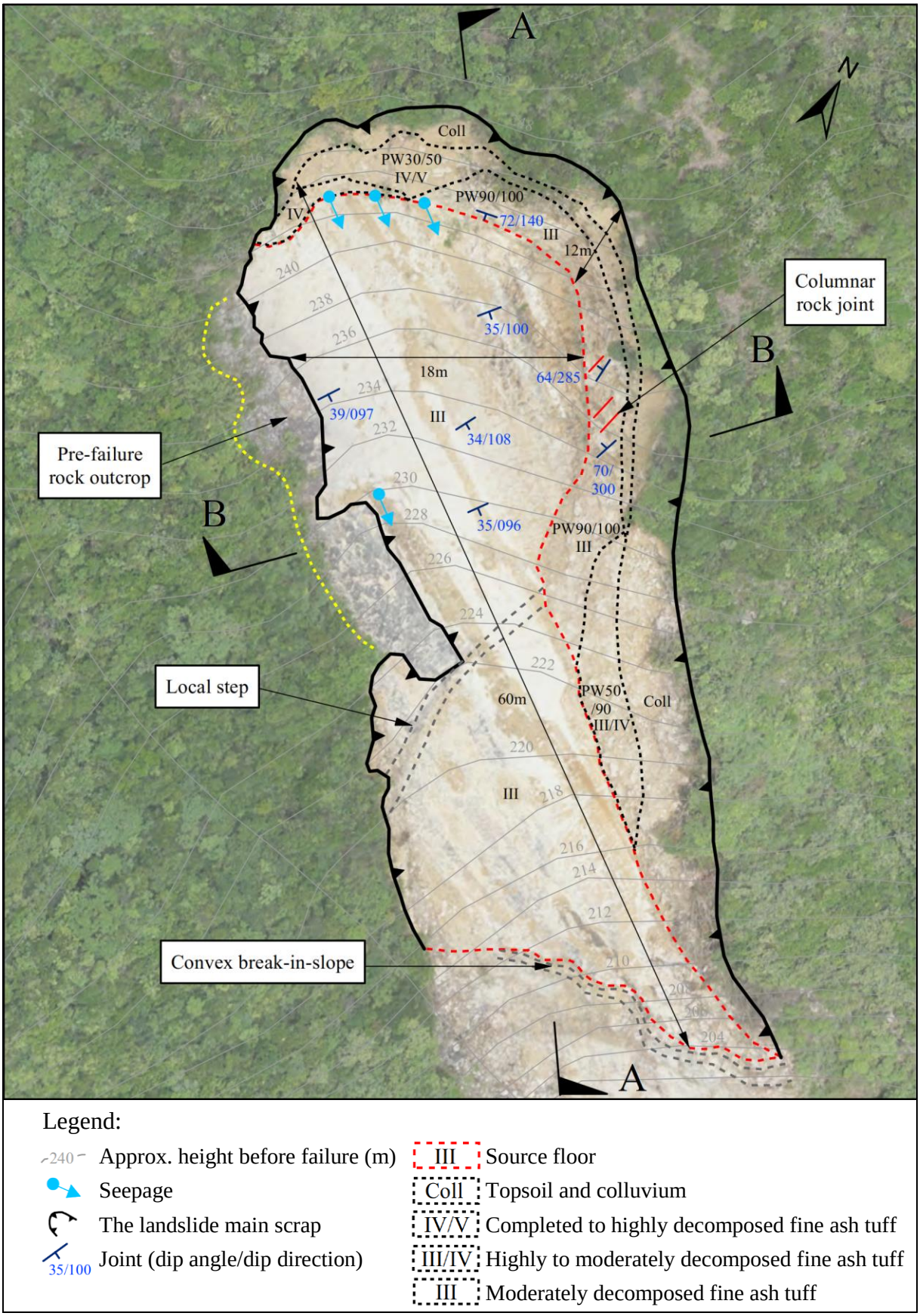

Figure 4.1 Plan of the Source Area

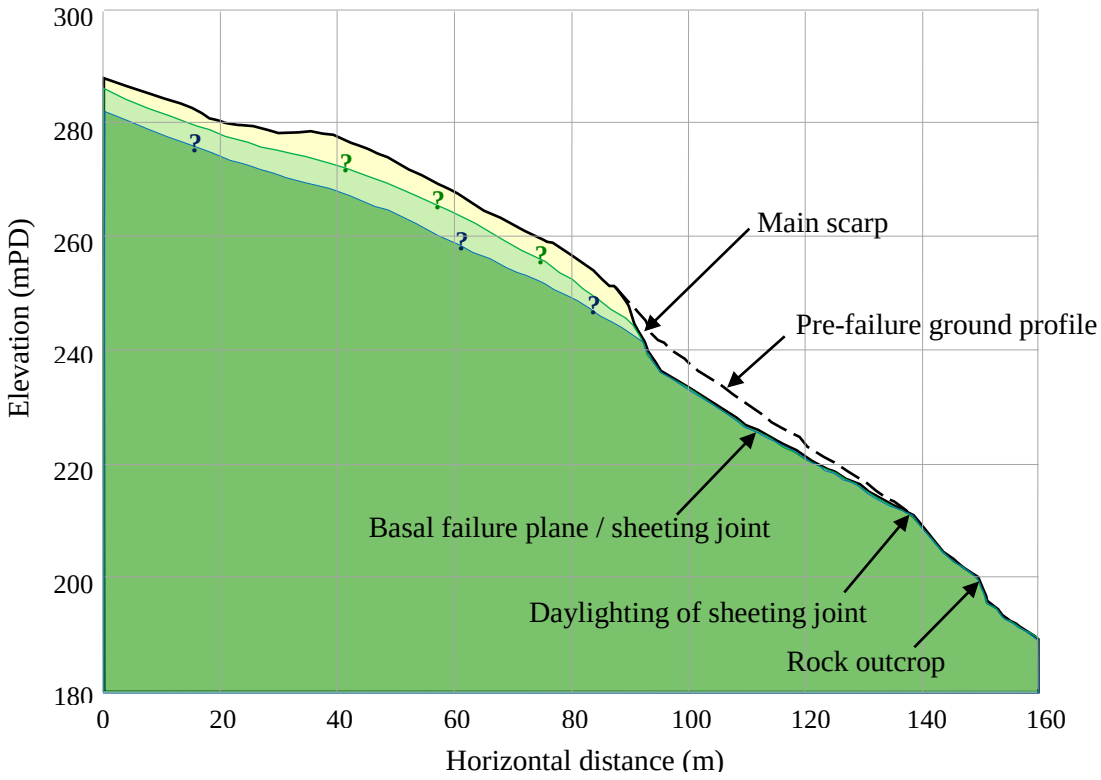

(a) Longitudinal Section through the Source Area, Section A-A

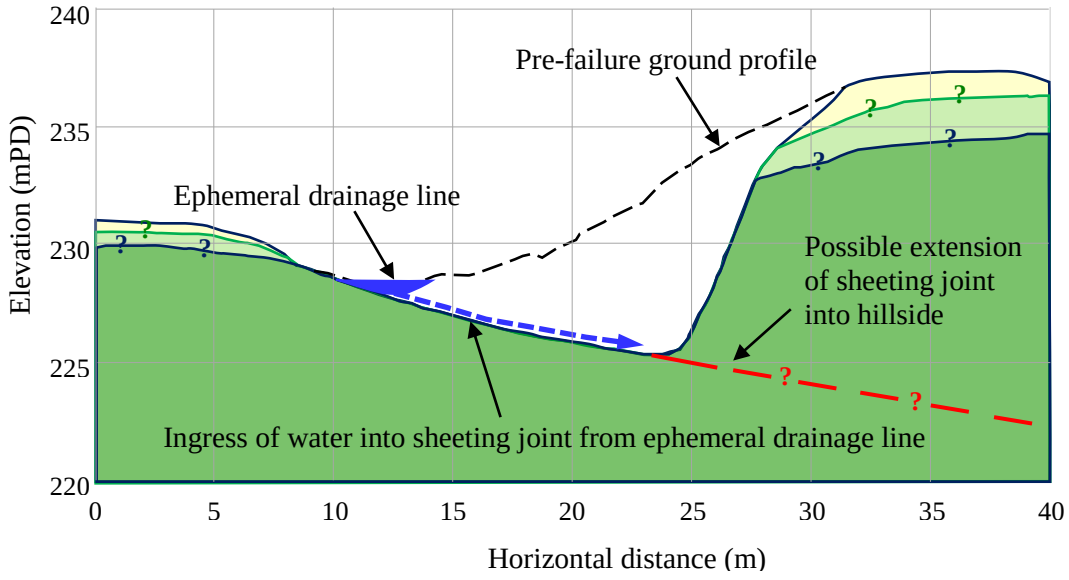

(b) Transverse Section through the Source Area, Section B-B

Legend:

Colluvium | Grade IV/V Tuff | Grade III Tuff

Note: Refer to Figure 4.1 for location of the sections.

Figure 4.2 Sections through the Source Area

4.3 Source Area (Chainage 0 to 60)

The landslide was a structurally controlled, translational rock slide with a distinctive, planar, basal failure surface (Figure 4.3). The crown of the source area is located at about 250 mPD and the dimensions of the source area are 18 m in width, 60 m in length and 12 m maximum in depth. A plan of the source area is shown in Figure 4.1 and longitudinal and transverse sections are shown in Figure 4.2. The total volume of detached material from the source is estimated at about 2,100 m^3 based on field measurements and comparison between pre-failure LiDAR survey data and post-failure photogrammetric topographic survey data obtained by unmanned aerial vehicle (UAV). Images of the actual source area topography and estimated detached material thickness are shown in Figure 4.4.

The source floor is formed from a persistent, planar sheeting joint (providing a basal failure plane) inclined at approximately 34° to 40°, and with an easterly dip direction (average 100°) such that the source floor dips across the source area as well as downslope giving an asymmetric morphology in transverse section, and with the sheeting joint probably extending into the adjacent hillside (Figures 4.2 and 4.5). This asymmetry gives the source area a wedge failure-type geometry with a steep (70°) scarp at the east flank up to 12 m in height, but with no scarp at all on the west flank of the source area. The exposed sheeting joint forming the source floor comprises moderately decomposed tuff with a distinctive polygonal joint pattern observed on the surface (Figure 4.6), where the columnar jointing in the tuff has been truncated. No infilling was observed on the joint surface, although thin iron and manganese oxide coating was observed locally. Elsewhere the tuff has typically weathered to an off-white colour. Distinctive striations were locally observed with a trend of approximately 140° (Figure 4.6) which is parallel to the direction of landslide movement but not the dip direction of the source floor. This suggests that the striations were formed during failure and not as part of any pre-failure incremental movement. The origin of the sheeting joint is considered to be related to stress relief.

Although the source floor is generally planar, some local, minor steps in the profile were observed (Figures 4.1 and 4.6). Near the base of the source floor, adjacent to the east flank, the dip angle of the surface reduces significantly to around 10° to 15° (Figure 4.7), and this joint orientation was observed to extend laterally eastwards into the adjacent hillside. Immediately below this area there is a convex break-in-slope which allows the sheeting joint to daylight (Figure 4.3). The break-in-slope is probably caused by local weakening of the rock mass along an E-W trending shear zone observed traversing the landslide below the source floor (Figure 4.5).

At the west flank of the source area the sheeting joint is exposed along a narrow band of rock outcrop which was the location of an ephemeral drainage line (Figures 3.3 and 4.3). The main scarp and east flank (Figure 4.8) comprise moderately decomposed tuff (up to 8 m deep), partially weathered rock mass (1 m to 2 m deep) and colluvium (2 m to 3 m deep). As a result of the significant portion of columnar jointed tuff rock that detached during failure (estimated at up to 1,200 m^3), the debris deposited downslope comprised intact joint-controlled rock blocks, smaller rock fragments that had broken up, and soil from the partially weathered rock mass and colluvium. Following failure, distinct polygonal 'columns' of tuff were partly exposed in the upper area of the east flank, typically with two joint faces (joint orientation approximately 70/300° and 64/285°) exposed over a height of up to 8 m (Figure 4.8) and

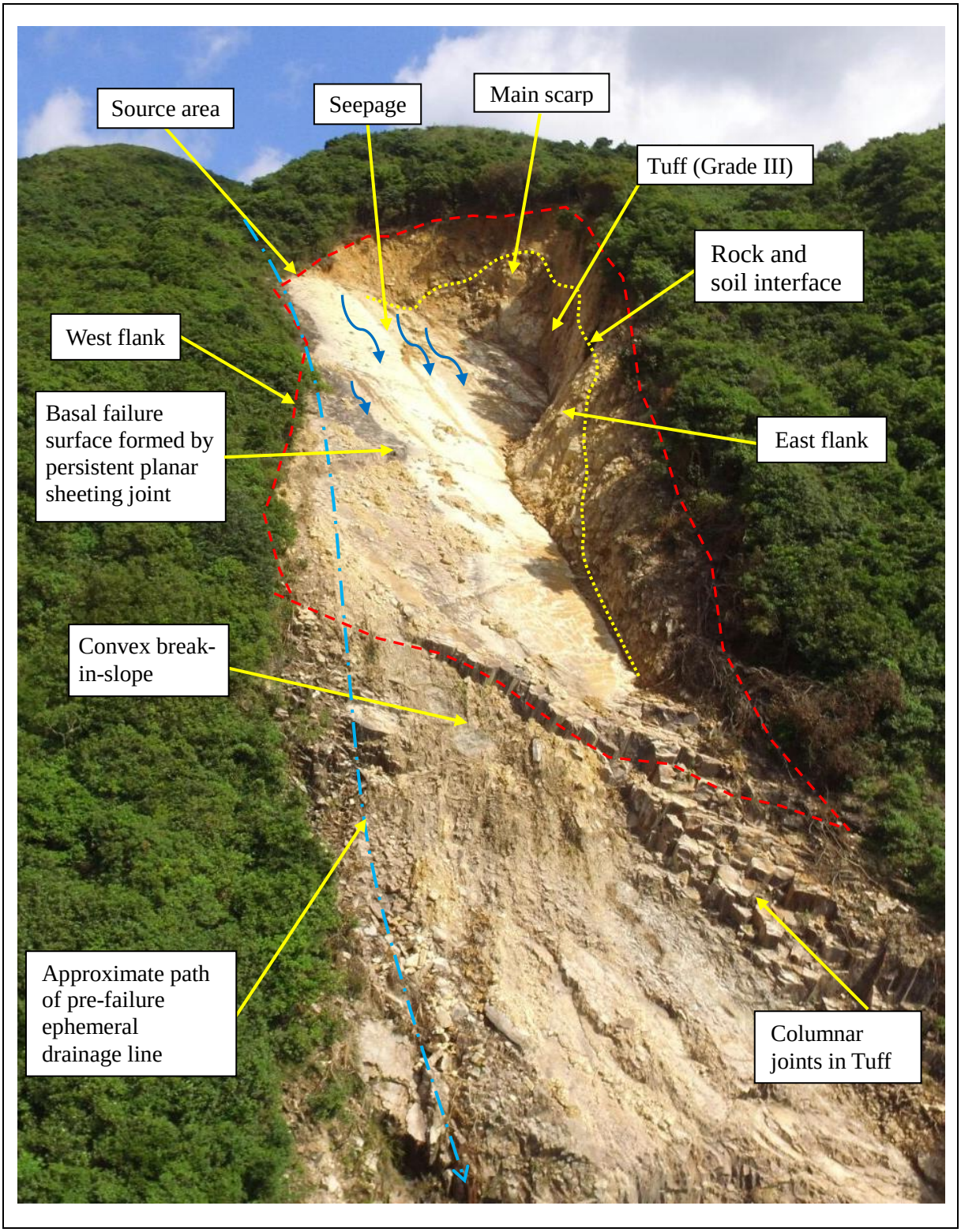

Figure 4.3 View of the Source Area and Upper Debris Trail (Photograph taken on 22 May 2016)

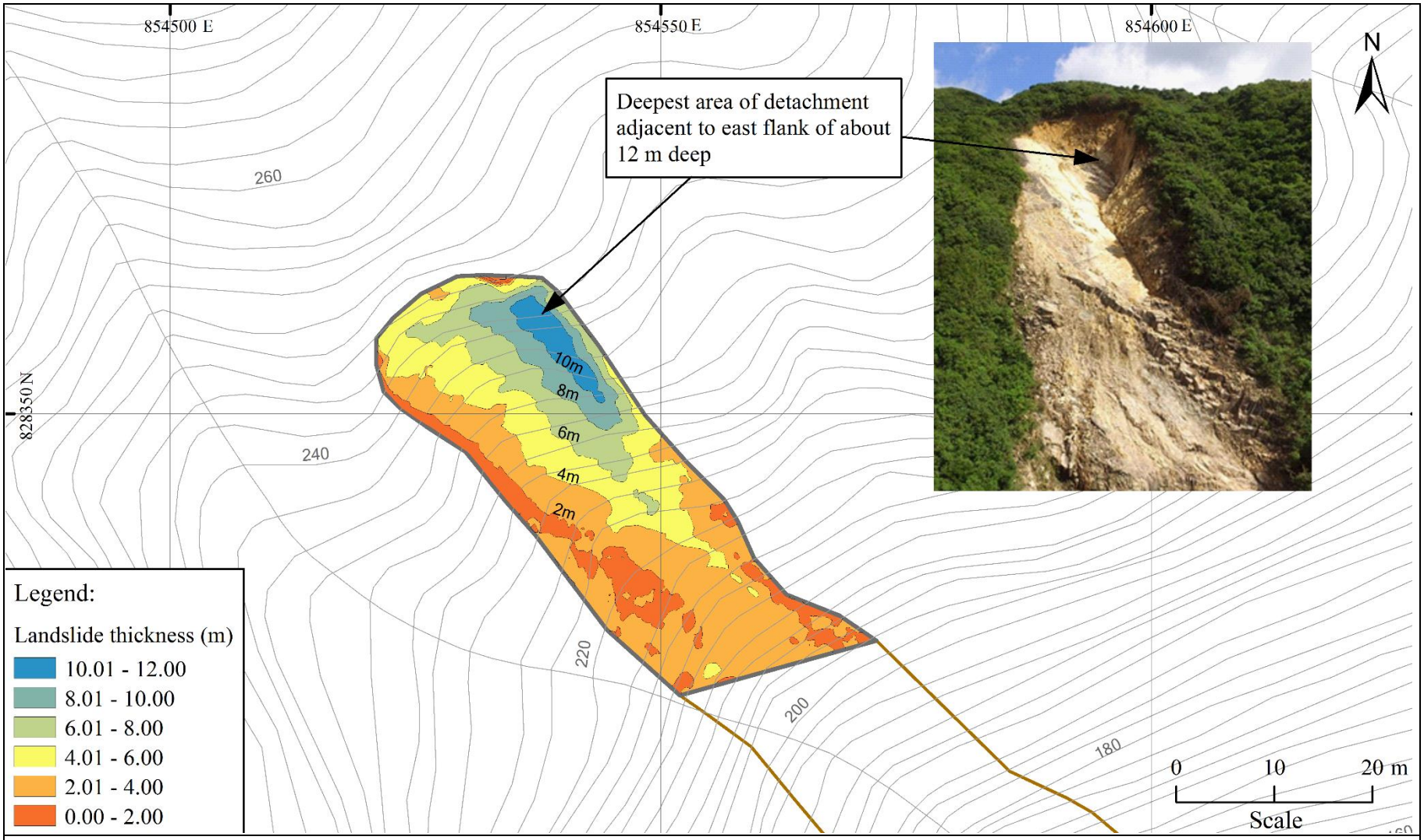

Note: Base plan is extracted from 1:1000 survey sheet No. 8SE-7A dated March 2016.

Figure 4.4 Source Volume Estimate from LiDAR and Photogrammetry

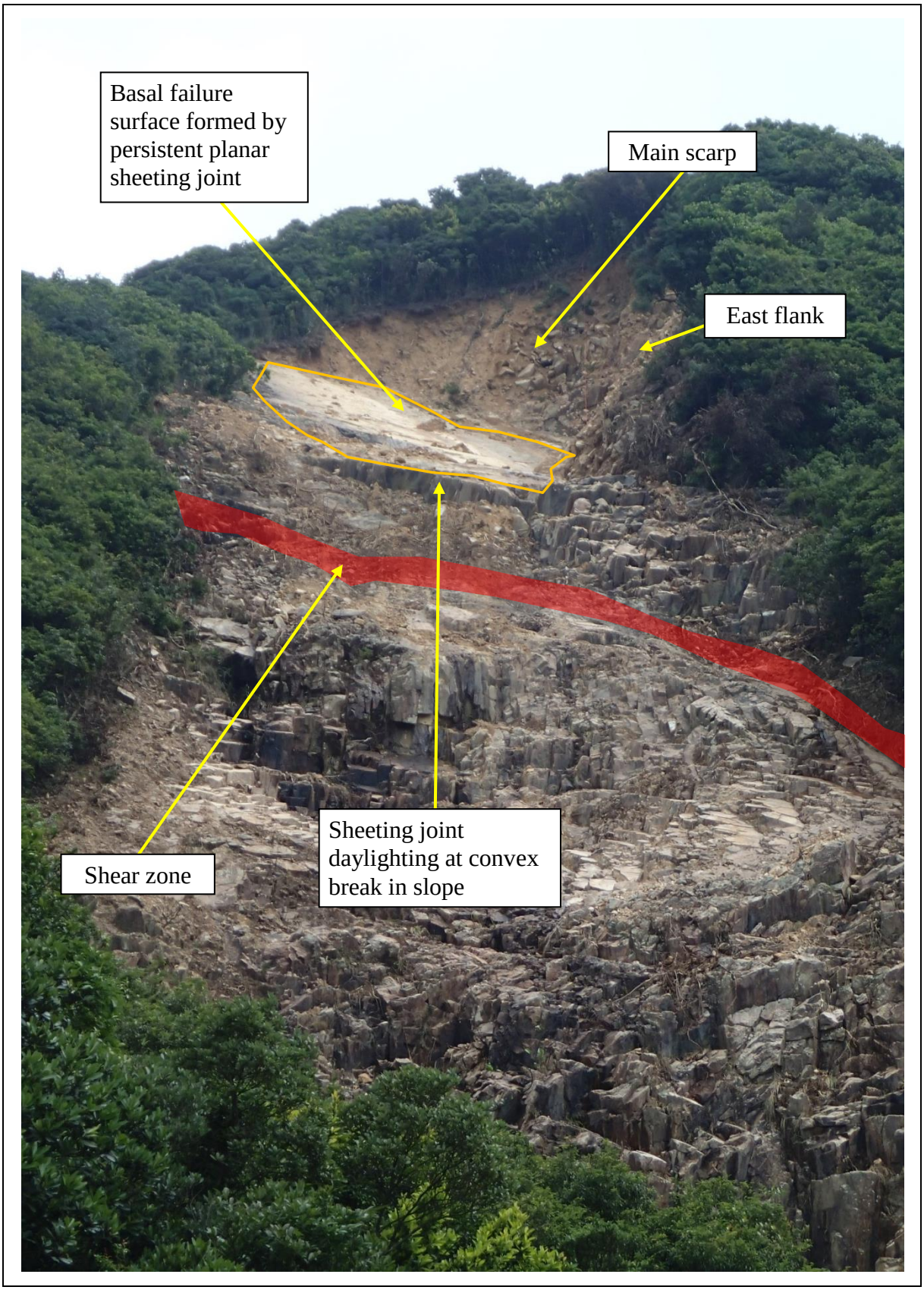

Figure 4.5 View of the Source Area and Upper Debris Trail Showing Asymmetric Source Profile (Photograph taken on 31 May 2016)

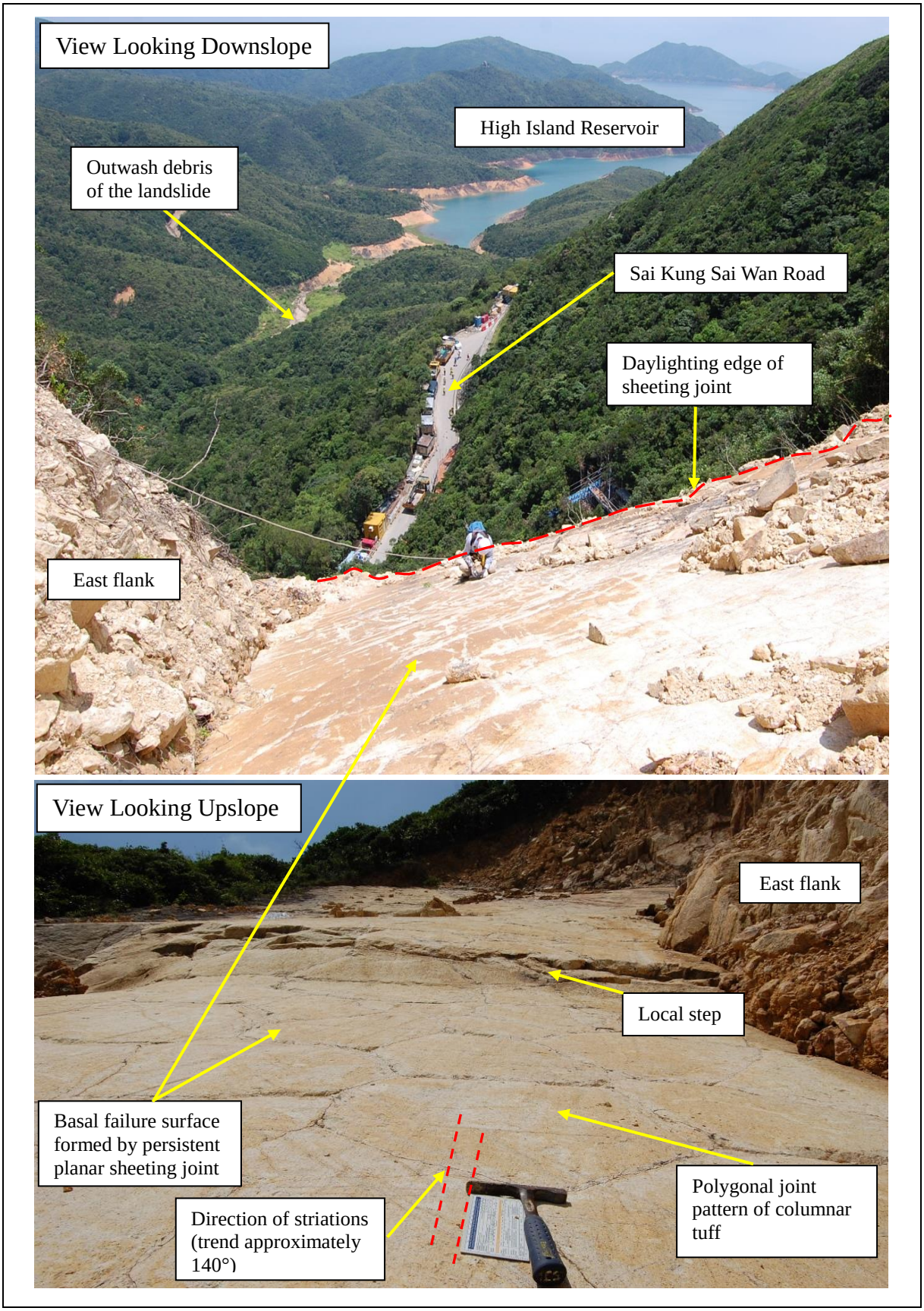

Figure 4.6 View Upslope and Downslope of the Persistent Planar Sheeting Joint Forming the Basal Surface of Rupture (Photograph taken on 26 July 2016)

Figure 4.7 View of the Base of Source Floor Showing Sharp Decrease in Dip Angle (Photograph taken on 26 July 2016)

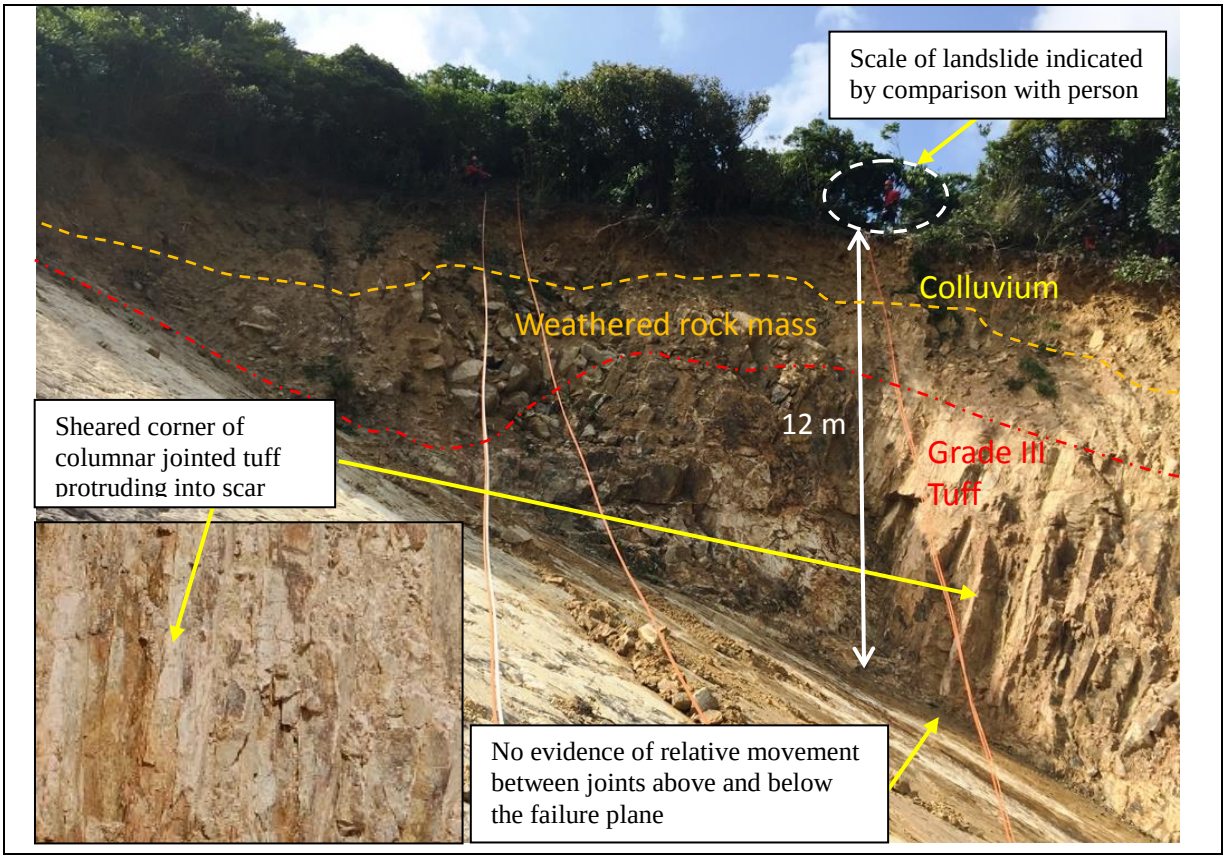

Figure 4.8 View Looking Northeast of the Source Floor, Main Scarp and Upper Part of East Flank Showing Geological Profile (Photograph taken on 31 May 2016)

forming sub-vertical corners where the joint faces intersect, protruding out from the east flank. Thus, with adjacent columns the surface profile along portions of the east flank is very irregular with a saw-tooth profile where the corners are intact. Locally, some exposed corners of the columnar jointed tuff were observed to have been crushed or sheared (Figure 4.8), indicating some shearing of intact rock asperities may have taken place to allow failure to occur (see Section 8).

The columns of tuff have a toppling orientation (inclined approximately 70° into the slope) and evidence of minor dilation of sub-vertical joints was observed, however, as these dilated joints are only exposed in the east flank, they are constrained from toppling failure into the source area. Observations of adjacent joints in the basal failure plane and the columnar joints exposed in the east flank, found no evidence of any relative movement (Figure 4.8) which would suggest pre-failure or post-failure movement.

Seepage was observed from the base of the main scarp along the intersection with the sheeting joint failure plane (Figure 4.9). The seepage was minor but fairly consistent when observed several times over a period of three months after the landslide, suggesting that the seepage is not likely to be a short-term response to intense rainfall events. Seepage water was flowing across the source floor towards the base of the east flank. As the intersection of the east flank and the sheeting joint is extremely narrow to tight, surface water was observed draining directly along the surface downslope.

In order to gain access to the source area, access paths were cut through the thick vegetation above the source area and along the flanks. Inspections were carried out along these access paths to look for tension cracks or other signs of distress over a distance of over 60 m above the crown of the source area, and 20 m adjacent to the flanks. Some minor vertical 'steps' were observed above the main scarp, the largest one of which had 400 mm vertical displacement (Figure 2.1), but with no apparent lateral movement and the exposed soil was weathered, indicating the feature was not recent. This feature was approximately 20 m above the crown and was targeted for further investigation during the post-landslide ground investigation (GI), as described in see Section 5.3. No other signs of significant distress could be observed within the source area or adjacent to the main scarp or east flank. An area of intermittent rock outcrop about 30 m west of the source area, observed from API with apparent planar joint surfaces dipping downslope, was inspected and found to have no obvious adverse structure.

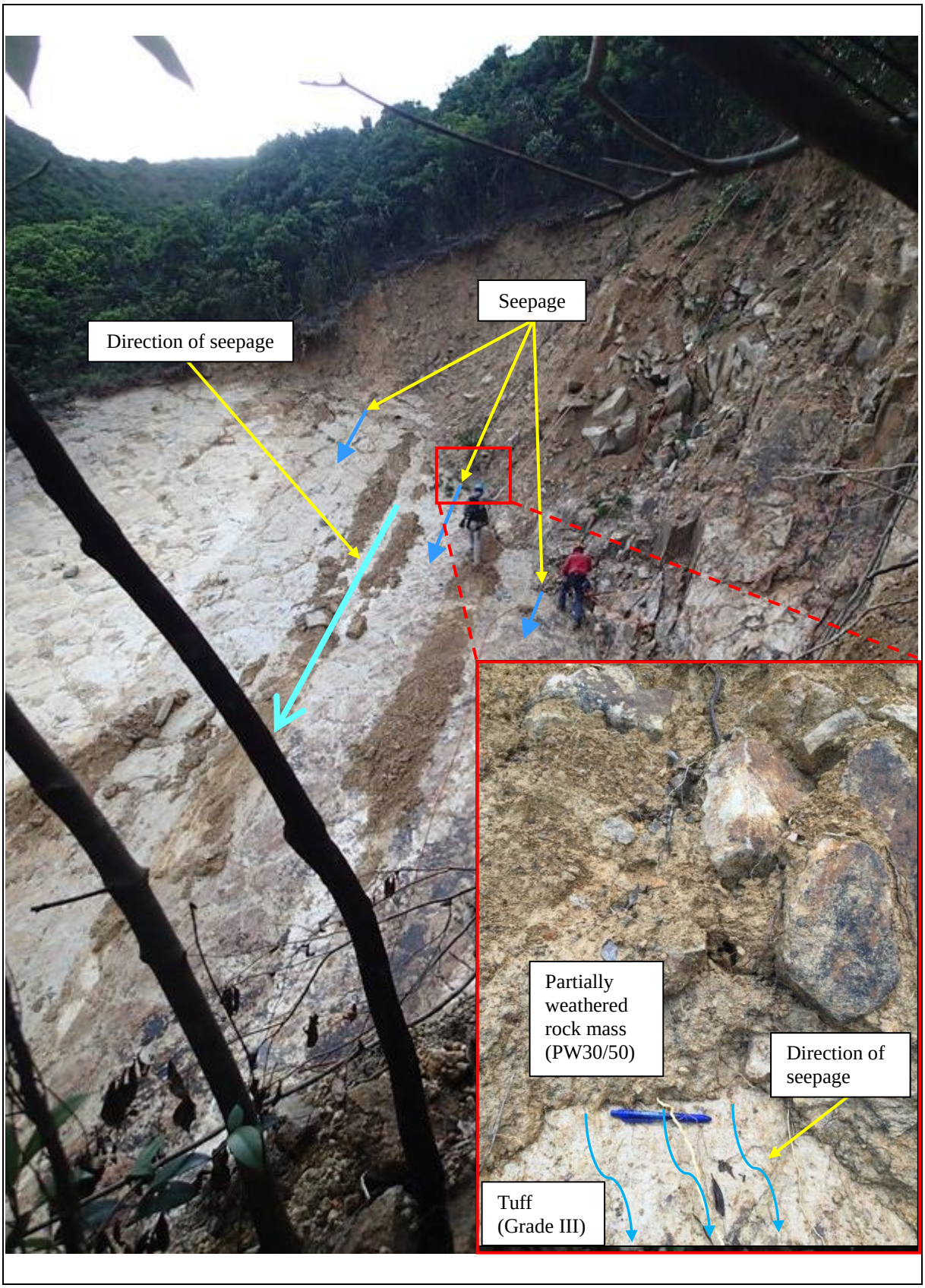

Figure 4.9 View Upslope of the Main Scarp and Upper Source Floor Showing Seepage (Photograph taken on 31 May 2016)

4.4 Upper Debris Trail above Sai Kung Sai Wan Road (Chainage 60 to 116)

Erosion is the dominant process in this section of the debris trail below the source area and above Sai Kung Sai Wan Road (Figures 4.3 and 4.5). The trail steepens to about 50° providing additional energy and erosive power to the debris which contains a significant rock component. The exposed substrate mainly comprised tuff rock with a peripheral area of partially weathered rock mass and colluvium exposed where it has been partly entrained. The debris trail is between 15 m and 21 m wide along this section and most of the pre-failure regolith has been stripped off due to the erosive power of the debris. Even so, the total entrainment was estimated at just over 200 m^3 which suggests that the regolith was not very deep in this section. This is corroborated by aerial photograph evidence which indicates that prior to the failure the area was partly rock outcrop or thinly vegetated, especially in the upper part of this section of debris trail. The debris trail gradually becomes more confined below the source area at the intersection with perennial drainage line DL1 (Figure 3.3).

4.5 Sai Kung Sai Wan Road (Chainage 116 to 137)

Sai Kung Sai Wan Road is elevated above the associated upslope culvert area and proved a significant obstruction to the debris flow despite the high calculated velocity. Significant deposition of landslide debris occurred on the road and upslope in the culvert area, estimated at about 460 m^3 from the number of truck loads removed from site (Figure 1.3). Debris height of up to 4 m was observed on the road and possibly increased to about 6 m within the upslope culvert area, which was topographically lower than the road and was completely filled in. Debris on the road comprised a mixture of cobble- to boulder-sized rock blocks, in a fine matrix of sandy silt, with clastic accumulations of angular cobble- and boulder-sized rock blocks on the lateral periphery.

4.6 Lower Debris Trail below Sai Kung Sai Wan Road (Chainage 137 to 237)

Over the initial portion of this section of debris trail below Sai Kung Sai Wan Road (up to Chainage 162), erosion was the dominant process as the debris that cascaded over the road (about 1,830 m^3), passed over fill slope No. 8SE-A/F34, and entrained about 250 m^3 from the fill slope. The northern portion of the fill slope was especially eroded by the debris, over a width of about 9 m, undermining the road pavement above to a depth of about 3 m (Figure 1.4). The downslope culvert pipe was exposed intact (Figure 2.3) but the wing walls and associated structures were entrained by the debris flow and deposited further downstream. Deposition of approximately 200 m^3 also took place with peripheral accumulations (levees) of clastic and remoulded debris along the flanks of the debris trail, as well as remnant clastic material deposited within the debris trail.

From Chainage 162 to 237, the drainage line becomes more incised and rock is commonly exposed in the base of the debris trail which is consistent with pre-failure aerial photographs showing a rocky substrate between Chainage 170 and 190 where there is no tree cover. Also, eroded colluvial deposits are exposed in the flanks of the debris trail which is consistent with the API findings (Figures 3.1 and 3.3), where a lobe of colluvial debris

borders the southern portion of the debris trail from Chainage 175. However, flow-aligned vegetation (Figures 4.10 and 4.11) observed on the eroded colluvial flanks, and the rocky substrate, suggest that the amount of entrained material was relatively modest in this section (about 40 m^3). With relatively little overall deposition (about 90 m^3), transportation was the dominant process, with most of the debris flow material (about 1,780 m^3), passing through this section. The overall slope angle is approximately 24°, although there are some small local 'steps' in the drainage line profile (e.g. at Chainage 195).

4.7 Lower Debris Trail (Chainage 237 to 560)

Between Chainage 237 and 300, the debris trail reduces in slope angle to about 15°, negotiates two sharp bends at about Chainage 270 (Figure 4.12) and Chainage 300, and the drainage line becomes less deeply incised, with some relatively flat terrace-like areas on the south side of the drainage line. The change in drainage line morphology and slope angle resulted in the onset of significant deposition. Between Chainage 245 and Chainage 305, over 500 m^3 of mainly coarse clastic debris was deposited (Figures 4.12 to 4.14) with minor amounts of finer material and remoulded debris observed towards the flanks of the drainage line as levees (Figure 4.15). Superelevation marks could be observed along the sharp bends at Chainage 273 and Chainage 300 with maximum superelevations of approximately 2.5 m and 1 m respectively (Figure 4.15). A tributary drainage line enters the main drainage line at Chainage 270. Some large concrete fragments, several metres long and probably part of the culvert wing wall or base slab structure, were observed at Chainage 273 (Figures 4.14 and 4.15 and Figure B2).

After Chainage 300, the drainage line initially becomes more confined again and more irregular in profile with a series of rocky steps of 2 to 3 m high (Figures 4.16 and 4.17), but with an overall gradient of about 8°. The largest step (about 3 m high at Chainage 325) coincides with a geological boundary between the tuff and trachydacite and rhyolite lava (Figure 4.17). Minor entrainment could be observed along the flanks of the drainage line (Figure 4.16) but deposition is the dominant process, with coarse clastic debris deposited in semi-continuous lobes within the drainage line and local remoulded debris typically forming levees higher up on one flank.

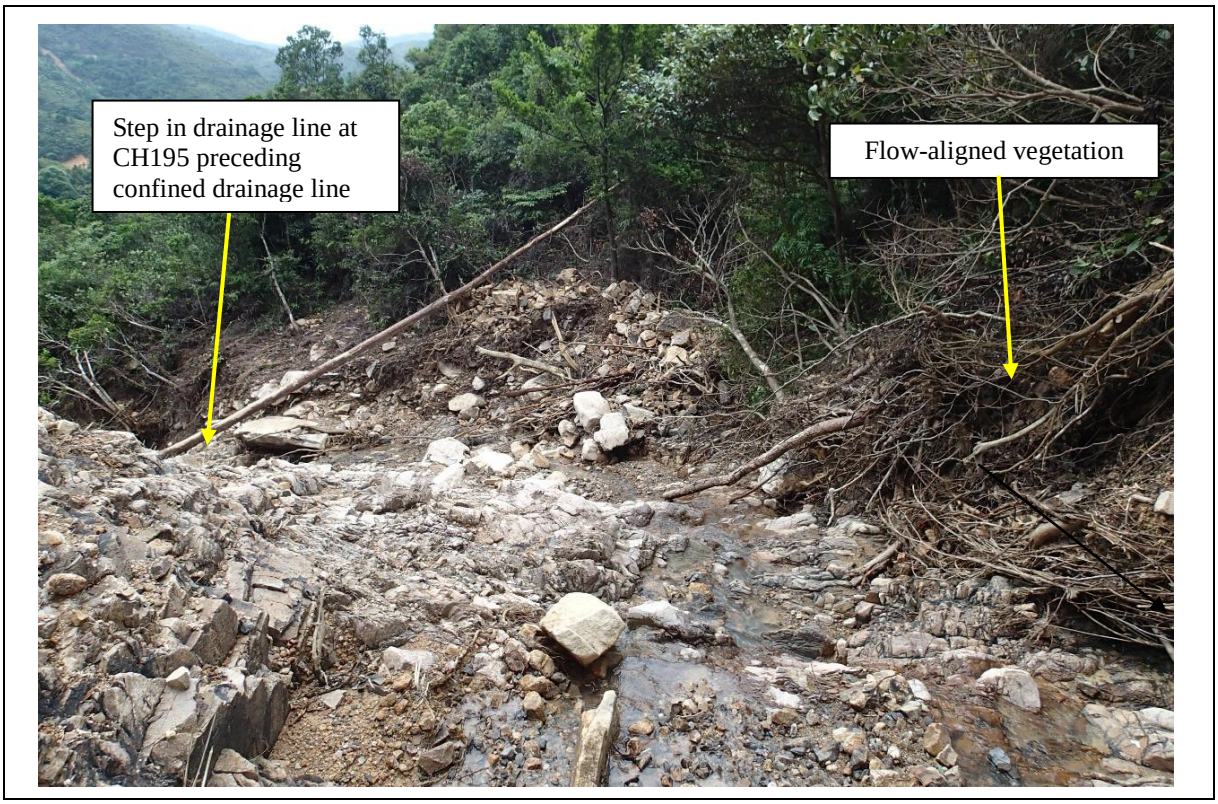

Figure 4.10 View Downslope from CH180 to CH192 (Photograph taken on 14 June 2016)

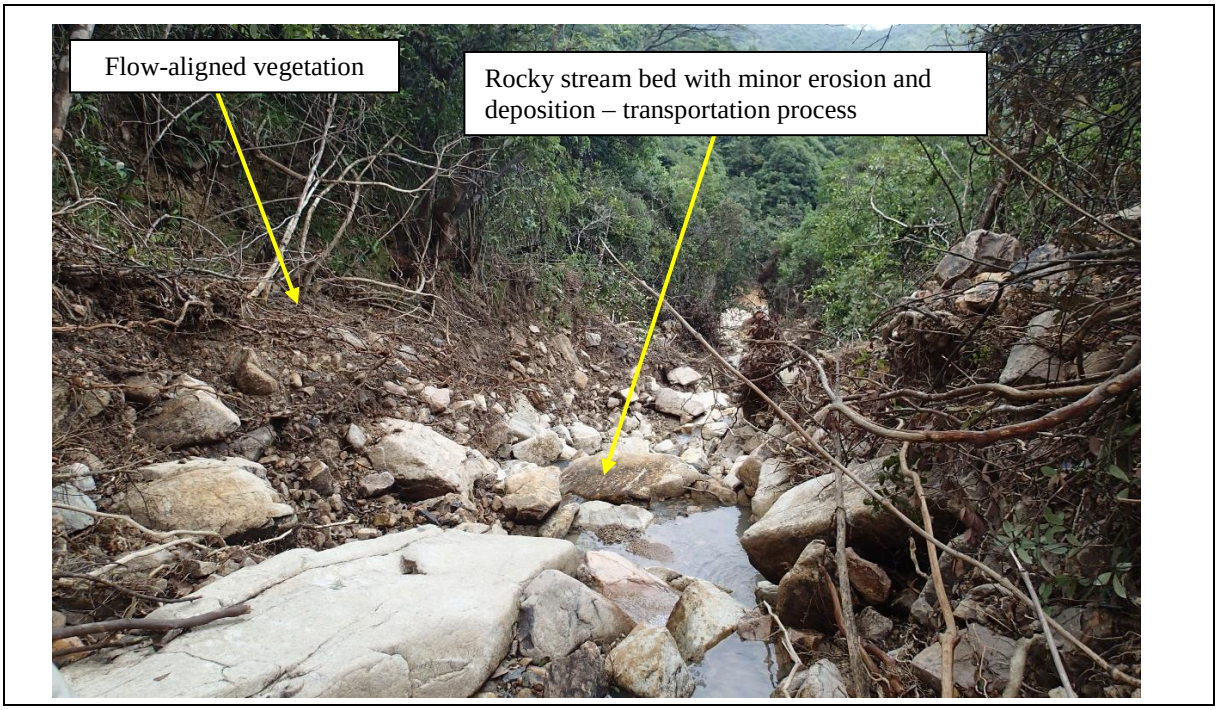

Figure 4.11 View Downslope from CH200 to CH210 (Photograph taken on 14 June 2016)

Figure 4.12 View Downslope from CH260 to CH275 (Photograph taken on 14 June 2016)

Figure 4.13 View Upslope from CH250 to CH265 (Photograph taken on 14 June 2016)

Figure 4.14 View Downslope from CH275 to CH290 (Photograph taken on 14 June 2016)

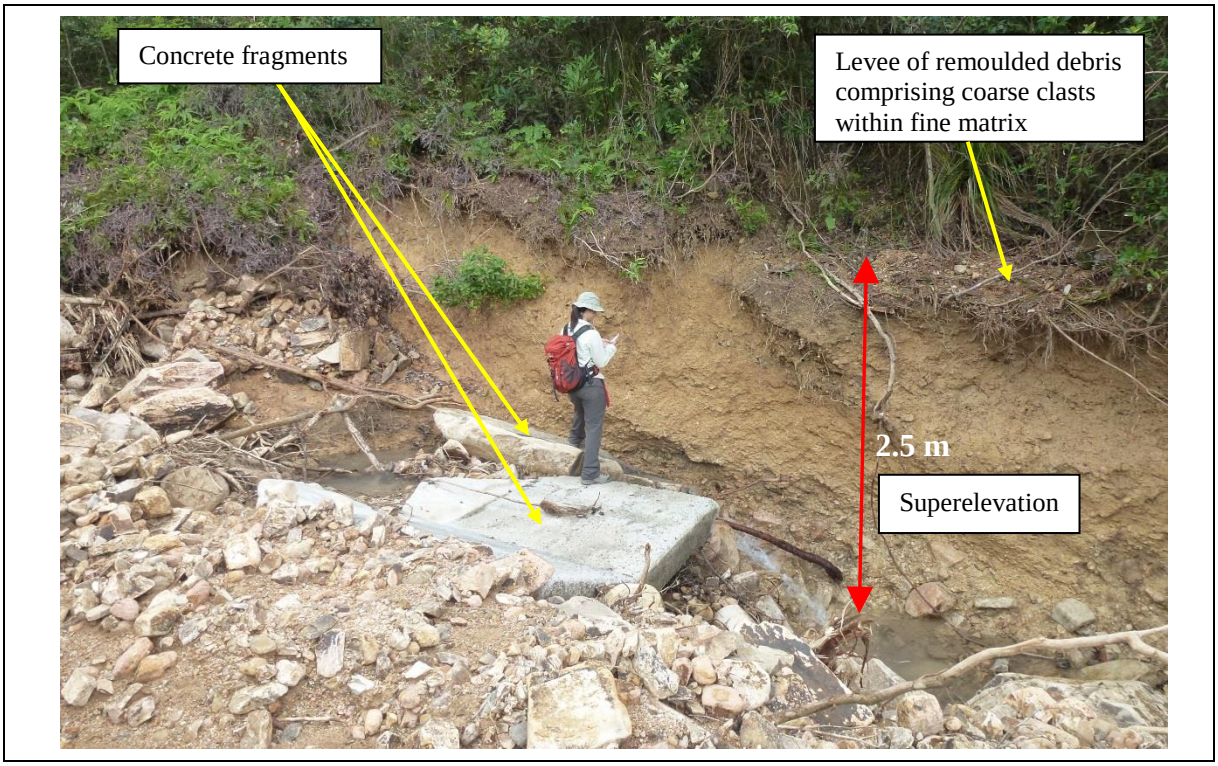

Figure 4.15 View of Superelevation at CH273 Where a Sharp Bend in the Drainage Line Occurs (Photograph taken on 14 June 2016)

Figure 4.16 View Downslope from CH305 to CH320 (Photograph taken on 14 June 2016)

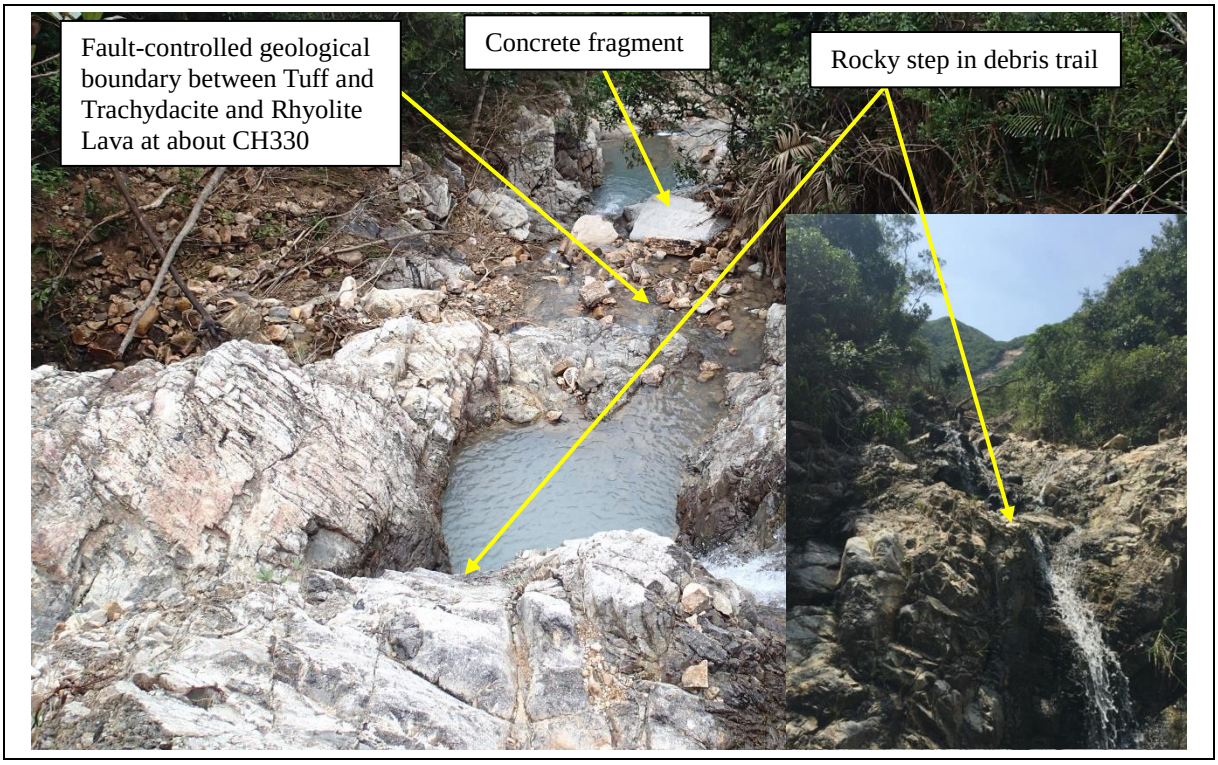

Figure 4.17 View Downslope from CH325 to CH345 (Photograph taken on 14 June 2016)

Concrete fragments could be observed at Chainage 330 and Chainage 410, again likely to be from the culvert structure below Sai Kung Sai Wan Road. Tributary drainage lines enter the main drainage line at Chainage 330, 370, 380 and 480, likely contributing to mobility of the debris. A small landslide observed during the field inspections has slumped into the drainage line at Chainage 410 (Figure 4.18). As it was a shallow, small magnitude failure, it did not contribute any significant debris to the landslide. Another sharp bend was encountered in the drainage line at Chainage 490 but no superelevation marks could be observed. The drainage line has a few more small steps (Figure 4.19) but overall the gradient decreases and deposition was observed to be slowly decreasing (Figure 4.20) and the last observation of remoulded debris could be seen at Chainage 560 (Figure 4.21), suggesting that debris flow processes terminated at this point.

4.8 Outwash Deposits

After Chainage 560, intermittent coarse clastic and sand deposits could still be observed within the drainage line all the way to High Island Reservoir but appear sorted or washed and have probably been moved or remobilized by post-failure fluvial processes rather than landslide processes. While most of the coarse boulder-sized material was deposited before Chainage 560, the more dilute, sediment charged flow (i.e. debris flood) may have continued (Hungr, 2002). At Chainage 590 there is a confluence with another major drainage line (Figure 2.2) which would have added considerable discharge during the rainstorm (Figure 4.22).

Figure 4.18 View Downslope from CH400 to CH410 (Photograph taken on 14 June 2016)

Figure 4.19 View Upslope from CH415 to CH430 (Photograph taken on 14 June 2016)

Figure 4.20 View Downslope from CH430 to CH445 (Photograph taken on 14 June 2016)

Figure 4.21 View at around CH560 of Remoulded Debris Forming Levees on Top of the Flank (Photograph taken on 14 September 2016)

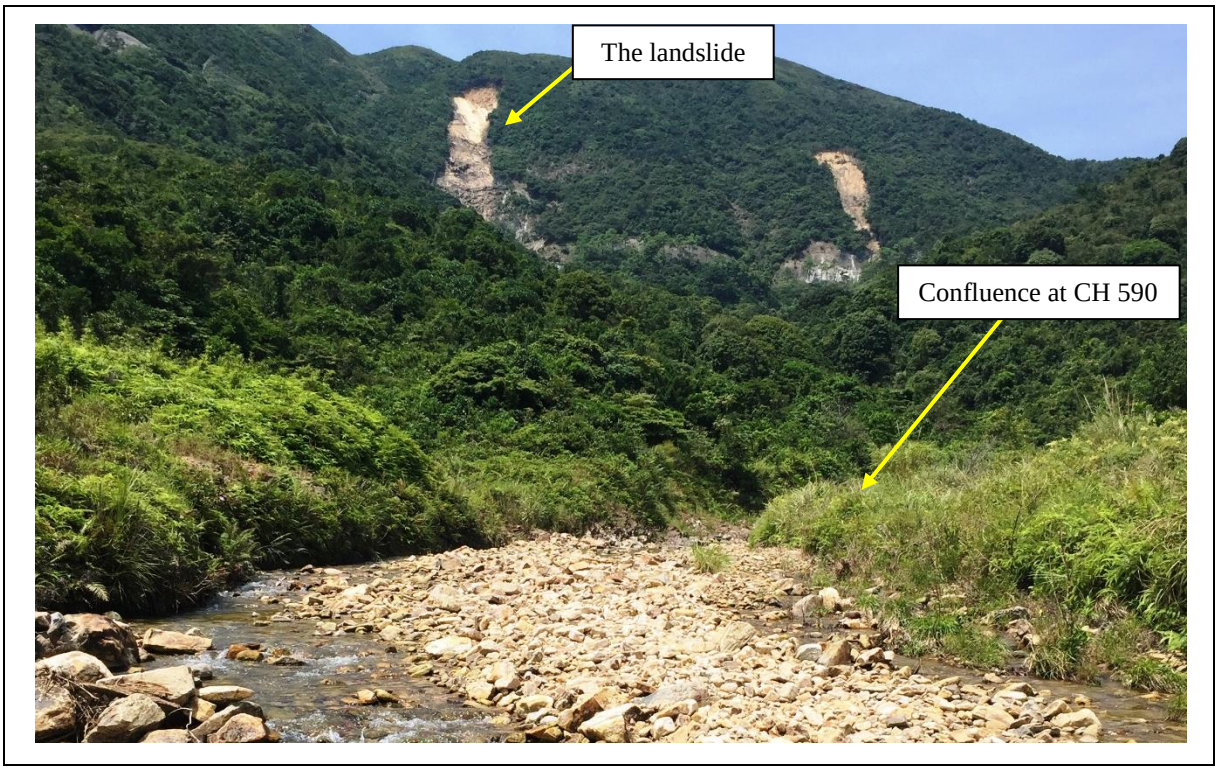

Figure 4.22 View of Outwash Deposits and Upslope from CH630 to CH710 (Photograph taken on 14 September 2016)

5 Geology and Geomorphology

5.1 Geological and Geomorphological Setting

The study area is characterised by a broad topographic depression, with local deposits of colluvium accumulated in relatively flat, unconfined areas adjacent to drainage lines and occasional bands of rock outcrop traversing the hillside. The geological structure controls these lateral bands of rock outcrop (Figures 1.5 and 3.3), where local shears have caused preferential weathering. No sheeting joints similar in orientation or persistence to the landslide failure plane are apparent in other areas of rock outcrop within the study area.

The source area of the landslide almost exactly coincides with a local topographic depression, considered to be formed by a relict landslide, probably a typical shallow failure in 1 m to 2 m of colluvium or saprolite (Figure 3.2). This relict landslide is located below a rounded convex break-in-slope in the hillside above and thus is consistent with the location of typical shallow landslides. However, the landslide does not appear to be a retrogressive failure of the relict landslide scar or hillside retreat, such as that postulated by Hansen (1984), as there seems to be no upslope erosion from the crown of the existing relict landslide depression, and the failure mechanism (structurally controlled, asymmetric rock slide) appears different to that of the relict landslide.

5.2 Hydrological and Hydrogeological Setting

The underlying geological structure of the study area, typically comprising sub-vertical preferentially weathered joints, has formed numerous drainage lines along these zones of relative weakness (Figure 3.3), giving a dendritic drainage pattern in the study area (Figure 5.1). The drainage pattern and number of tributary drainage lines entering the main drainage line, result in a high (4^{th}) order (Strahler, 1952) drainage catchment which probably had a high discharge of water during intense rainfall. Aerial photographs show a narrow, vertical band of rock outcrop at the west flank of the source area, where a minor ephemeral drainage line is located (Figures 4.1 and 4.3). This band of rock outcrop coincides with the exposed western extent of the sheeting joint that forms the surface of rupture. As the sheeting joint is exposed along the outcrop, it would have probably facilitated ingress of water into the joint during the rainstorm.

5.3 Post-landslide Ground Investigation

No previous GI information at the study area is available. The post-landslide GI was limited to trial pit excavation and vegetation clearance strips due to access difficulties in the steep, densely vegetated terrain. As the failure occurred along a basal, persistent, planar sheeting joint, the GI strategy aimed at looking for indirect evidence of extension of the sheeting joint into the adjacent terrain, in the form of signs of distress or instability. Vegetation clearance areas were proposed to identify such features, including pre- or post-failure tension cracks and deformation, and if identified, a trial pit would be excavated through the features to investigate the nature. A 400 mm vertical step (Figure 2.1) was identified 20 m above the main scarp during the initial site inspection, and a trial pit was proposed to investigate this feature. Thus, the GI comprised one trial pit (No. TP1) an

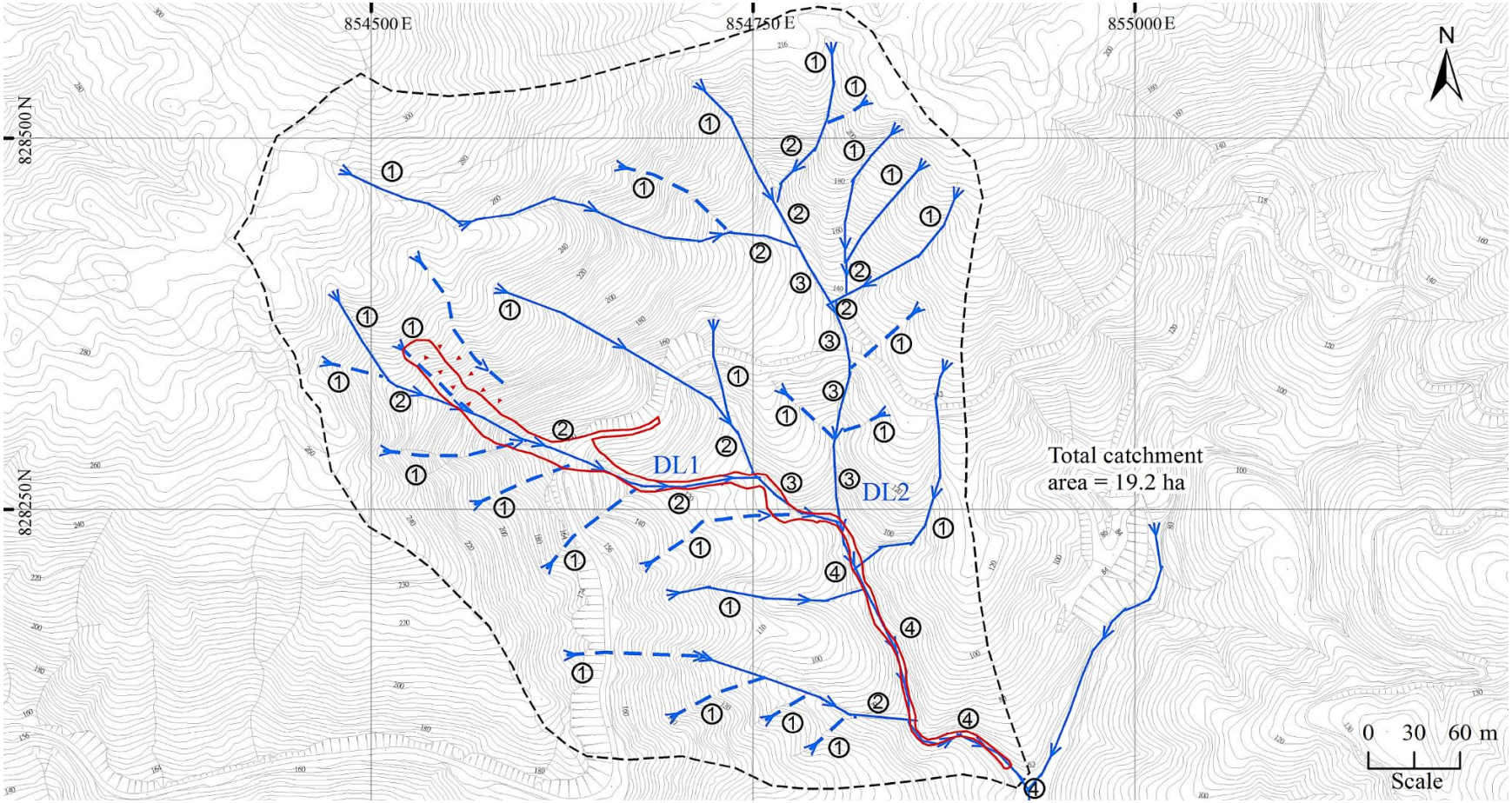

Legend:

The landslid | Study area | Perennial drainage line | Ephemral drainage line | (1) Stream order (Strahler,1952)

Note: Base plan is extracted from 1:1000 survey sheet Nos. 8SE-7A, 8SE-7B, 8SE-7C and 8SE-7D dated March 2016.

Figure 5.1 Site Catchment Drainage

three vegetation clearance strips each above the main scarp (Nos. VC1 to VC3) and adjacent to the east flank (Nos. VC4 to VC6). The locations of the GI stations are shown in Figure 5.2 and the trial pit record is presented in Figure 5.3.

The vegetation clearance strips were carried out 60 m above the main scarp (Nos. VC1 to VC3) and 40 m adjacent to the east flank (Nos. VC4 to VC6). Vegetation was cut down to soil surface so that any distress, such as tension cracks or deformation, significant enough to be manifested on the ground surface could be observed. However, no signs of distress were observed from the hillside above the main scarp or adjacent to the east flank (Figure 5.4).

Trial pit TP1 was excavated to investigate the 400 mm vertical step, suspected to be a relict tension crack, above the main scarp. The trial pit was excavated to 3 m depth and exposed 0.45 m of colluvium, underlain by 0.35 m of residual soil, which became very stiff, completely decomposed tuff (clayey silt) until termination at the base. However, no evidence of any tension crack, disturbance or dilation could be observed in the exposed soil faces below the step (Figure 5.4).

No rock outcrop was observed above the source area and no evidence of daylighting of the basal failure sheeting joint was observed outside the source area.

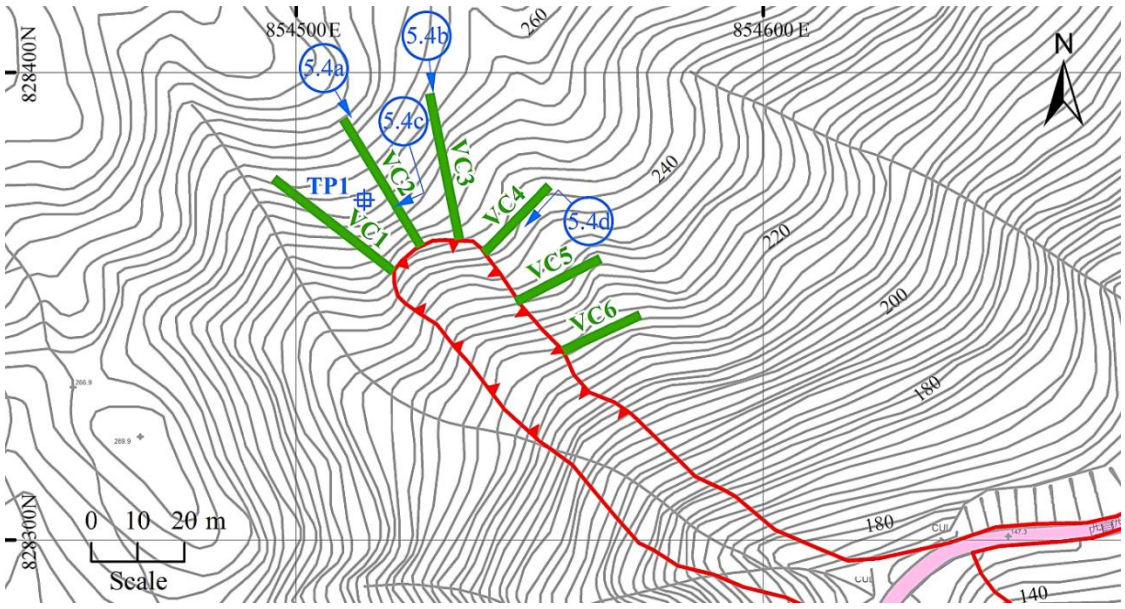

Legend:

The landslide
TP1 Post-landslide trial pit
VC1 Post-landslide vegetation clearance strip
Sai Kung Sai Wan Road
5.4a Location and direction of photograph in Figure 5.4(a)

Note: Base plan is extracted from 1:1000 survey sheet No. 8SE-7A dated March 2016.

Figure 5.2 Plan of Ground Investigation Works

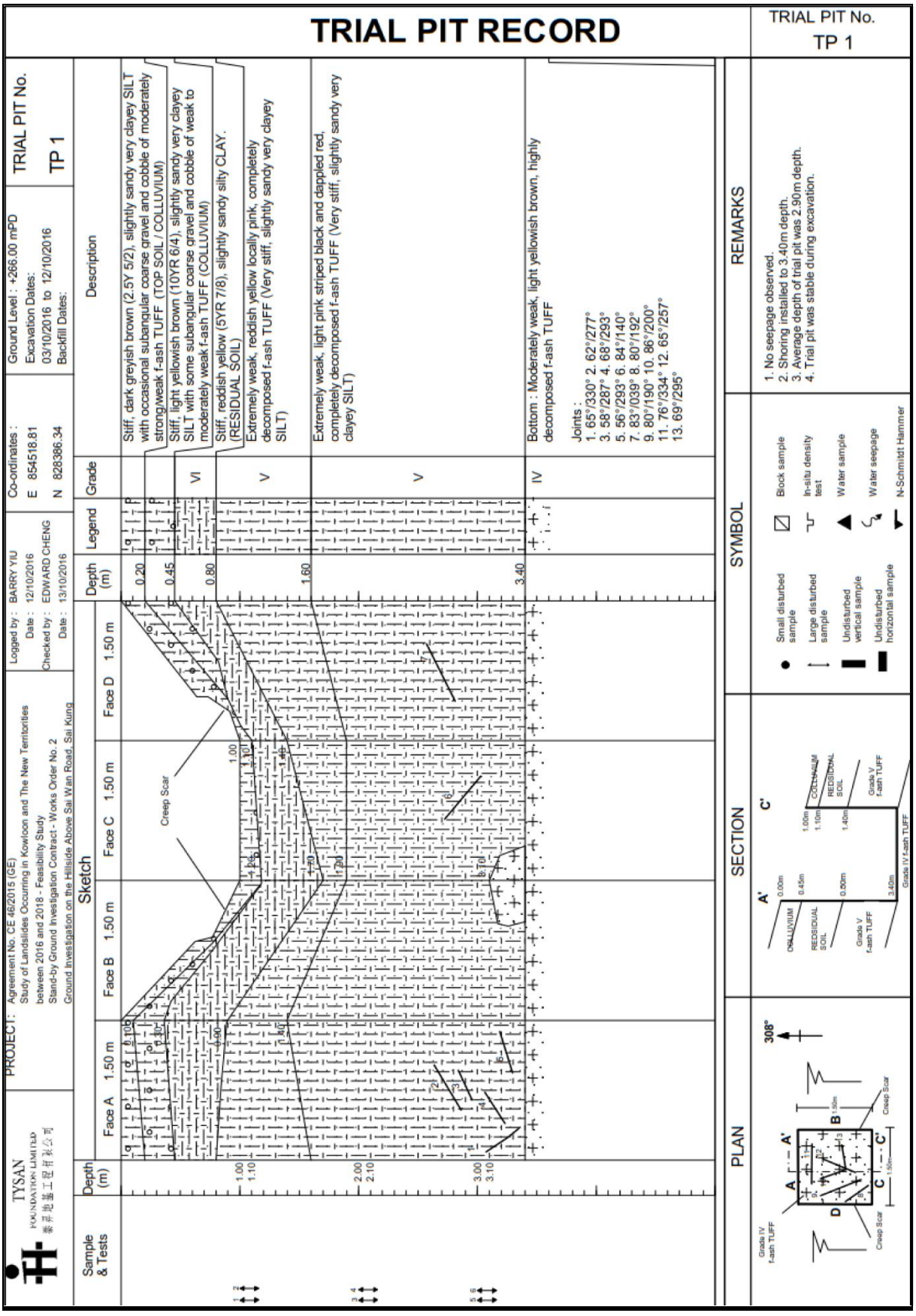

Figure 5.3 Record of Trial Pit TP1

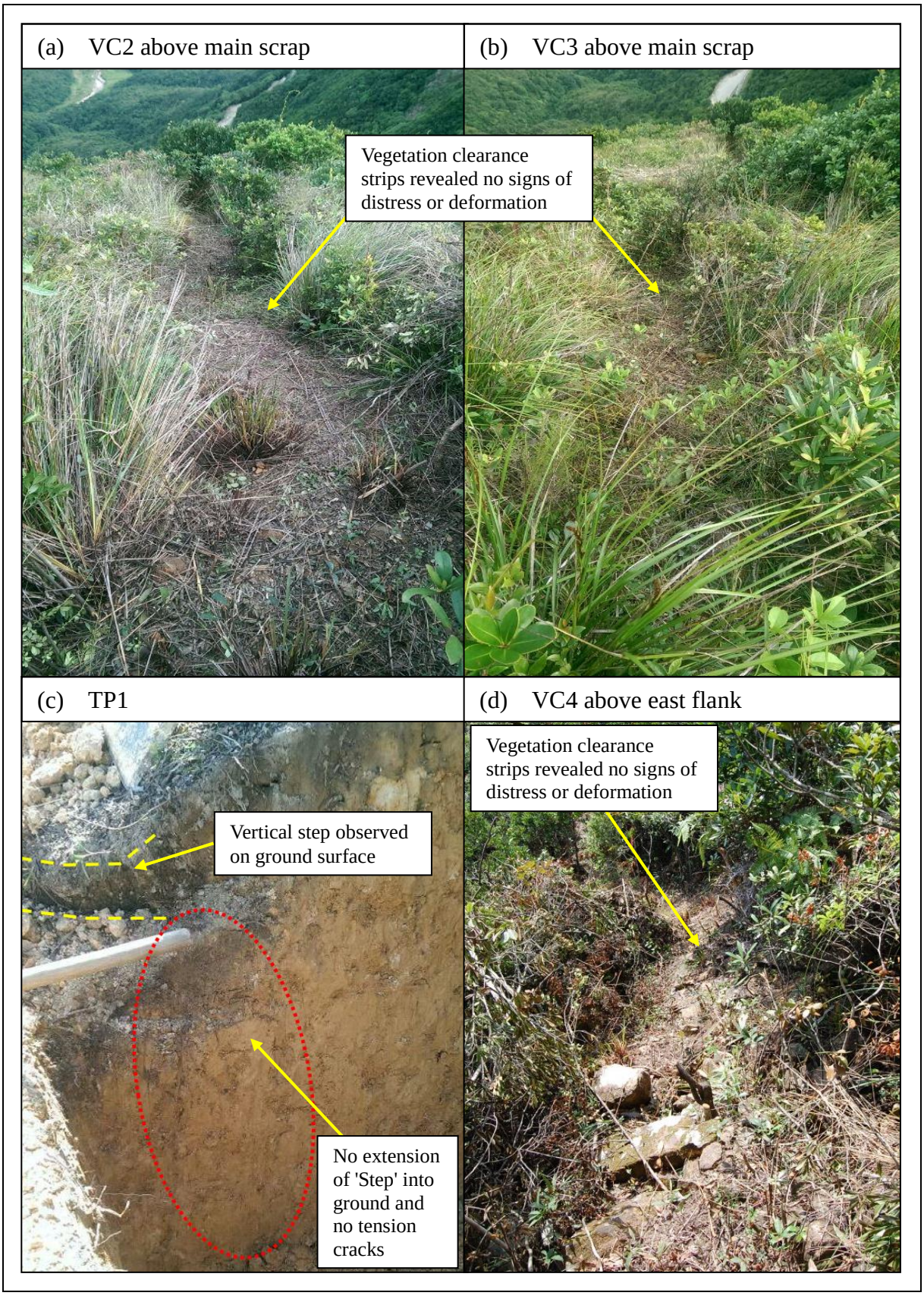

Figure 5.4 View of GI Works including Vegetation Clearance Strips and Trial Pit (Photograph taken on 6 and 13 October 2016)

6 Analysis of Rainfall Records

Rainfall data was obtained from the nearest GEO automatic raingauge No. N13 located at Yuen Ng Fan, High Island Reservoir, Sai Kung, which is about 2.5 km to the southwest of the study area (Figure 1.1). GEO Raingauge No. N13 was established in 1983 and records and transmits rainfall data at 5-minute intervals to the GEO and the Hong Kong Observatory (HKO). Based on these data, the daily rainfall recorded between 19 April 2016 and 25 May 2016 and the hourly rainfall recorded between 12:00 a.m. on 20 May 2016 to 11:00 p.m. on 21 May 2016 were prepared and are presented in Figure 6.1.

The rainstorm started at about 8:00 p.m. on 20 May 2016 with intensive rainfall recorded within the subsequent hours up to 6:00 a.m. on 21 May 2016. The landslide was first reported by FSD at about 8:30 a.m. on 21 May 2016. Without any further witness accounts it is not possible to verify the exact time of failure, however, for the purpose of the rainfall analysis, the landslide was assumed to have occurred at 6:00 a.m. which coincides with the end of the intense rainfall period. The rainfall analysis was carried out by estimating the maximum rolling rainfall preceding the assumed time of occurrence of the landslide for various durations from 5 minutes to 31 days. Results of the rainfall analysis based on the rainfall data recorded by GEO Raingauge No. N13 are presented in Table 6.1. The maximum rolling rainfall for short-duration 2 hours, 4 hours, 6 hours and 8 hours at GEO Raingauge No. N13 is 196.5 mm, 280 mm, 346 mm and 362 mm respectively (Table 6.1).

An analysis of the return periods for various durations of rolling rainfall recorded by GEO Raingauge No. N13, with reference to historical rainfall data recorded at the raingauge since 1983 (Tang & Cheung, 2011) shows that the rainfall duration of 6 hours was the most severe with a corresponding return period of about 200 years (Table 6.1). Other short-duration rainfalls of 8-hour and 4-hour durations were also severe with an estimated return period of 150 and 93 years respectively.

The maximum rolling rainfall of the 21 May 2016 rainstorm has also been compared with previous major rainstorms recorded at GEO Raingauge No. N13 and the results are presented in Figure 6.2. The 21 May 2016 rainstorm recorded at GEO Raingauge No. N13 preceding the landslide, was the most severe with respect to short-duration rainfall (viz. between 1 hour and 12 hours durations) since the operation of the raingauge in 1983.

7 Debris Mobility

7.1 General

Theoretical analyses of the mobility of the debris trail resulting from the source area were carried out using GEO's 2-dimensional Debris Mobility Model, 2d-DMM (Version 1.2). Details of the analyses are given in Appendix C.

7.2 Travel Angle and Distance

The detached debris from the source area entered perennial drainage line DL1 where

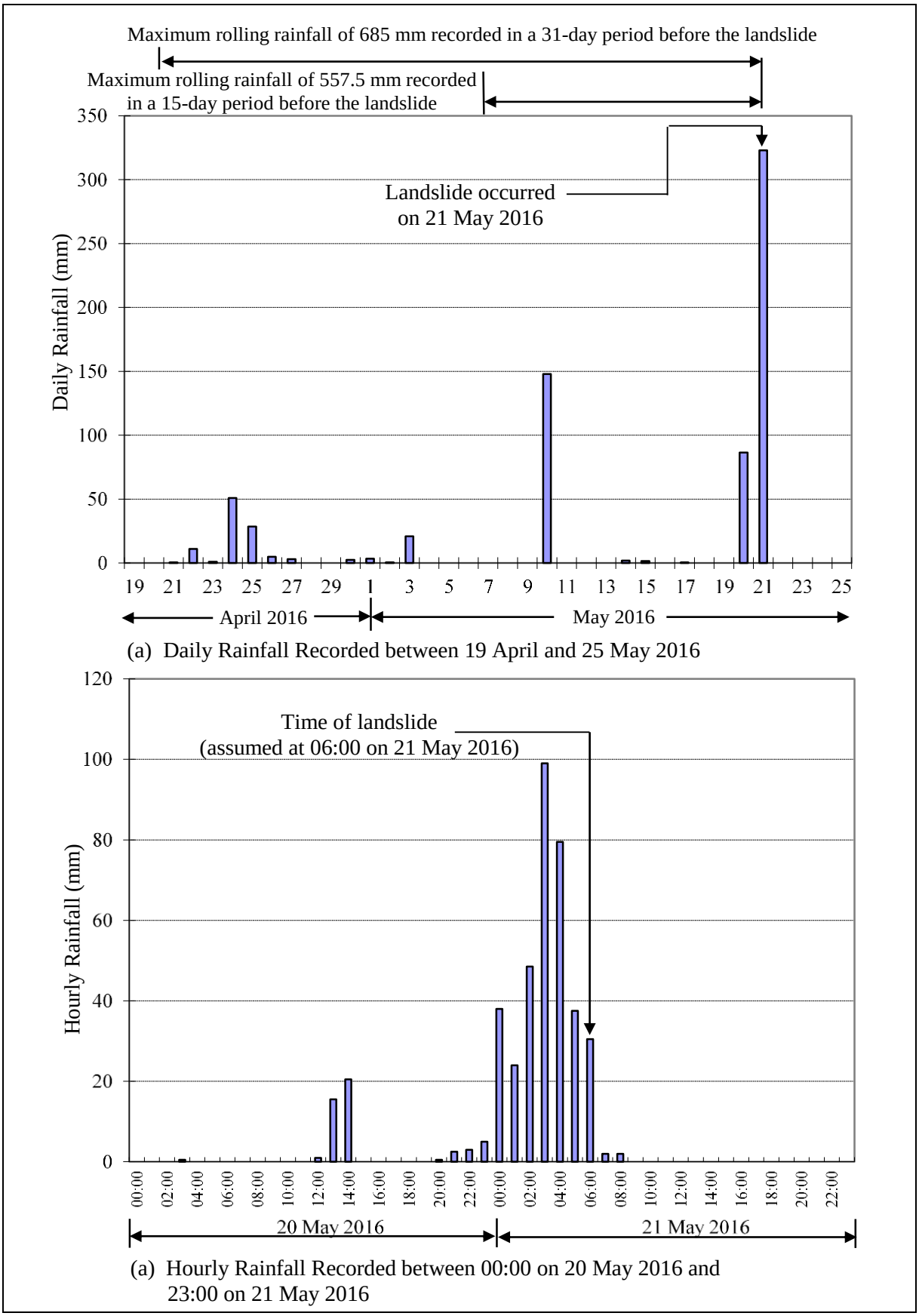

Figure 6.1 Daily and Hourly Rainfall Recorded at GEO Rainguage No. N13

Table 6.1 Maximum Rolling Rainfall at GEO Raingauge No. N13 for Selected Durations Preceding the Landslide and Estimated Return Periods

Duration	Maximum Rolling Rainfall (mm)	End of Period (Hours)	Estimated Return Period (Years) Note 4
5 Minutes	13	02:35 on 21 May 2016	< 2
15 Minutes	32	02:40 on 21 May 2016	3
30 Minutes	56.5	02:55 on 21 May 2016	4
1 Hour	104.5	03:25 on 21 May 2016	9
2 Hours	196.5	03:45 on 21 May 2016	62
4 Hours	280	05:35 on 21 May 2016	93
6 Hours	346	05:35 on 21 May 2016	200
8 Hours	362	05:40 on 21 May 2016	150
12 Hours	368	06:00 on 21 May 2016	51
24 Hours	405	06:00 on 21 May 2016	23
48 Hours	405.5	06:00 on 21 May 2016	6
4 Days	406	06:00 on 21 May 2016	3
7 Days	407.5	06:00 on 21 May 2016	< 2
15 Days	557.5	06:00 on 21 May 2016	< 2
31 Days	685	06:00 on 21 May 2016	< 2

Notes:
(1) Maximum rolling rainfall was calculated from 5-minute rainfall data.
(2) GEO Raingauge No. N13 is located at Yuen Ng Fan, High Island Reservoir, Sai Kung about 2.5 km to the southwest of the landslide.
(3) For the purpose of rainfall analysis, the landslide was assumed to have occurred at 6:00 a.m. on 21 May 2016.
(4) The return periods were estimated based on the method described by Tang & Cheung (2011).

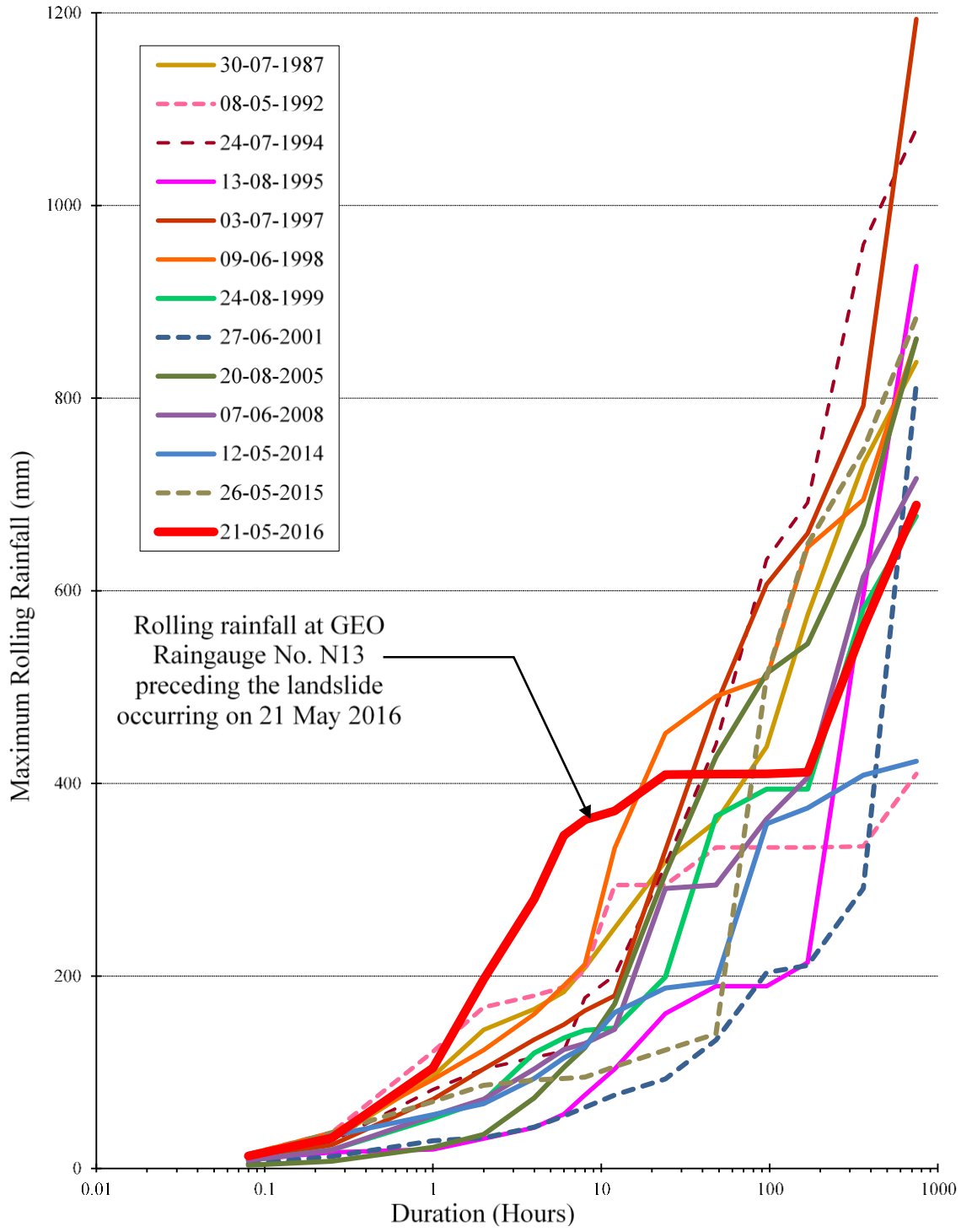

Notes:

(1) Rainfall data are evaluated from 5-minute readings from GEO Raingauge No. N13 located at Yuen Ng Fan, High Island Reservoir, Sai Kung which is about 2.5 km to the southwest of the landslide.

(2) The GEO Raingauge No. N13 started its operation since 1983. The maximum rolling rainfalls are estimated from rainstorms afterwards.

Figure 6.2 Maximum Rolling Rainfall Preceding the Landslide and Selected Previous Major Rainstorms Recorded at GEO Raingauge No. N13

the debris became confined and channelized before coming to rest in a natural drainage line above High Island Reservoir. The total travel distance was about 500 m and the travel angle, measuring from the crown of the source area to the end of the debris trail was about 18°.

7.3 Theoretical Modelling of Debris Runout

The topography adopted for the modelling was based on the pre-failure LiDAR survey. The initial thickness of the displaced material within the source area was estimated from a comparison of the pre-failure LiDAR survey topography, and the post-failure photogrammetric topographic survey by UAV together with field measurements (see Section 4). A Voellmy rheological model was adopted in the analyses and, for simplicity, it has been assumed that all the materials in the source area displaced simultaneously. Analyses with different key parameters were carried out in order to provide a reasonable fit to the extent and profile of the debris trail, deposition of debris and mass balance as observed on site.

The site setting with respect to debris trail morphology was reviewed when adopting the mobility parameters. A combination of a base friction angle of 18º with a turbulence coefficient of 1,000 m/s^2 from the source area to Sai Kung Sai Wan Road and 8º with a turbulence coefficient of 500 m/s^2 for the downhill area of Sai Kung Sai Wan Road where the drainage line become incised, was found to provide a reasonable fit to the debris trail topography.

The maximum velocity profile generated by the debris mobility analysis (Figure C1) indicates that the debris flow would accelerate from the source area and reach its peak velocity of about 19 m/s, when the debris front reached approximately Chainage 123 immediately above Sai Kung Sai Wan Road. At this point the debris was about 4.3 m thick, reaching a maximum of about 4.7 m just below Sai Kung Sai Wan Road when the debris entered the main drainage line and became channelized (Figure C1).

The debris velocity and thickness reduced gradually to about 15 m/s and 2.7 m respectively, where the onset of significant deposition occurred at Chainage 245. Over the next 100 m, several sharp bends occur in the drainage line (Figure 2.2), and the debris velocity and thickness were sufficient to produce superelevation of the debris surface around the bends, with superelevations of 2.5 m and 1 m observed at Chainage 273 (Figure 4.15) and Chainage 300 respectively. The superelevation marks indicated a velocity of approximately 10 m/s and 7 m/s respectively, which corresponds reasonably well, albeit slightly lower than the calculated debris front velocity generated by 2d-DMM along this section of the debris trail (Figure C1).

The calculated velocity continues to decrease and the debris thickness remains above 2 m until about Chainage 440, corresponding to a velocity of about 6 m/s, where the debris thickness rapidly decreases. By Chainage 500, the velocity had reduced to about 3 m/s and the thickness of debris was calculated to be 1.2 m, which is comparable to the field observations (about 1 m). The debris came to a halt at Chainage 560 where the slope gradient is gentle (< 5º).

8 Engineering Analyses

8.1 General

Theoretical stability and seepage analyses were carried out to assist in the diagnosis of the mechanisms and causes of the failure.

The source area had a wedge failure geometry (Figure 4.2) and the frictional resistance from the basal, planar sheeting joint and the irregular, saw-tooth profiled columnar jointed tuff exposed in the east flank could be considerably different. In addition, the morphology of the failure on plan was irregular on the east flank and included a soil portion in the upper few metres. A 3-dimensional approach was therefore adopted for the stability analyses to address these observations more realistically. The stability analyses, together with the seepage analyses, also assisted in investigating the likely range of cleft water pressure on the failure surface at the time of failure for the operative shear strength parameters for tuff rock exposed along the basal sheeting joint and the east flank of the landslide.

The stability analyses were conducted using the computer program 'Slope3D' (Cheng & Yip, 2007), which adopts the limit equilibrium method by considering both force and moment equilibrium (Morgenstern - Price approach) of each imaginary 'column' of the ground mass.

A 3-dimensional geological model was developed based on detailed field mapping and using the pre-failure LiDAR survey data, and post-failure photogrammetric topographic survey data obtained by UAV to construct a digital elevation model (DEM) for the stability analyses. The geological interfaces projected into the adjacent hillside both longitudinally and laterally were carefully established with reference to the geomorphology and geology of the study area.

Assumptions on adopted engineering parameters were made based on field observations and engineering judgement, as described in the following sections, in view of the limited GI undertaken.

8.2 Groundwater Response

8.2.1 Infiltration and Water Ingress

Given the scale and geological setting of the landslide, cleft water pressure was likely to have developed within the planar sheeting joint at the time of failure. Based on the findings from the post-landslide inspections (see Section 4.3), direct water ingress from the ephemeral drainage line at the west flank of the source area and direct infiltration over the entire hillside were two possible water sources for the development of cleft water pressure (Figure 8.1).

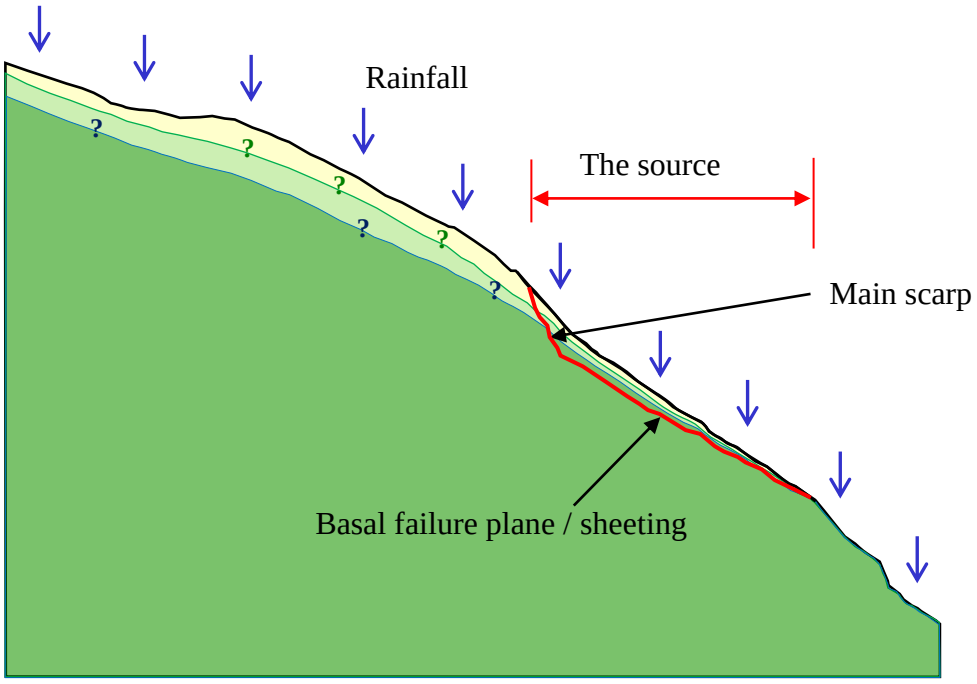

(a) Infiltration over the entire hillside including the source area

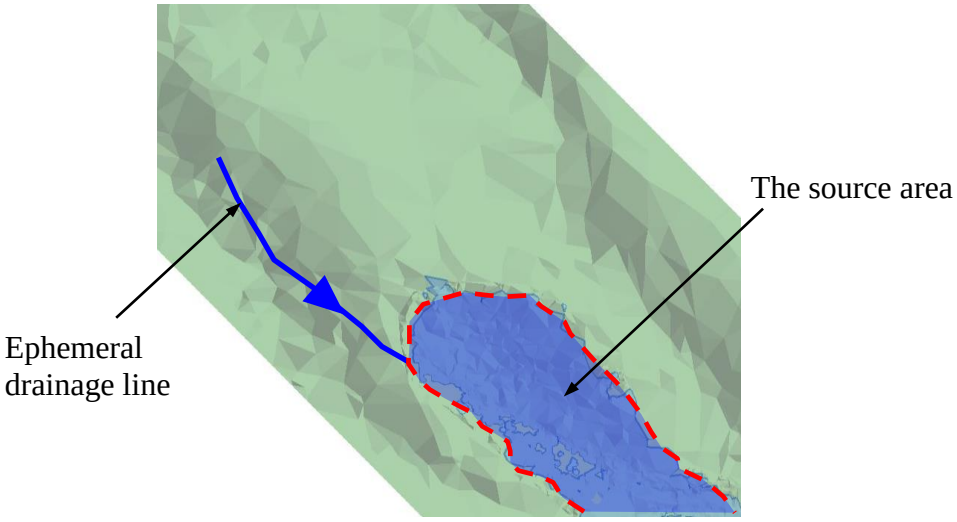

(b) Direct water ingress from ephemeral drainage line at west flank

Legend:

Colluvium | Grade IV/V Tuff | Grade III Tuff

Note: Refer to Figure 4.1 for location of the sections.

Figure 8.1 Groundwater Regime along Sheeting Joint

8.2.2 Seepage Analyses

To evaluate a possible range of the cleft water pressure developed within the planar sheeting joint at the time of failure, two sets of seepage analyses were carried out to model the effect of infiltration from the ground surface and direct water ingress from the west flank to the sheeting joint respectively. The computer program SEEP/W was employed for both analyses.

The seepage analyses for infiltration have taken into account the severe rainstorm on 21 May 2016 as well as the preceding rainstorms on 10 and 20 May 2016. Owing to the time-dependent nature of the problem, transient analyses were conducted to assess the potential development of cleft water pressure at the planar sheeting joint. Apart from the geology and topography, the rate of infiltration at different rainfall intensities and the permeability of the ground materials are key inputs to the analyses. The results of the seepage analyses indicate that at the time of failure, only limited cleft water pressures would have developed within the sheeting joint due to infiltration from the ground surface. Infiltration alone was not the main source of water contributing to the cleft water build-up at the sheeting joint. The results of the seepage analyses, showing considerable response time to infiltration from intense rainfall, are also consistent with the steady, minor seepage observed around the main scarp during several post-failure site inspections. These site inspections were carried out several days after any significant rainfall over a period of about three months after the landslide.

Another set of seepage analyses was carried out to look for the other possible source of water due to direct water ingress from the west flank to the planar sheeting joint and to assess its potential contribution to the development of cleft water pressure at the sheeting joint at the time of failure. The mechanism by which the cleft water pressure could develop was rather different to that in the above infiltration scenario. In this set of seepage analyses, surface water was assumed to directly enter the planar sheeting joint primarily from along the west flank due to the surface run-off from the ephemeral drainage line above it (see Section 5.2). On the other hand, as the sheeting joint was seen extremely narrow to tight along the intersection of the joint surface and the base of the east flank, and surface water was observed to flow along the intersection and not into the east flank, the seepage model assumed an 'impermeable' boundary along the east flank, and assessed how the cleft water pressure was developed on the basal sheeting joint at the time of failure under such boundary conditions. Results of the analyses showed a variation of the developed cleft water pressure across the sheeting joint, typically increasing with joint depth from west to east, with a maximum located at the landslide scar 'nose' along the east flank (Figure 8.2). This cleft water pressure distribution was applied to the subsequent 3-dimensional back analysis in order to evaluate the most likely operative range of the maximum cleft water pressures developed within the sheeting joint at the time of failure.

8.3 Basal and Side Friction

The wedge failure geometry defines a basal sliding plane along the sheeting joint in tuff rock and a secondary side release surface along the east flank comprising columnar persistent surface without any infilling materials. Under these joint conditions, a typical

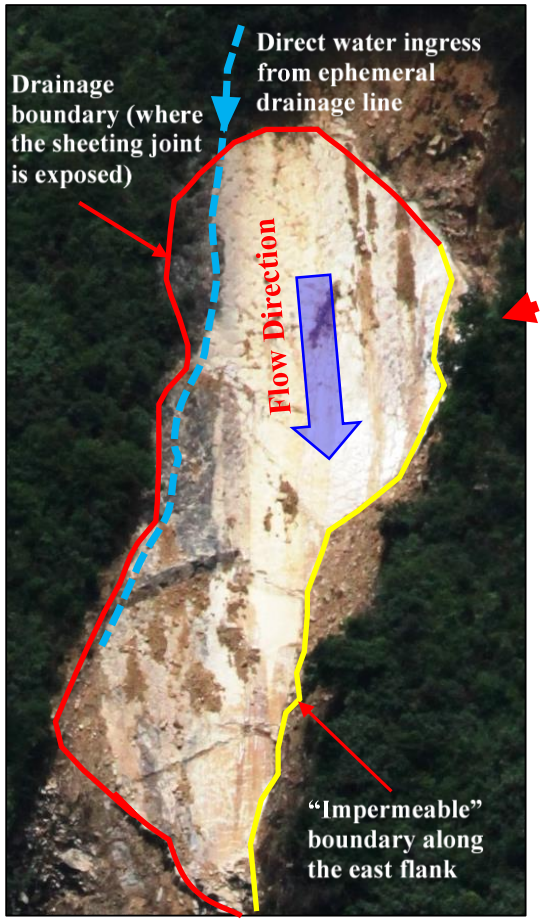

Assumptions for seepage analysis (steady-state)

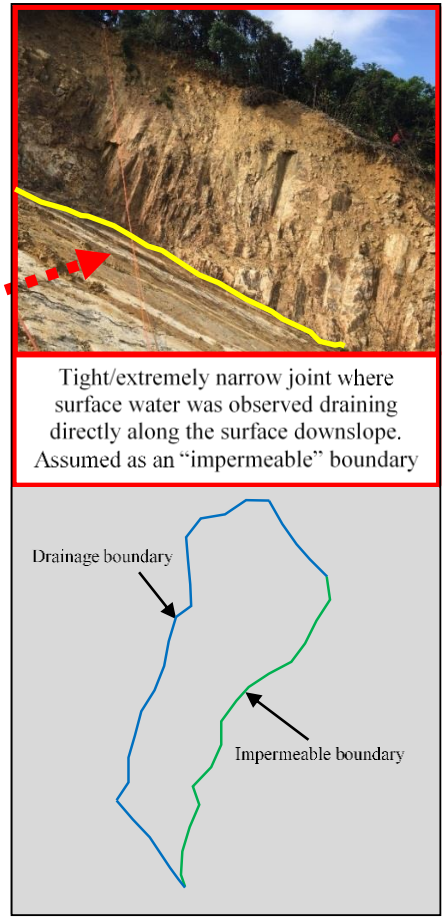

Model set-up for seepage analysis (steady-state)

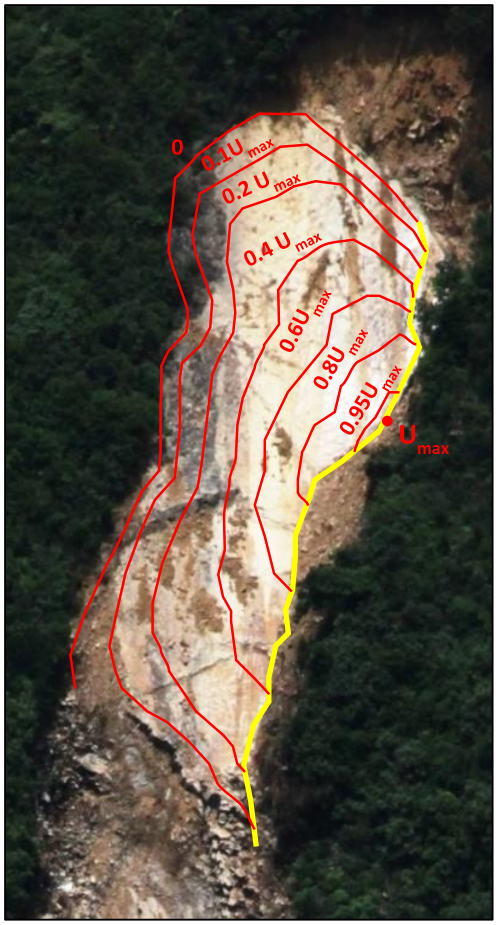

Cleft water pressure distribution developed across the sheeting joint at the landslide source area

Note: "Drainage boundary" refers to where the water pressure is set to zero in the analysis, and the boundary can be a source or exit point for water depending on the calculated hydraulic gradient.

Figure 8.2 Seepage Analysis (Steady State) at Time of Failure

range of shear strength parameters $c' = 0$ kPa and ϕ' varying between 40° and 45° were adopted for the purpose of the stability analyses, which is consistent with local rock slope engineering practice.

Shearing resistance at the east flank comprised the resistance from soil (viz colluvium and completely to highly decomposed tuff) and rock with columnar jointing, although the latter is considered to have contributed to most of the shearing resistance for the landslide. Theoretically, shearing in rock would have taken place along the individual joint faces of the rock columns assuming that the joints were exposed and that the rock columns remained intact. However, post-landslide observations noted that the corners formed by two sides of the sub-vertical columnar rock joints were often protruding into the landslide scar, and that local shearing had occurred across these corners in order to overcome the frictional resistance to failure. Under this circumstance, the frictional resistance in rock would likely be higher than that in intact rock joint (between 40° and 45°). Therefore, for the purposes of the sensitivity analysis, higher shear strength parameters c' of 60 kPa to 65 kPa and $\phi' = 50°$ were adopted for moderately decomposed tuff with columnar jointing, reflecting the additional resistance generated due to local shearing of the rock columns. Typical shear parameters for soils (GEO, 1993) were adopted for the shear resistance of the soil part in the east flank.

8.4 Slope Stability Findings

Stability analyses were carried out to back calculate the likely range of cleft water pressure development on the failure surface at the time of failure for the operative shear strength parameters for sheeting joint ($c' = 0$ kPa and $\phi' = 40°$ and 45°) and for columnar jointed rock ($c' = 60$ kPa to 65 kPa and ϕ' adopted at 50°). The results of the back analyses are presented in Figure 8.3. The results indicate that for the likely range of the shear strength parameters for both the sheeting joint and rock with columnar jointing, a maximum cleft water pressure between 33 kPa and 43 kPa in the sheeting joint would have been sufficient for the failure to occur (i.e. FoS = 1).

9 Discussion

9.1 'Atypical' Setting of the Landslide

9.1.1 General

During the 21 May 2016 rainstorm, a total of 34 natural terrain landslides occurred in the vicinity of Sai Kung Sai Wan Road (Figure 1.1). With the exception of the landslide, most of these other landslides were typically shallow (< 2 m deep) debris avalanches and debris flows initiating within colluvium and saprolite soil, had little or no structural control, and involved detached source volumes of less than 300 m^3. In contrast, the landslide had a significantly larger source volume (2,100 m^3), which was due to its considerable depth of failure (maximum of 12 m) and which in turn was due to the nature of the failure (structurally controlled, translational rock slide). This type of failure is relatively uncommon and is considered to be the result of an 'atypical' setting, where a combination of several contributory factors, other than steep natural terrain, have acted at this particular location. The contributory factors are discussed in the following sections.

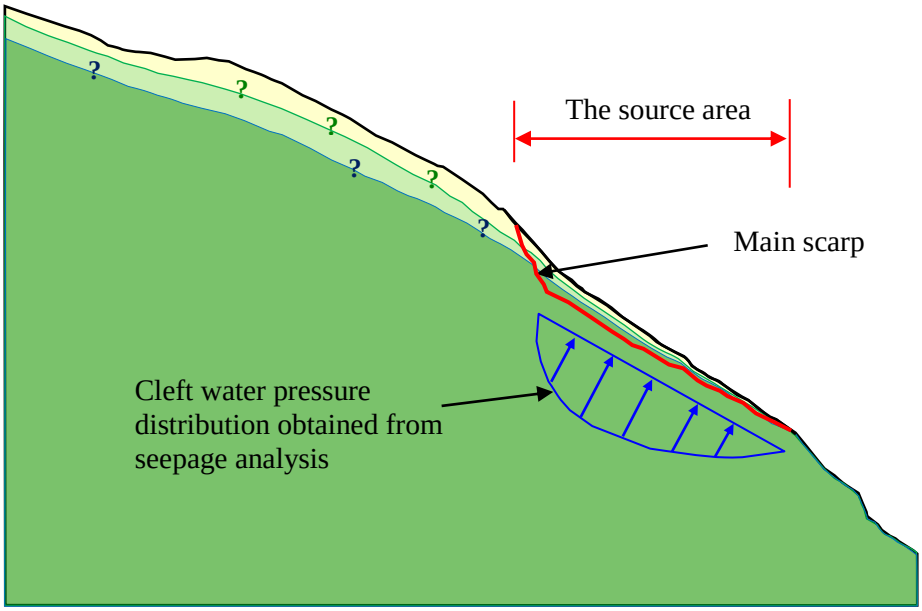

(a) Geological model for stability analysis

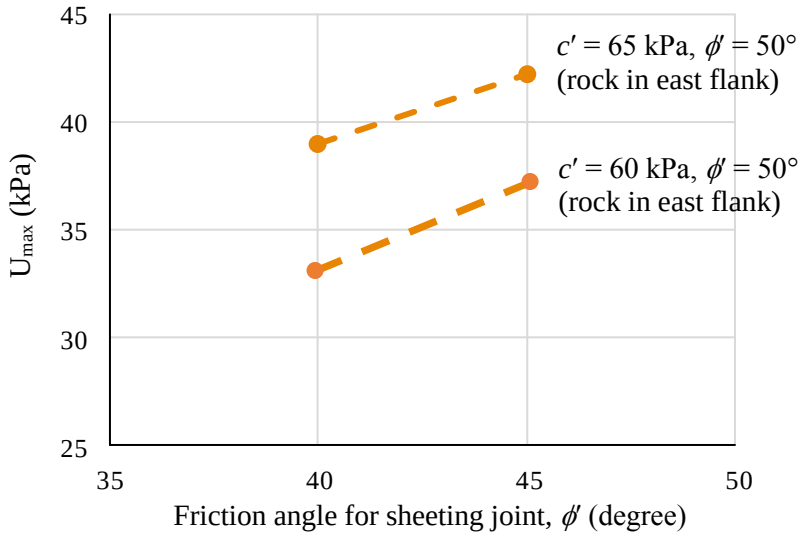

(b) Plot of shear strength parameters corresponding to various cleft water pressures

Legend:

Colluvium | Grade IV/V Tuff | Grade III Tuff

U_{max} that resulted in computed factor of safety equals to unity

Notes:

(1) In the stability analysis, the cohesion c' of the grade III tuff with columnar jointing was set to be 60 kPa and 65 kPa whereas the friction angle ϕ' set to be 50°.

(2) U_{max} refers to the maximum cleft water pressure of the contour plot estimated from the seepage analysis (see also Figure 8.2).

(3) Refer to Figure 4.1 for location of the section.

Figure 8.3 Results of Stability Analysis (Back Analysis of the Landslide)

9.1.2 Presence of a Planar, Persistent, Adversely-orientated Sheeting Joint near Ground Surface

The presence of an extensive sheeting joint within the columnar jointed tuff below the source area facilitated a basal surface of rupture on which structurally controlled failure could occur. In terms of geometry, the exposed surface of rupture was planar, persistent (greater than 60 m), steep (35° to 40°) and adversely orientated relative to the hillside. The sheeting joint also dipped across the hillside from west to east at approximately 15°. On the west flank the joint was exposed at ground level and then dipped to a maximum of approximately 12 m deep at the intersection with the east flank, giving an asymmetric profile (Figure 4.5), and facilitating concentrated water ingress into the joint.

The geometry and extent of the sheeting joint likely contributed to the large-scale of failure. No other sheeting joint with a similar orientation to the surface of rupture was observed in the surrounding hillside, although a few cases of persistent sheeting joints are known to exist in coastal settings around the Sai Kung area.

9.1.3 Presence of Ephemeral Drainage Line facilitating Direct Water Ingress into Sheeting Joint

An ephemeral drainage line was located along the vertical outcrop of tuff along the west flank of the source area (Figures 3.3 and 4.3). As the sheeting joint was exposed along the outcrop and likely open at this location due to stress relief, it would have facilitated ingress of water into the joint during the rainstorm.

The sheeting joint was observed to be extremely narrow to tight at the intersection with the east flank with surface water flowing along the intersection and not into the east flank after the failure. This suggests that water flow within the joint below the east flank was impeded and that cleft water pressures would have developed, increasing with depth towards the east flank, with associated reduction in shear strength between the joint surfaces. Minor seepage was observed at the base of the main scarp for three months after failure. The discharge rate and duration of the seepage indicate a possible delayed response from infiltration further upslope, which is consistent with the results of seepage analyses that direct infiltration is considered not to have had a significant effect on the landslide initiation.

9.1.4 Presence of Break-in-Slope

A convex break-in-slope is present just below the source area allowing the pre-failure sheeting joint to daylight and facilitating detachment (Figure 4.3). The break-in-slope is characterized by a narrow band of steep rock outcrop that traverses across the adjacent hillside to the east and is probably due to a local shear zone observed below the source area, causing preferential weathering and the steep break-in-slope. Although the band of rock outcrop could be traced laterally across the hillside to the east of the source, the orientation of the sheeting joint changes such that the dip angle reduces to between 10° and 15° (Figure 4.7) becoming less adverse. No other similar break-in-slope with daylighting sheeting joints was observed in the surrounding hillside.

9.2 Probable Causes of Failure

The close correlation between the landslide and the preceding intense rainstorm suggests that the failure was probably rain-induced. The landslide was a translational rock slide involving basal failure along an adversely orientated, persistent, planar sheeting joint in columnar jointed tuff, and was likely caused by direct water ingress from an adjacent drainage line into the joint which was exposed along the west flank of the source area resulting in the development of cleft water pressure within the sheeting joint, reducing shear strength and triggering failure. These unfavourable combination of factors had given rise to an atypical setting which was critical to the landslide initiation.

9.3 Potential for Further Large-scale Failure

The loose materials exposed in the main scarp were relatively small in volume. The potential for further large-scale failure was examined assuming a similar failure mechanism with the basal failure plane continuing into the hillside above the failure and into the east flank. This assumption is considered conservative as observations from the field mapping and GI, including vegetation clearance strips to investigate tension cracks upslope and to the east of the failure, indicate no signs of distress or deformation adjacent to the source area, which could indicate movement along a projected sheeting joint extension. Upslope of the main scarp, no outcrop is observed and no evidence of any daylighting joint could be observed, suggesting it might have changed orientation to follow the topography, or it discontinued.

For the hillside area adjacent to the east flank of the source area, the sheeting joint is dipping relatively steep into the east flank and the depth of the overburden increases rapidly eastwards (Figure 4.2). Consequently, the degree of weathering eastwards along the joint would likely be less and the associated shear strength be higher across the joint. Also the sheeting joint is extremely narrow to tight along the intersection of the joint surface and the base of the east flank, and surface water was observed to flow along the intersection and not into the east flank, suggesting the development of cleft water pressure in the east flank with similar magnitude as the failed portion is unlikely. The rock outcrop observed to the east of the source area near the break-in-slope indicates the orientation of the sheeting joint inside the east flank changes direction with the dip angle reducing to between 10° and 15°. This implies the orientation of the basal plane becoming less adverse. Thus, the susceptibility of large-scale failure extending eastward of the source is considered low.

Observations from the 33 other natural terrain landslides that occurred on 21 May 2016, revealed that none of them had any significant structural control and they were typically shallow failures within the regolith. The atypical setting of the landslide with respect to the combination of several geological and geomorphological factors resulting in the large-scale failure, is considered to be unusual and localised and the adjacent terrain is not susceptible to similar large-scale instability.

The field observations have been supplemented with engineering analyses to review the post-failure stability conditions. For the hillside area upslope of the main scarp, engineering analyses have been carried out with assumptions reflecting a worst-case scenario

of the sheeting joint extending with a similar orientation into the upslope terrain (given in Appendix D). Using a limit equilibrium 3-dimensional slope stability program and the strength parameters and water pressures described earlier, the results indicate that the change in stability conditions of the remaining hillside with respect to another large-scale failure before and after the landslide is insignificant and the computed factors of safety associated with potential large-scale failure of the remaining hillside exceed unity. Considering the hillside as a whole, the hillside is deemed to be less susceptible to large-scale failure after the landslide. Details of the analyses are given in Appendix D.

9.4 Debris Mobility

The mobility analyses show that a combination of base friction angles of 18º with a turbulence coefficient of 1,000 m/s^2 from the source area to Sai Kung Sai Wan Road and 8º with a turbulence coefficient of 500 m/s^2 for the downhill area of Sai Kung Sai Wan Road where the drainage line become incised, provides a reasonable fit to the debris trail. This is consistent with characteristics of four other notable mobile landslide events in Hong Kong that occurred in June 2008 (GEO, 2011), and a comparison is shown in Table C2. The study area setting includes a sizeable catchment with a long flow path into which many tributaries and drainage lines contain entrainable material. Thus it is considered that the landslide setting related to the catchment characteristics to be adverse with regards to being prone to development of sizeable channelized debris flows with watery debris of high mobility (Wong, 2009).

10 Conclusions

The landslide initiated as a structurally controlled, translational rock slide along a planar and persistent sheeting joint basal failure surface, and was probably triggered by the intense rainstorm in the early morning of 21 May 2016. The rainstorm was the most severe since 1983 for short duration rainfall (1 hour to 12 hours). Failure was probably induced by direct water ingress from an adjacent drainage line resulting in development of cleft water pressure within an adversely orientated sheeting joint in the underlying tuff rock mass. A narrow convex break-in-slope laterally traversing across the hillside facilitated daylighting of the sheeting joint and kinematic feasibility of failure. The landslide occurred at the location of a topographic depression inferred to be an existing relict landslide, although it is considered to have had limited direct influence on the landslide which is structurally controlled.

In addition to the landslide, another 33 natural terrain landslides occurred in the vicinity of Sai Kung Sai Wan Road in the same morning. All these landslides were more 'typical' shallow landslides within the regolith, and with a maximum volume of 300 m^3. In the study area, a total of 46 relict and recent natural terrain landslides have been identified, none of which appear to be structurally controlled. Within the Sai Kung Sai Wan Road area, the landslide is 'atypical' in terms of both its significant magnitude and unusual type, and is considered to have occurred due to a number of setting-specific factors that in combination resulted in the failure. These factors include structural geology, geomorphology, hydrology and hydrogeology.

In this respect, the landslide may be considered a low-frequency, large-magnitude landslide and the surrounding hillside is not particularly susceptible to similar events even during intense rainfall.

11 References

Cheng, Y.M. & Yip, C.J. (2007). Three-dimensional asymmetrical slope stability analysis - extension of Bishop's and Janbu's techniques. *Journal of Geotechnical and Geoenvironmental Engineering*, ASCE, December 2007, pp 1544-1555.

GCO (1989). *Sai Kung Peninsula: Solid and Superficial Geology, Hong Kong Geological Survey, Map Series HGM 20,* Sheet 8, 1:20,000 scale. Geotechnical Control Office, Hong Kong.

GEO (1993). *Guide to Retaining Wall Design (Geoguide 1)(2nd Edition)*. Geotechnical Engineering Office, Civil Engineering Department, Hong Kong, 258 p.

GEO (2011). *Guidelines on the Assessment of Debris Mobility for Channelized Debris Flows (GEO Technical Guidance Note 29)*. Geotechnical Engineering Office, Civil Engineering and Development Department, Hong Kong, 6 p.

Hansen, A. (1984). Engineering geomorphology: the application of an evolutionary model of Hong Kong's terrain. *Zeitschrift fur Geomorphologie*, supplementary vol. 51, pp 39-50.

Hungr, O. (2002). Hazard and risk assessment in the runout zone of rapid landslides. *Proceedings of the Conference Natural Terrain – A Constraint to Development*. The Institution of Mining and Metallurgy, Hong Kong Branch, pp 21-38.

IAEG Commission on Landslides (1990). Suggested nomenclature for landslides. International Association of Engineering Geology (IAEG) Commission on Landslides. *Bulletin of the International Association of Engineering Geology*, no. 41, pp 13-16.

Scott Wilson (1999). *Specialist API Services for the Natural Terrain Landslide Study - Task B Final Report*. Scott Wilson (Hong Kong) Limited. Report to Geotechnical Engineering Office, Civil Engineering Department, Hong Kong, 9 p. plus 4 maps.

Sewell, R.J., Campbell, S.D.G., Fletcher, C.J.N., Lai, K.W. & Kirk, P.A. (2000). *The Pre-Quaternary Geology of Hong Kong*. Geotechnical Engineering Office, Civil Engineering and Development Department, Hong Kong, 181 p. plus 4 maps.

Strahler, A.N. (1952). Hypsometric (area-altitude) analysis of erosional topography. *Geological Society of America Bulletin*, vol. 63, no. 11, pp 1117-1142.

Tang, C.S.C. & Cheung, S.P.Y. (2011). *Frequency Analysis of Extreme Rainfall Values (GEO Report No. 261)*. Geotechnical Engineering Office, Civil Engineering and Development Department, Hong Kong, 209 p.

Wong, H.N. (2009). Rising to the challenges of natural terrain landslides. *Proceedings of the HKIE Geotechnical Division Annual Seminar on Natural Hillsides: Study and Risk Management Measures*, Hong Kong Institution of Engineers, pp 15-53.

Appendix A

Aerial Photograph Interpretation

Contents

List of Table

List of Figure

A.1 Introduction

An Aerial Photograph Interpretation (API) has been carried out as part of the desk study for the purposes of establishing the site history, past instability and geomorphological characteristics of the study area. A review of available aerial photographs taken between 1924 and 2014 was undertaken (see list in Table A1). Based primarily on the 1963 aerial photographs, with some additional observations from other relevant aerial photographs, observations relating to the site history are shown on Figure 3.1, with the morphology and hydrology shown in Figures 3.3 and 5.1 respectively. Pertinent observations from the API are summarised in Figure A1.

A.2 Summary

The study area comprises natural terrain. In the earliest aerial photographs reviewed (1924 to 1963), the area of concern can be seen to be located on a southeast-facing catchment, bounded by ridges and spurlines. The catchment contains a dendritic drainage network feeding into an incised main drainage line (DL1) which although meanders locally, generally trends southeast. Several tributary, ephemeral drainage lines form the drainage network within the study area, one of which is located on the west flank of the source area. A convex break-in-slope is discernible near the toe of the landslide source where a band of rock outcrop can be seen.

The catchment is generally vegetated although along the ridgeline there are some local areas of high reflectivity, inferred as bare soil surface, and which probably indicates surface erosion. Rock outcrop is observed as continuous narrow bands and intermittent outcrop.

A number of relict landslides (RL1 to RL42) can be identified within the study area, which are predominantly distributed in the mid to upper portion of the catchment or on steep drainage line flanks in the lower portion of the catchment. Relict landslide RL1 is located at the approximate location as the landslide and appears as a rounded depression.

In the early 1970s Sai Kung Sai Wan Road, traversing across the mid-slope of the study area, was constructed. This was probably associated with the construction of High Island Reservoir which was constructed in the 1970s.

No significant changes can be seen in the study area after 1974.

A.3 Detailed Observations

This appendix sets out the detailed observations made from an interpretation of aerial photographs taken between 1924 and 2014. A list of the aerial photographs studied is presented in Table A1 and a location plan is shown in Figure A1.

Year	Observations
1924	Poor resolution, high-flight photographs preclude detailed interpretation. The study area covers a southeast-facing catchment, bounded by an east-west trending ridge at crest, and south- to southeast-trending spur at eastern and western flanks respectively. The catchment contains several drainage lines in a dendritic pattern. The incised main drainage line at the lower portion of the catchment is generally trending southeast. Several well-defined, southeast- to southwest-trending drainage lines are located on the valley flanks, draining towards the main drainage line (DL1). The catchment is generally lightly vegetated, while local patches of high reflectivity can be observed along the ridgeline, which are probably patches of soil surface erosion.
1945	Poor resolution, high-flight photographs preclude detailed interpretation. Photolineaments trending NE-SW are visible. Surface areas of high reflectivity can be locally observed at the western portion of the catchment, which are inferred as rock outcrop. In general the upper portion of the study area near the ridgeline is steeper and is lightly vegetated with low shrubs and grass. The lower portion of the study area is not as steep as the upper portion and is generally characterised by the presence of trees and tall shrubs.
1963	These photographs are of good resolution and the terrain morphology is much clearer. The study area morphology is generally a concave depression containing several drainage lines in a dendritic pattern. Interfluves can be discerned further dividing the study area into sub-catchments. The upper portion of the catchment is generally steep and the gradient gradually reduces towards the bottom of the catchment. Steep terrain is present along the flanks of drainage lines and where rock outcrop exposed. Rock outcrop is visible near the ridgeline and locally on the mid-slopes. A number of relict landslides (RL1 to RL42) can be identified within the catchment, which are predominantly distributed near the crest and at the mid-slope area. Among those, 18 Nos. of them have a sharp morphology (Class A), 13 Nos. of them have a rounded morphology (Class B) and 11 Nos. of them are shallow depressions with a gentle break in slope (Class C). These relict landslide features are generally vegetated with grass. The relict landslides are predominately located at the head of drainage lines and at the oversteepened flanks of incised drainage lines. Most of these landslides appear shallow in depth. Photolineaments trending NE-SW and NW-SE can be observed, which are probably associated with geological structures. Some of the lineaments are sub-parallel to each other, probably reflecting the dominant joint set orientation. NE-SW trending photolineaments are apparent at relict landslides RL1, RL6 and

Year	Observations
	RL26, and probably reflect rock joint surface exposures at the relict scar. It is possible that these joint surfaces have contributed to the relict landslide initiation. Relict landslide RL1 (ENTLI No. 08SEA0034E) is located at the approximate location as the landslide, and appears as a rounded depression with a linear rock outcrop discernible along the southwest edge of the depression dipping downslope. The morphology of relict landslide RL1 appears rounded with a gentle break-in-slope along the main scarp and is inferred as a degraded landslide feature. A colluvial lobe can be discerned at the middle portion of the catchment, which is located downstream (about 180 m) from relict landslide RL1.
1964	No observable changes.
1973	Sai Kung Sai Wan Road was under construction, traversing across the mid-slope of the catchment. The associated cut slopes above the road have been formed, while the fill slopes below the road were still under construction. Recent landslide LS1 (ENTLI No. 08SEA0589E) can be discerned at the lower portion of the catchment, where a highly reflective surface and detached raft of debris can be observed at the flank of main drainage line (DL1). The location of LS1 is approximately the same as relict landslide RL38. Landslide LS1 may represent retrogressive failure of RL38.
1974	Construction works of Sai Kung Sai Wan Road and its associated slopes have been completed. Recent landslide LS2 can be identified at the lower portion of the catchment, approximately 50 m to the southwest. This recent landslide was not previously recorded in the ENTLI and is located at the outer bank of a drainage bend. Fluvial erosion at the slope toe may be a contributing factor for the failure.
1975	No observable changes.
1976	No observable changes.
1978	No observable changes.
1979	Recent landslide LS3 (ENTLI No. 08SEA0623E) is observed at the southern portion of the catchment. It is located near the crest of a southeast-trending spur and at the head of a northeast-trending ephemeral drainage line. The debris trail is approximately 50 m in length.

Year	Observations
1981	Recent landslide LS4 (ENTLI No. 08SEA0626E) can be discerned at the eastern portion of the catchment, which is located at the flank of a southwest-trending drainage line. The debris trail of LS4 reaches the main drainage line (DL1) approximately 50 m to the southwest.
1983	No observable changes.
1985	No observable changes.
1986	No observable changes.
1988	No observable changes.
1989	No observable changes.
1990	No observable changes.
1991	No observable changes.
1992	No observable changes.
1993	No observable changes.
1994	No observable changes.
1995	No observable changes.
1996	No observable changes.
1997	No observable changes.
1998	No observable changes.
1999	No observable changes.
2000	No observable changes.
2001	No observable changes.
2002	No observable changes.
2003	No observable changes.
2004	No observable changes.
2005	No observable changes.

Year	Observations
2006	No observable changes.
2007	No observable changes.
2008	No observable changes.
2009	No observable changes.
2010	No observable changes.
2011	No observable changes.
2013	No observable changes.
2014	No observable changes.

Table A1 List of Aerial Photographs (Sheet 1 of 2)

Date taken	Altitude (ft)	Photograph Number
1924	11100	Y00071-72
10 November 1945	20000	Y00662-63
17 February 1963	3900	Y10271-73
26 February 1963	7000	Y10614-15
13 December 1964	12500	Y12982-83
13 December 1964	12500	Y13019-20
30 January 1973	6000	2997-98
28 February 1974	12500	8242-43
27 February 1975	4000	10997-98
30 June 1976	4000	14421-22
23 November 1976	12500	16532-33
10 January 1978	12500	20714-15
29 November 1979	10000	28153
27 October 1981	10000	39169-70
22 December 1983	10000	52203-04
22 April 1985	4500	65452-53
12 December 1986	10000	A08085-86
16 January 1988	10000	A12020-21
20 November 1989	10000	A19343-44
3 December 1990	10000	A24306-07
19 October 1991	10000	A28266-67
11 November 1992	10000	A33282-83
6 December 1993	10000	CN5614-15
12 October 1994	10000	CN8512-13
24 November 1995	10000	CN12351-52
9 November 1996	10000	CN15862-63
1 November 1997	10000	CN18814-15
11 November 1998	8000	CN21467-68

Note: All aerial photographs are in black and white except for those prefixed with CN, CW, CS or RS.

Table A1 List of Aerial Photographs (Sheet 2 of 2)

Date taken	Altitude (ft)	Photograph Number
24 November 1999	8000	CN24863-64
20 January 2000	4000	CN25886
21 June 2001	8000	CS00429-30
9 February 2002	8000	CW44855-56
27 September 2003	4000	CW50561-62
19 November 2004	4000	CW61900-01
21 November 2005	8000	CW69059-60
8 February 2006	4000	CW70876-77
6 January 2007	6000	CS05574-75
27 July 2008	6000	CS15718-19
23 November 2009	6000	CS24910-11
6 August 2010	2500	CW86636-37
2 November 2010	6000	RS04992-93
10 January 2011	6000	CS31792-93
1 January 2013	3000	CW99028-29
28 January 2014	8000	CW105349-50

Note: All aerial photographs are in black and white except for those prefixed with CN, CW, CS or RS.

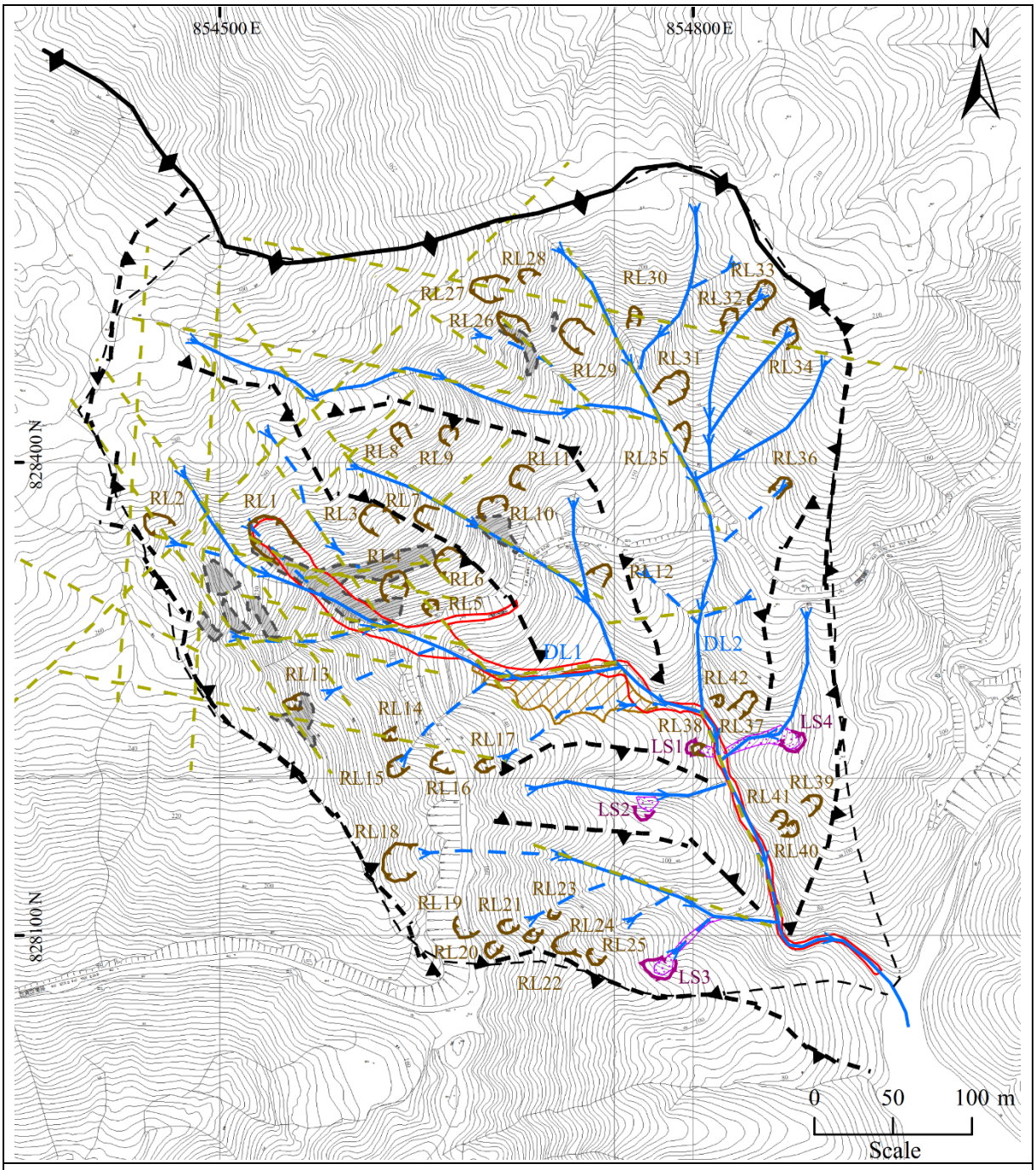

Legend:

- The landslide
- Study area
- Perennial drainage line
- Ephemeral drainage line
- Ridgeline
- Spurline
- LS1 Recent landslide
- RL1 Relict landslide
- Photolineament
- Rock outcrop
- Recent landslide debris
- Lobe of relict colluvial debris

Note: Base plan is extracted from 1:1000 survey sheet Nos. 8SE-7A, 8SE-7B, 8SE-7C and 8SE-7D dated March 2016.

Figure A1 Aerial Photograph Interpretation

Appendix B

Landslide Mapping Plans

Contents

List of Figures

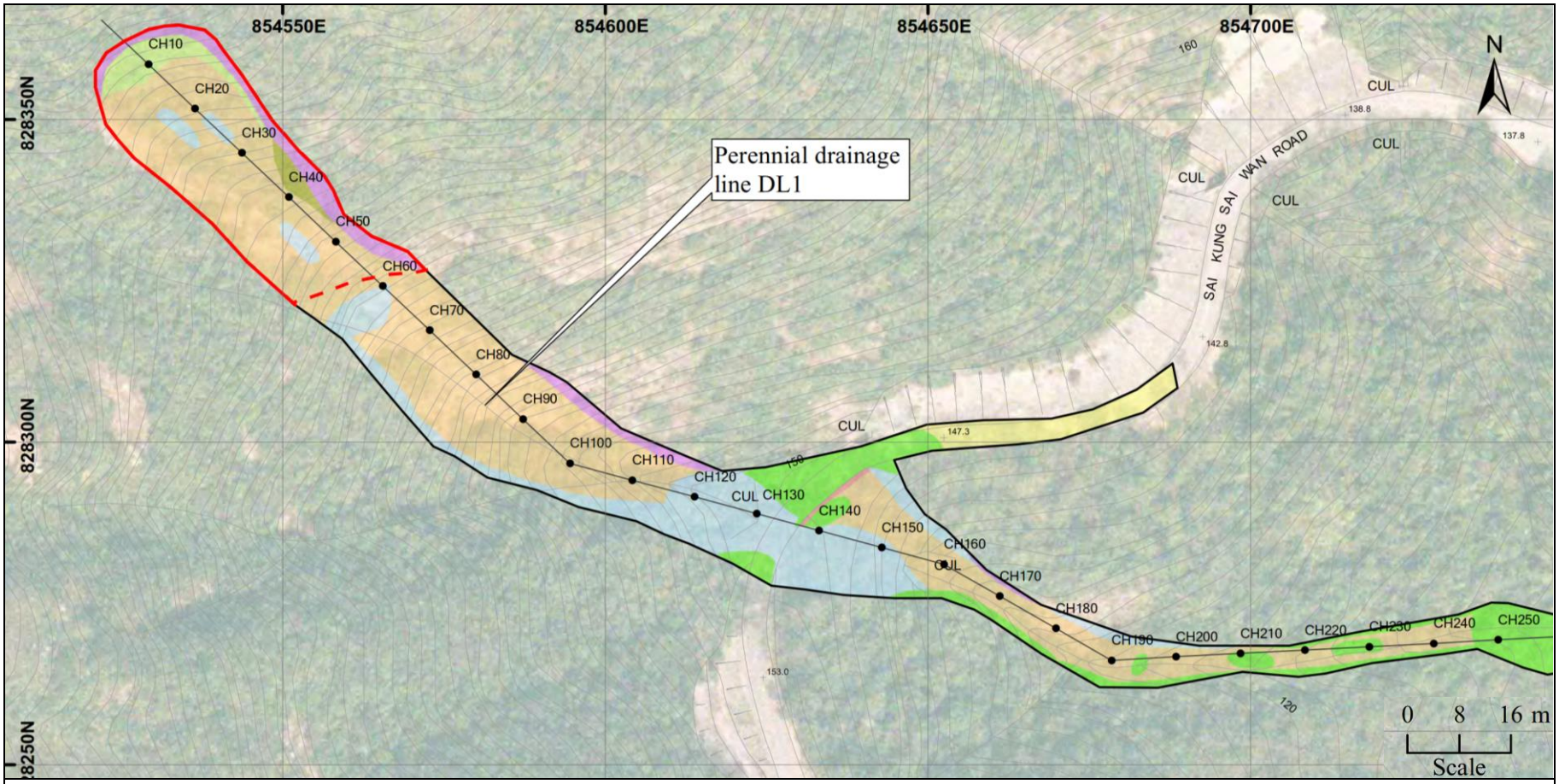

Note: Base plan is extracted from 1:1000 survey sheet Nos. 8SE-7A dated March 2016.

Figure B1 Sketch Plan of Debris Trail (CH0 to CH250)

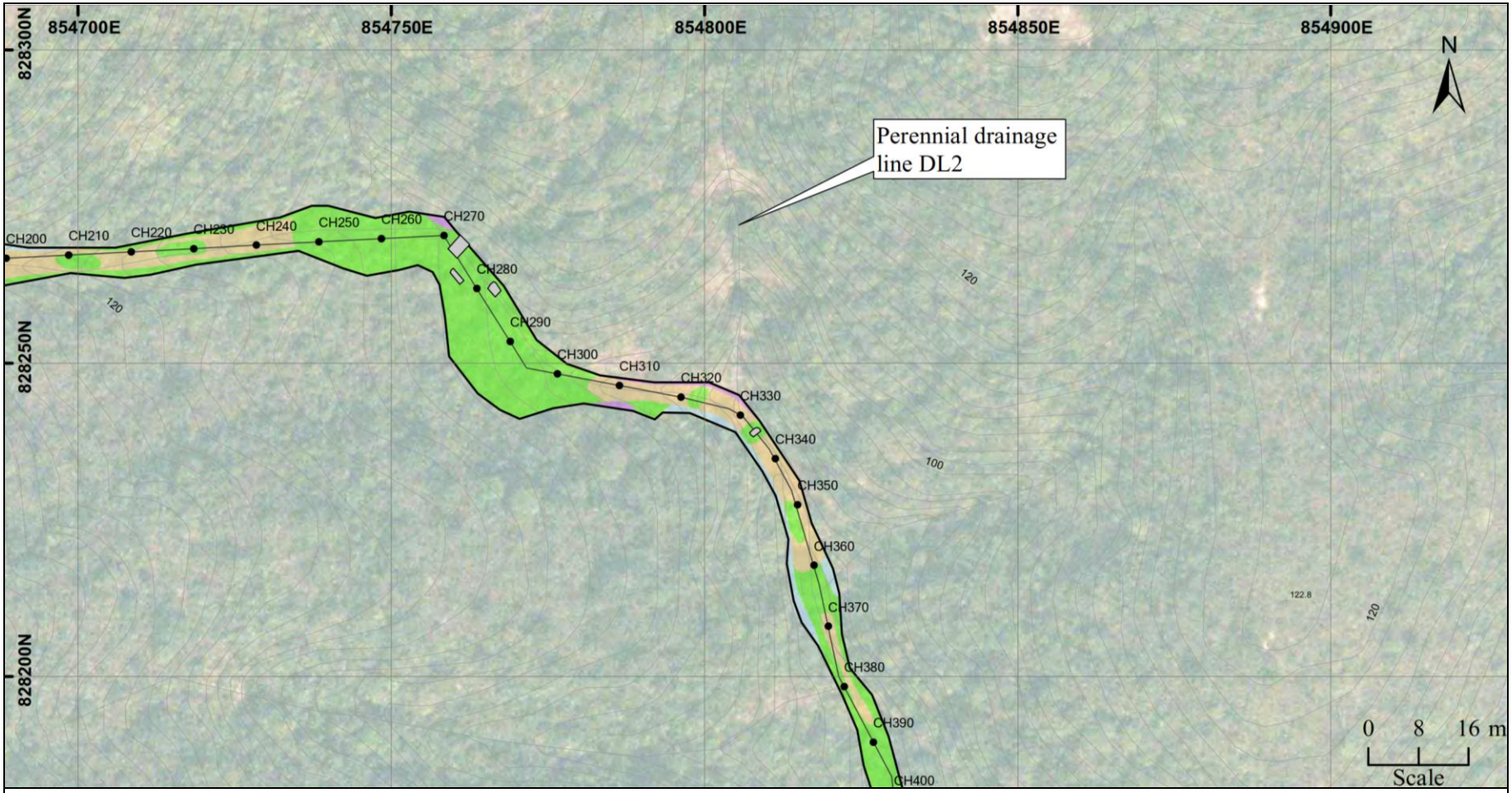

Legend:

Exposed source and substrate

Debris trail

Concrete fragment

MT1 – Colluvium

MT3 – H/MDT

MT4 – MDT

Deposition materials

MT5 – Remoulded debris (mixed fine and coarse)

MT6 – Clastic debris (coarse gravel to boulder sized)

Note: Base plan is extracted from 1:1000 survey sheet Nos. 8SE-7A, 8SE-7B, 8SE-7C and 8SE-7D dated March 2016.

Figure B2 Sketch Plan of Debris Trail (CH200 to CH400)

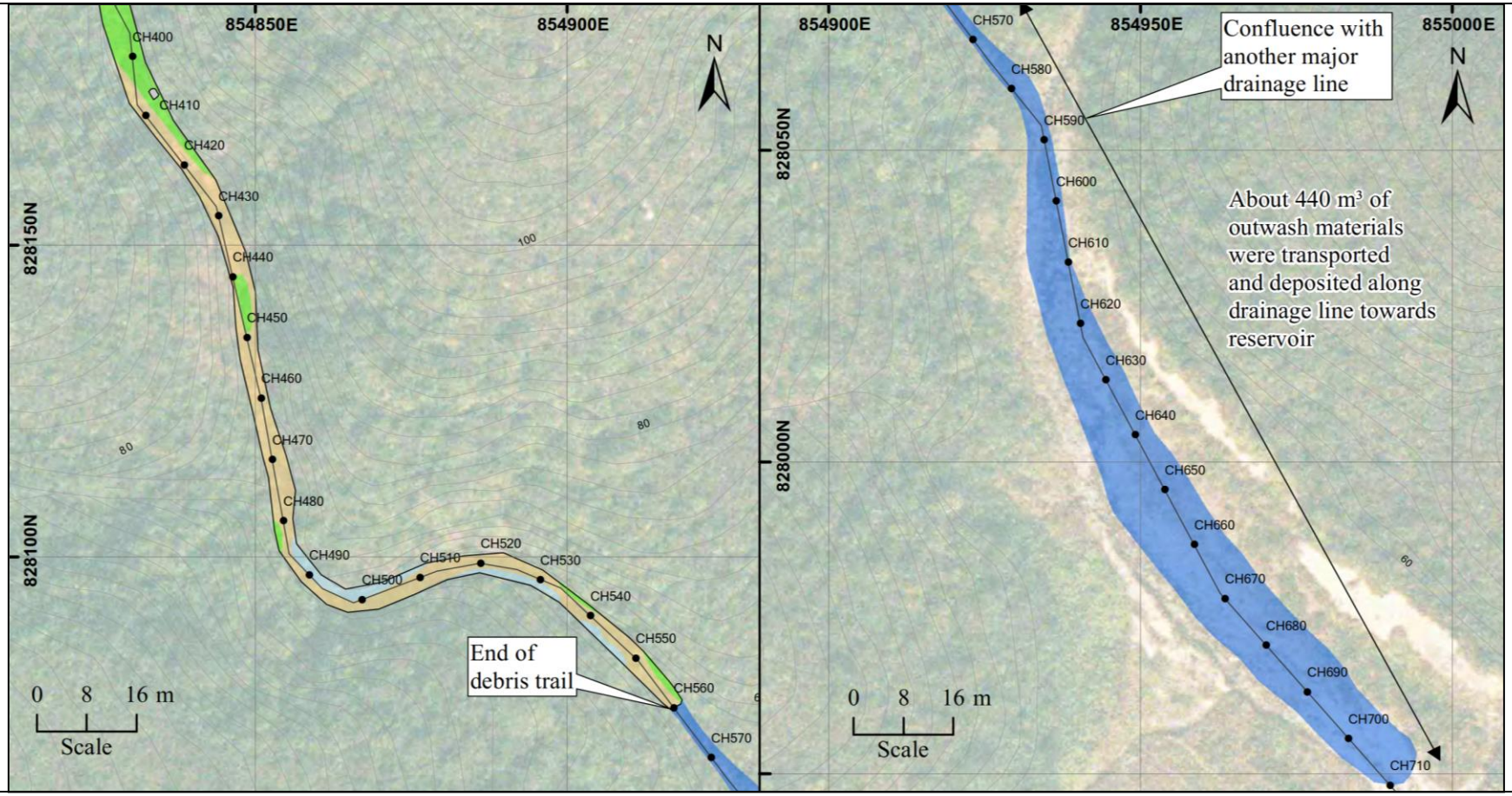

Note: Base plan is extracted from 1:1000 survey sheet Nos. 8SE-7C and 8SE-7D dated March 2016.

Figure B3 Sketch Plan of Debris Trail (CH390 to CH710)

Appendix C

Theoretical Debris Mobility Analysis

Contents

List of Tables

List of Figures

C.1 General

The landslide was back-analysed using the GEO's 2-dimensional Debris Mobility Model, 2d-DMM (Version 1.2). The program incorporates consideration for a trapezoidal cross-section to define the cross-sections of the landslide debris flow path. The program has also incorporated a functionality module for simulating motion of landslide debris using the sliding-consolidation model. Two rheologies, the frictional and Voellmy models, are available in the numerical simulation package.

Where a debris flow travels at high velocity around a bend in a drainage channel, a difference of surface elevation (superelevation) of the debris across a drainage channel may occur due to banking effects. By recording the geometry of the channel and debris marks, velocity of the debris can be estimated and used to compare with results obtained from modelling (Figure C1 and Table C3). A commonly used method is the forced vortex equation (Hungr et al, 1984; Johnson & Rodine, 1984) and illustrated below from Ho & Roberts (2016). Mean flow velocity *v*, is given by:

$$v = \sqrt{\frac{R_c g}{k}\frac{\Delta h}{b}}$$ where

v	mean flow velocity
Rc	the channel's radius of curvature
g	acceleration due to gravity
Δh	super-elevation height
k	correction factor for viscosity and vertical sorting
b	the flow width

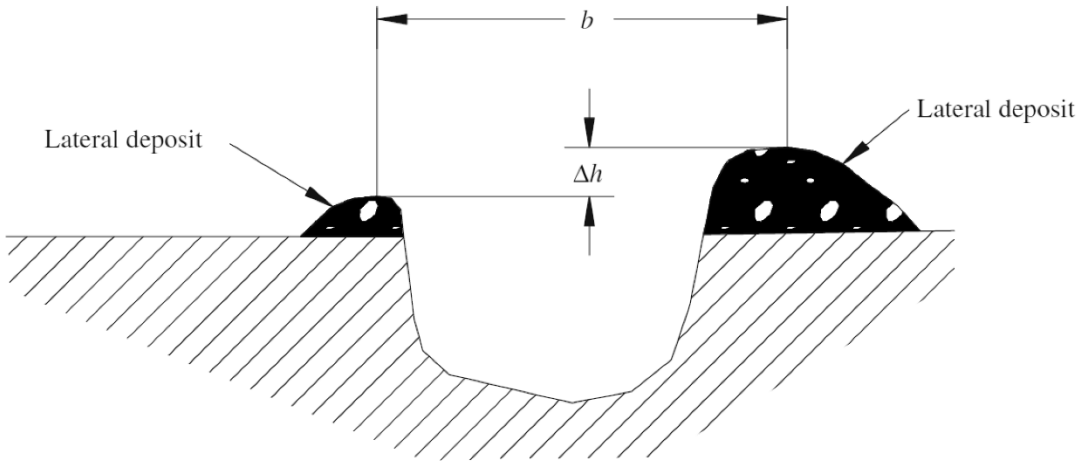

Superelevation marks were observed at two locations at bends in the debris trail, at Chainage 273 and Chainage 300, indicating elevation differences of 2.5 m and 1.0 m respectively.

C.2 The Model

The topography adopted for the modelling comprised post-failure topography for the source area, derived from photogrammetric survey, and pre-failure topography for the debris trail based on LiDAR survey data. The initial thickness of the displaced material within the source area was estimated from the difference between the topographic surface from the pre-failure LiDAR survey, and the post-failure topographic surface from photogrammetric survey by UAV, supplemented by field measurements. According to the site observations, the source area involved a detachment of about 2,100 m^3. For simplicity, the model assumes all the materials detached in one go.

Within the debris trail, erosion and channel width were recorded from field mapping for each critical section of chainage, as shown in Table 4.1. In two portions along the debris trail, at CH60 to CH116 and CH137 to CH162, tangible entrainment of 210 m^3 and 250 m^3 respectively were considered in the analysis. Due to the inherent variability, the channel width was averaged for each chainage section but varied from between 2 m and 17 m, and the input for the model was derived from a polynomial trend through this data. The channel side angles adopted in the analysis were 89º, 40º and 30º for grouped sections of debris trail between CH 0 to CH155, CH155 to CH340 and CH340 to CH560 respectively, based on field observations.

It is suggested in GEO Technical Guidance Note Nos. 29 and 38 (GEO, 2011; 2014) that Voellmy flow models may be used to represent the failure within topographic depression catchments and channelized debris flows. The landslide involved a topographic depression failure above Sai Kung Sai Wan Road and the debris became channelized when it reached the drainage line downslope of Sai Kung Sai Wan Road. As the major portion of the debris trail is below Sai Kung Sai Wan Road it is considered that the Voellmy rheology is appropriate to be adopted for the entire debris trail in the analyses.

C.3 Summary of Results

Several analyses were carried out for a range of base friction angle in order to provide a reasonable correlation to the observed extent of the debris trail, deposition of debris and mass balance. The results indicated that the base friction angle has a marked effect on the mobility of the debris flow. For example, if a typical base friction angle (i.e. 11º) was adopted for the channelized debris flow section, lower mobility of the debris would result where the debris would stop further upslope from the observed end of the debris trail.

The findings of these analyses show that a combination of base friction angles of 18º with a turbulence coefficient of 1,000 m/s^2 from the source area to Sai Kung Sai Wan Road and 8º with a turbulence coefficient of 500 m/s^2 for the downhill area of Sai Kung Sai Wan Road where the drainage line become incised, could provide a reasonable fit to the debris trail topography. The best-fit parameters determined are summarised in Table C1. Table C2 shows a comparison of debris flow characteristics from the landslide with four mobile landslides that occurred in June 2008.

The maximum velocity generated by the 2d-DMM indicates that the debris flow would

accelerate from the source area as it entered the steep hillside below with a gradient of about 50º and reached its peak velocity of about 19 m/s when the debris front reached approximately Chainage 123 immediately above Sai Kung Sai Wan Road (Figure C1). At this point the debris was about 4.3 m thick, reaching a maximum of about 4.7 m just below Sai Kung Sai Wan Road.

From Chainage 123 to 200, the velocity only slightly decreases to about 18 m/s due to the steep confined drainage line morphology, and the debris thickness remains at least 3 m. However, after Chainage 200 the velocity gradually decreases as the gradient slowly decreases. Significant deposition of coarse material occurred between Chainage 245 and 305 where the drainage line broadened out with some relatively flat, vegetated areas adjacent to the drainage line and consequently the corresponding velocity reduced to between 15 m/s and 11 m/s, and the debris thickness reduced to between 2.7 m and 2.2 m. Within this area, the debris velocity and thickness were sufficient to produce superelevation of the debris surface around two of the bends with superelevations of 2.5 m and 1 m observed at Chainage 273 (Figure 4.15) and Chainage 300 respectively. The superelevation marks indicated a velocity of approximately 10 m/s and 7 m/s respectively, which corresponds reasonably well with the

Table C1 Parameters Determined for Theoretical Debris Mobility Analysis

Chainage (m)	Model Type	Base Friction Angle ϕ_a (°)	Turbulence Coefficient, ξ (m/s^2)
0-135	Voellmy	18	1000
135-560	Voellmy	8	500

Table C2 Comparison of Debris Flow Characteristics with Mobile Landslides in June 2008 (GEO, 2011)

Landslide case	Catchment size	Source volume	Total maximum active volume	Runout distance	Travel angle	Back analysed Voellmy parameters (based on 2d-DMM)	
						ϕ_a	ξ
Sai Wan Road	**192,000 m^2**	**~ 2,100 m^3**	**~ 2,220 m^3**	**> 500 m**	**18.0°**	**8.0°**	**500 m/s^2**
Yu Tung C30	102,000 m^2	~ 2,350 m^3	~ 3,300 m^3	> 590 m	16.6°	7.7°	500 m/s^2
Shek Pik 2	165,000 m^2	~ 1,000 m^3	> 8,500 m^3	> 910 m	17.7°	7.6°	500 m/s^2
Shek Pik 4	672,000 m^2	~ 150 m^3	> 5,000 m^3	> 1,700 m	15.8°	7.3°	500 m/s^2
Shek Mun Kap	121,000 m^2	~ 220 m^3	> 1,700 m^3	> 980 m	23.6°	8.7°	500 m/s^2

calculated debris front velocity generated by 2d-DMM along this section of the debris trail (Figure C1 and Table C3).

The calculated velocity continues to decrease and the debris thickness remains above 2 m until about Chainage 440, corresponding to a velocity of about 6 m/s, where the debris thickness rapidly decreases. By Chainage 500, the velocity had reduced to about 3 m/s and the thickness of debris was calculated to be 1.2 m, which is comparable to the field observations (about 1 m). The debris came to a halt at Chainage 560 where the slope gradient is gentle (< 5º).

Table C3 Calculation of Debris Velocity from Superelevation Observation Using a Forced Vortex Equation (Hungr et al, 1984; Johnson & Rodine, 1984)

Estimation of Velocity Based on Superelevation Observations			
CH 273			
h_1	1	m	Debris height on inside of bend
h_2	3.5	m	Debris height on outside of bend
Δh	2.5	m	Superelevation height = $h_2 - h_1$
b	6	m	Flow Width
Rc	24	m	Channel's radius of curvature (Bend radius)
k	1		Correction factor for viscosity and vertical sorting
v	**9.90**	**m/s**	Flow velocity = $((\Delta h * R_c * 9.81)/(k * b))^{0.5}$
CH 300			
h_1	1.5	m	Debris height on inside of bend
h_2	2.5	m	Debris height on outside of bend
Δh	1	m	Superelevation height = $h_2 - h_1$
b	7	m	Flow Width
Rc	32	m	Channel's radius of curvature (Bend radius)
k	1		Correction factor for viscosity and vertical sorting
v	**6.70**	**m/s**	Flow velocity = $((\Delta h * R_c * 9.81)/(k * b))^{0.5}$

C.4 References

GEO (2011). *Guidelines on the Assessment of Debris Mobility for Channelised Debris Flows (GEO Technical Guidance Note No. 29).* Geotechnical Engineering Office, Civil Engineering and Development Department, Hong Kong, 6 p.

GEO (2014). *Guidelines on Assessment of Debris Mobility for Failures within Topographic Depression Catchments (GEO Technical Guidance Note No. 38).* Geotechnical Engineering Office, Civil Engineering and Development Department, Hong Kong, 8 p.

Ho, H.Y. & Roberts, K.J. (2016). *Guidelines for Natural Terrain Hazard Studies (GEO Report No. 138, 2nd Edition).* Geotechnical Engineering Office, Civil Engineering and Development Department, Hong Kong, 173 p.

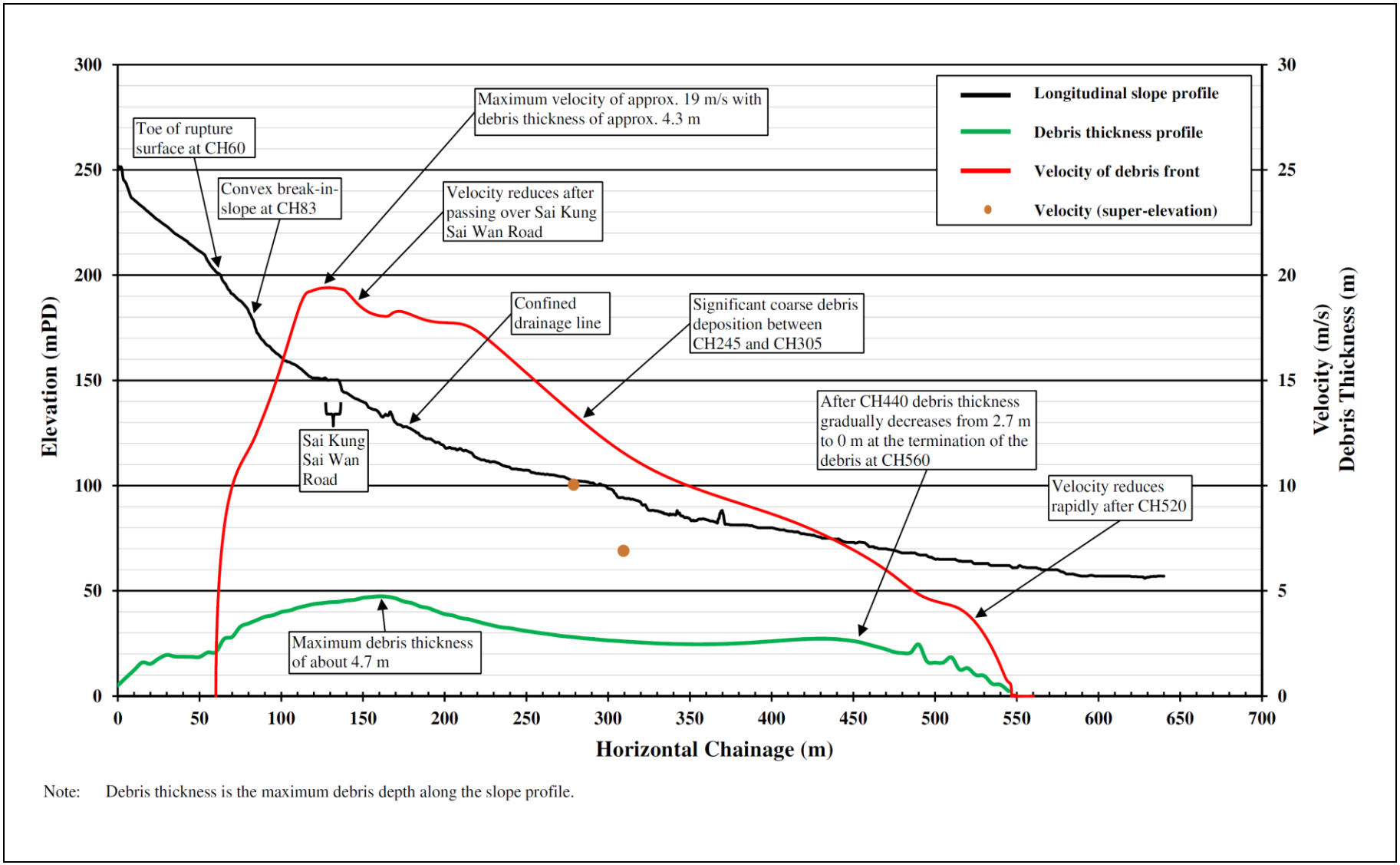

Figure C1 Debris Velocity and Thickness versus Chainage

Hungr, O., Morgan, G.C. & Kellerhals, R. (1984). Quantitative analysis of debris torrent hazards for design of remedial measures. *Canadian Geotechnical Journal*, vol. 21, pp 663-677.

Johnson, A.M. & Rodine, J.R. (1984). Debris flow. In: Brunsden, D. & Prior, D.B. (Eds), *Slope Stability*, John Wiley and Sons Ltd, NY, pp 257-361

Appendix D

Engineering Analysis for Further Large-scale Failure

Contents

List of Figures

D.1 General

The engineering analysis provided a quantitative assessment on the likelihood of a further large-scale failure occurring on the hillside surrounding the landslide and supplemented the findings from site reconnaissance. The natural hillside upslope of the main scarp was considered more critical than the east flank (see Section 9.3) and has been selected for this assessment. A slope stability analysis was conducted to evaluate the change of the overall factor of safety (FoS) of the hillside before and after the landslide. Owing to the 3-dimensional nature of the slope stability problem (see Section 8.1), the computer program 'Slope3D' (Cheng & Yip, 2007) using the limit equilibrium method (Morgenstern - Price approach) was adopted.

D.2 Analytical Model

The pre-failure and post-failure topography of the landslide site adopted for the modelling was based on the LiDAR survey and the photogrammetric topographic survey data obtained by UAV respectively. The topography of the surrounding hillside was based on the LiDAR survey, which was commonly used for the modelling of both pre- and post-failure conditions. The geological interfaces projected into the adjacent hillside both longitudinally and laterally were carefully established with reference to the geomorphology and geology of the study area.

With the assumption on 'large-scale failure' (see Section 9.3), prescribed failure slip surfaces with basal sliding plane principally along the sheeting joint extension were adopted in the stability analysis to reflect the worst case scenario. For simplicity, elliptical (on plan) slip surfaces with a planar side face along the perimeter of the slips were derived. Such planar side face was assumed to have a similar dip to that exposed on the east flank of the landslide. As a result, the slip surfaces adopted in the 3-dimensional analysis would be pan-shaped. This assessment employed three prescribed slip surfaces (namely S1, S2 and S3) in an attempt to obtain a convergent solution while keeping the amount of the computation work manageable.

The hillside upslope of the failure was assumed to have a similar geological profile inferred from the exposed landslide scar and similar material properties (principally shear strength parameters) adopted in the back analysis of the landslide (see Section 8.3). Only the case with cohesion intercept (c') of rock with columnar jointing of 60 kPa was considered for the sake of simplicity (i.e. the lower value of the range adopted in the back analysis, 60 kPa to 65 kPa in Section 8.3).

The stability of the hillside was assessed for scenarios before and after the landslide, with a view to evaluating the respective stability conditions. To simulate the pre-landslide groundwater condition, the cleft water pressure distribution due to direct water ingress as obtained from seepage analysis (see Section 8.2.2) was applied to the source area and a nominal water pressure of 10 kPa on the hillside above the main scarp was applied to account for any limited groundwater pressure that could develop at the sheeting joint due to direct infiltration. For the post-landslide scenario, as no rock outcrop or evidence of any daylighting joint could be observed at the hillside above the main scarp, direct water ingress

into the sheeting joint is unlikely. Therefore, only a nominal of water pressure of 10 kPa on the hillside above the main scarp was applied to account for any limited groundwater pressure that could develop at the sheeting joint due to direct infiltration.

D.3 Summary of Results

The computer program 'Slope3D' using Morgenstern - Price approach was employed to better reflect the asymmetric geometry of the landslide source area. The analytical model together with the material properties, groundwater conditions and prescribed failure slip surfaces outlined above, were utilised in the program to compute the respective FoS associated with potential large-scale failure of the remaining hillside. The results of the stability analysis, as shown in Figure D1, indicate that although the computed FoSs decrease slightly (from 4% to 9%) when comparing stability conditions before and after the landslide, all FoSs exceed unity. Considering the hillside as a whole, the hillside is deemed to be less susceptible to large-scale failure after the landslide.

D.4 References

Cheng, Y.M. & Yip, C.J. (2007). Three-dimensional asymmetrical slope stability analysis - extension of Bishop's and Janbu's techniques. *Journal of Geotechnical and Geoenvironmental Engineering*, ASCE, December 2007, pp 1544-1555.

GEO (1993). *Guide to Retaining Wall Design (Geoguide 1) (2nd Edition).* Geotechnical Engineering Office, Civil Engineering Department, Hong Kong, 258 p.

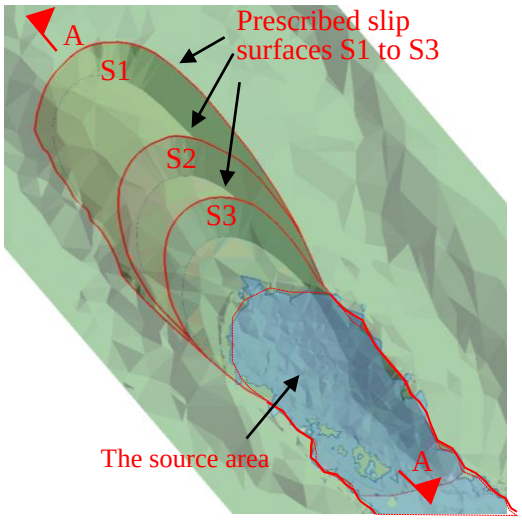

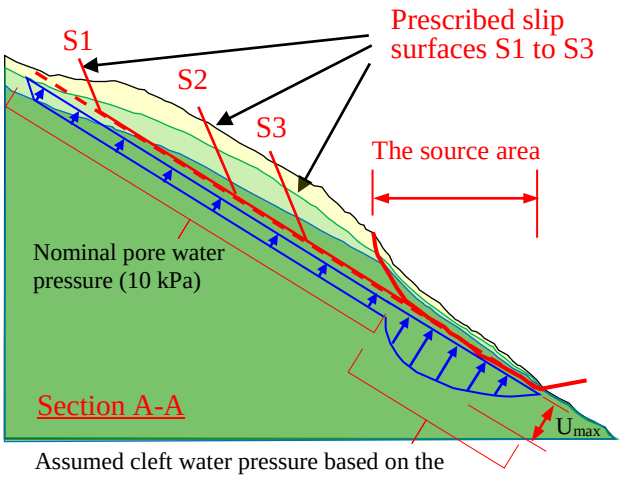

(a) Pre-landslide condition

Assumed cleft water pressure based on the results of seepage analysis and back analysis (U_{max} = 33 kPa and 37 kPa for ϕ' = 40° and 45° respectively)

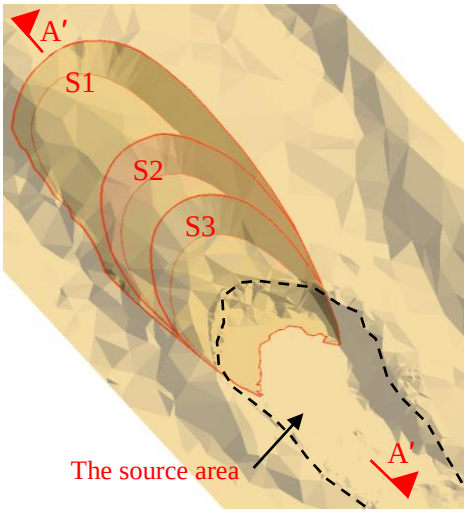

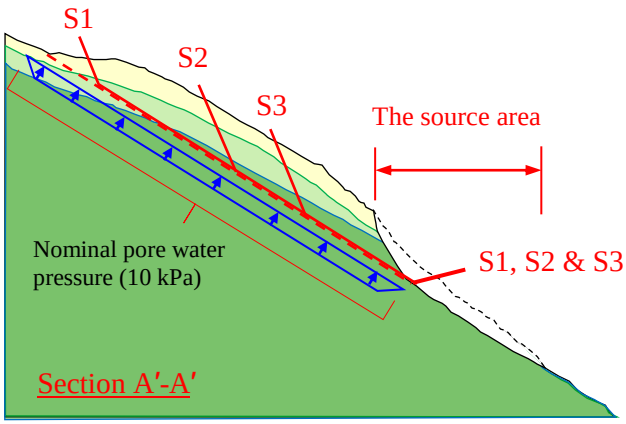

(b) Post-landslide condition

ϕ' = 40° (friction angle for sheeting joint)	FoS for Slip No.		
	S1	S2	S3
Pre-landslide condition	1.79	1.75	1.19
Post-landslide condition	1.68	1.59	1.10
ϕ' = 45° (friction angle for sheeting joint)	FoS for Slip No.		
	S1	S2	S3
Pre-landslide condition	1.88	1.83	1.24
Post-landslide condition	1.79	1.70	1.19

(c) Results of Stability Analysis

Legend: Colluvium; Grade IV/V Tuff; Grade III Tuff; Assumed sheeting joint extension (worst-case scenario)

Note: The adopted shear strength parameters for colluvium (c' = 0 kPa, ϕ' = 35°) and Grade IV/V tuff (c' = 10 kPa, ϕ' = 38°) are based on the typical ranges given in Table 8 of Geoguide 1 (GEO, 1993).

Figure D1 Results of Stability Analysis

GEO PUBLICATIONS AND ORDERING INFORMATION
土力工程處刊物及訂購資料

An up-to-date full list of GEO publications can be found at the CEDD Website http://www.cedd.gov.hk on the Internet under "Publications". The following GEO publications can also be downloaded from the CEDD Website:

i. Manuals, Guides and Specifications
ii. GEO technical guidance notes
iii. GEO reports
iv. Geotechnical area studies programme
v. Geological survey memoirs
vi. Geological survey sheet reports

詳盡及最新的土力工程處刊物目錄，已登載於土木工程拓展署的互聯網網頁http://www.cedd.gov.hk 的"刊物"版面之內。以下的土力工程處刊物亦可於該網頁下載：

i. 指南、指引及規格
ii. 土力工程處技術指引
iii. 土力工程處報告
iv. 岩土工程地區研究計劃
v. 地質研究報告
vi. 地質調查圖表報告

Copies of some GEO publications (except geological maps and other publications which are free of charge) can be purchased either by:

Writing to
Publications Sales Unit,
Information Services Department,
Room 626, 6th Floor,
North Point Government Offices,
333 Java Road, North Point, Hong Kong.

or

- Calling the Publications Sales Section of Information Services Department (ISD) at (852) 2537 1910
- Visiting the online Government Bookstore at http:// www.bookstore.gov.hk
- Downloading the order form from the ISD website at http://www.isd.gov.hk and submitting the order online or by fax to (852) 2523 7195
- Placing order with ISD by e-mail at puborder@isd.gov.hk

讀者可採用以下方法購買部分土力工程處刊物(地質圖及免費刊物除外):

書面訂購
香港北角渣華道333號
北角政府合署6樓626室
政府新聞處
刊物銷售組

或

- 致電政府新聞處刊物銷售小組訂購 (電話：(852) 2537 1910)
- 進入網上「政府書店」選購，網址為 http://www.bookstore.gov.hk
- 透過政府新聞處的網站 (http://www.isd.gov.hk) 於網上遞交訂購表格，或將表格傳真至刊物銷售小組 (傳真：(852) 2523 7195)
- 以電郵方式訂購 (電郵地址：puborder@isd.gov.hk)

1:100 000, 1:20 000 and 1:5 000 geological maps can be purchased from:

Map Publications Centre/HK,
Survey & Mapping Office, Lands Department,
23th Floor, North Point Government Offices,
333 Java Road, North Point, Hong Kong.
Tel: (852) 2231 3187
Fax: (852) 2116 0774

讀者可於下列地點購買1:100 000、1:20 000及1:5 000地質圖：

香港北角渣華道333號
北角政府合署23樓
地政總署測繪處
電話: (852) 2231 3187
傳真: (852) 2116 0774

Any enquires on GEO publications should be directed to:

Chief Geotechnical Engineer/Standards and Testing,
Geotechnical Engineering Office,
Civil Engineering and Development Department,
Civil Engineering and Development Building,
101 Princess Margaret Road,
Homantin, Kowloon, Hong Kong.
Tel: (852) 2762 5346
Fax: (852) 2714 0275
E-mail: florenceko@cedd.gov.hk

如對本處刊物有任何查詢，請致函：

香港九龍何文田公主道101號
土木工程拓展署大樓
土木工程拓展署
土力工程處
標準及測試部總土力工程師
電話: (852) 2762 5346
傳真: (852) 2714 0275
電子郵件: florenceko@cedd.gov.hk